CHARACTERIZATION OF THE HYDROGEN-BROMINE FLOW BATTERY FOR ELECTRICAL ENERGY STORAGE

By

Haley Maren Kreutzer

Submitted to the graduate degree program in Chemical and Petroleum Engineering and the Graduate Faculty of the University of Kansas in partial fulfillment of the requirements for the degree of Master of Science.

_____

Chairperson Dr. Trung Van Nguyen

_____

Dr. Laurence Weatherley

_____

Dr. Susan Williams

Date Defended: April 6, 2012

The Thesis Committee for Haley Maren Kreutzer
certifies that this is the approved version of the following thesis:

CHARACTERIZATION OF THE HYDROGEN-BROMINE FLOW BATTERY FOR ELECTRICAL ENERGY STORAGE

_____

Chairperson Dr. Trung Van Nguyen

_____

Dr. Laurence Weatherley

_____

Dr. Susan Williams

Date Approved: April 6, 2012

Abstract

A low-cost and efficient electrical energy storage system is needed to implement intermittent renewable energy sources such as solar and wind while maintaining grid reliability, and could also reduce the use of inefficient peak-load electrical generating units through peak shaving and load leveling. Batteries have proper energy and power densities for these applications. A flow battery is advantageous to a secondary battery because the reactants are stored externally and the electrodes are inert, allowing the power and energy densities to be separated and increasing durability and lifetime by eliminating physical and structural changes to the electrode surface. The hydrogen-bromine (H_2-Br_2) system is advantageous to other redox chemistries due to its fast kinetics, the high solubility of bromine in aqueous hydrobromic acid, the low cost of the electrolyte, and the ability to avoid water electrolysis. It is disadvantaged by the high cost of suitable electrodes and membranes, possible poisoning of the platinum catalyst at the hydrogen electrode by bromide, and the corrosiveness of aqueous HBr/Br_2 solution.

The effects of bromine concentration (0.7 M to 2 M), flow field design (serpentine or interdigitated), temperature (23 ˚C to 45 ˚C), hydrogen pressure (1 to 5 psig), flow rates, membrane thickness and bromine electrode materials on a hydrogen-bromine flow battery are presented. The cell consists of compressed graphite powder flow field blocks treated with polymer sealant, Nafion membrane, stainless steel current collectors and end plates, SGL 35BC with platinum catalyst as the hydrogen electrode, and plain Toray 090 with platinum or graphite catalyst as the bromine electrode. A potentiostat/gavalnostat by Arbin Instruments was used to set the voltage and measure the steady state current.

A H_2-Br_2 flow battery using platinum as the catalyst for both sides is molecular transport limited, with decreases in performance at lower temperatures, lower aqueous HBr/Br_2 flow rates, and when using serpentine rather than interdigitated flow field channels. The decreased performance at higher membrane thickness also demonstrates ionic transport limitations. While platinum at the bromine electrode increases the performance for both charge and discharge, no metal catalyst is needed as graphite is active for both bromine reduction and evolution.

Acknowledgment

I'd like to thank my advisor, Dr. Trung Van Nguyen, for his support, extreme flexibility, time, and patience as I worked on this research project. Thank you also to committee members Dr. Laurence Weatherley and Dr. Susan Williams for their time and feedback.

Thank you to Erin Espenschied and Omar Al-Kaff for their help during the experimental set-up and initial testing. Omar Al-Kaff also provided the peristaltic pump calibrations in Appendix A. Thank you to Brian Yang for verifying the concentrations of the aqueous HBr/Br_2 solutions. I would also like to acknowledge my lab mates Venkata Yarlagadda and Dr. Azita Ahosseini for their support and helpful feedback during my research.

The researchers working on this collaborative effort at the University of California-Santa Barbara, Vanderbilt University, and the University of Texas-Arlington were very helpful with insightful questions and comments for much of the research discussed in this thesis.

Thank you also to my supervisors and co-workers in the Air Permitting & Compliance Branch at Region 7 EPA for their flexibility while I pursued my degree.

[The views and opinions expressed in this article are those of the author and do not necessarily reflect the views or policies of the United States Environmental Protection Agency or United States Government.]

The author also wishes to acknowledge the National Science Foundation for making this research possible through grant no. EFRI-1038234.

To Nellie, Maxine, Bart, Kelley, Brit, Max, Kenneth,

And the rest of my family for encouraging me to continue my education.

Table of Contents

Title i

Acceptance ii

Abstract iii

Acknowledgment v

Dedication vi

Table of Contents vii

List of Figures xi

List of Tables xiii

Nomenclature xv

Chapter 1: Importance of Electrical Energy Storage 1

1.1: Improving Efficiency and Reliability of Non-Intermittent Sources 1

1.2: Implementation of Solar and Wind Power 4

1.3: Electrical Energy Storage Technologies 5

1.3.1: Stored Electrically 5

1.3.1.1: Capacitors & Supercapacitors 5

1.3.1.2 Superconducting Magnetic Energy Storage (SMES) 6

1.3.2 Stored Mechanically 7

1.3.2.1 Pumped Hydro Storage (PHS) 7

1.3.2.2 Compressed Air Energy Storage (CAES) 8

1.3.2.3 Flywheels 9

1.3.3 Stored Chemically 10

1.3.3.1 Secondary Batteries 10

1.3.3.1.1 Developed Secondary Batteries 11
1.3.3.1.2 Developing Secondary Batteries 12
1.3.3.2 Flow Batteries 12
1.3.3.2.1 Iron-Chromium 14
1.3.3.2.2 All-Vanadium 15
1.3.3.2.3 Vanadium-Polyhalide 16
1.3.3.2.4 Bromine-Polysulfide 16
1.3.3.2.5 Hydrogen-Oxidant 17
1.3.3.3 Hybrid Flow Batteries 19
1.3.4 Stored Thermally 19
1.3.5 Comparing Electrical Energy Storage Technologies 20
Chapter 2: Overview of the Hydrogen-Bromine Flow Battery 23
2.1: H_2-Br_2 Flow Battery Operation 23
2.2: History of the H_2-Br_2 Flow Battery 27
2.3: Literature Review 28
2.3.1: Properties of HBr-H_2O-Br_2 Solution 29
2.3.2: Open Circuit Potential 30
2.3.3: Electrode Catalyst Materials 30
2.3.3.1: Both Electrodes of the Same Material 30
2.3.3.2: Hydrogen Electrode 30
2.3.3.3: Bromine Electrode 31
2.3.4: Membrane 32
2.3.4.1: Structure of the Nafion Membrane 32

2.3.4.2: Properties of Nafion Membrane in an HBr Environment 33
2.3.4.3: Transport of Bromine Within Nafion 34
2.3.4.4: Alternate Membrane Performance 35
2.3.5: Catalyst/Membrane Interface 36
2.3.6: Overall Cell Performance 38
2.3.6.1: Experimental Studies 38
2.3.6.1.1: Fuel Cell Lifetime Study 38
2.3.6.1.2: Temperature, Concentration, Flow Rate and Catalyst Studies 40
2.3.6.2: Simulation Studies 41
2.3.6.2.1: Liquid Phase Flow Battery: Heat Effects 41
2.3.6.2.2: Liquid Phase Fuel Cell 42
2.3.6.2.3: Gas Phase Flow Battery 43
2.4: Advantages of the Hydrogen Bromine Flow Battery 45
2.5: Disadvantages of the Hydrogen Bromine Flow Battery 46
2.6: Experimental Objectives 46
Chapter 3: Experimental Studies 49
3.1: Typical Fuel Cell/Flow Battery Behavior 49
3.2: Preliminary Studies 51
3.2.1: Flow Field Block Material & Design 51
3.2.2: Membrane Electrode Assembly 52
3.2.3: Set-Up and Procedure 54
3.2.4: Comparison to H_2-O_2 System 54
3.2.5: Looping Phenomena 57

3.3: Case Studies 60
3.3.1: Experimental Design 60
3.3.1.1: Flow Field Block Material & Design 60
3.3.1.2: Membrane Electrode Assembly 61
3.3.1.3: Flow Battery Set-Up 62
3.3.1.4: Experimental Procedure 65
3.3.2: Effect of Bromine Concentration 67
3.3.3: Effect of Flow Field Design 70
3.3.4: Effect of Br_2/HBr Flow Rate 72
3.3.5: Effect of Temperature 74
3.3.6: Effect of H_2 Pressure and Flow Rate 76
3.3.7: Effect of Membrane Thickness 78
3.3.8: Effect of Br_2/HBr Electrode 80
3.4: Summary of Experimental Findings 84
Chapter 4: Recommendations for Further Studies 85
4.1: Catalyst Design 85
4.2: Membrane Design 86
4.3: Cell Design 87
4.4: Development of Model 88
References 89
Appendix A: Calibration Data 95
Appendix B: Experimental Data from Preliminary Studies (Sections 3.2.4-5) 100
Appendix C: Experimental Data from Case Studies (Sections 3.3.2-8) 104

List of Figures

Figure 1.1: Electrical energy storage used for peak shaving and load leveling[2] 2

Figure 1.2: World net electricity generation in trillion kilowatt hours (created from data provided by the EIA)[4] 3

Figure 1.3: Schematic of pumped hydro storage system for energy storage[10] 7

Figure 1.4: Compressed air energy storage system[9] 8

Figure 1.5: Secondary battery[7] 10

Figure 1.6: Diagram of a redox flow battery[11] 13

Figure 1.7: Capital cost per power and per energy of several EES technologies[25] 22

Figure 2.1: Hydrogen-bromine flow battery operation 23

Figure 2.2: Structure of Nafion membrane[41] 32

Figure 2.3: Cluster-Network model in Nafion membrane[43] 33

Figure 2.4: Electrode-membrane interface at hydrogen electrode[46] 36

Figure 3.1: Generic voltage-current plot for a fuel cell or flow battery during discharge[7] 49

Figure 3.2: Flow field design used in preliminary studies 52

Figure 3.3: Components of an MEA[38] 53

Figure 3.4: Comparison of H_2-Air fuel cell performance to H_2-Br_2 flow battery performance ... 55

Figure 3.5: Example of looping behavior observed during preliminary studies 58

Figure 3.6: Flow field dimensions used for the case studies in sections 3.3.2-8 60

Figure 3.7: Experimental set-up to obtain hydrogen-bromine flow battery data 62

Figure 3.8: Hydrogen path connected to the flow battery 64

Figure 3.9: Effect of bromine concentration on H_2-Br_2 flow battery performance 68

Figure 3.10: Effect of bromine concentration on H_2-Br_2 flow battery performance, adjusted for open circuit potential 69
Figure 3.11: Interdigitated and serpentine flow field designs 70
Figure 3.12: Interdigitated and serpentine flow field performance in the H_2-Br_2 flow battery ... 71
Figure 3.13: Effect of Br_2/HBr flow rate on H_2-Br_2 flow battery performance, interdigitated flow fields 72
Figure 3.14: Effect of Br_2/HBr flow rate on H_2-Br_2 flow battery performance, serpentine flow field for Br_2/HBr solution, interdigitated flow field for H_2 73
Figure 3.15: Effect of temperature on H_2-Br_2 flow battery performance 75
Figure 3.16: Effect of H_2 flow rate on H_2-Br_2 flow battery performance 77
Figure 3.17: Effect of H_2 pressure on H_2-Br_2 flow battery performance 78
Figure 3.18: Effect of membrane thickness on H_2-Br_2 flow battery performance 79
Figure 3.19: Effect of bromine electrode catalyst on H_2-Br_2 flow battery performance, platinum or XC-72 on Toray 090 and plain SGL 10AA 81
Figure 3.20: Effect of bromine electrode catalyst on H_2-Br_2 flow battery performance, platinum or XC-72 on Toray 090 82
Figure 3.21: Effect of bromine electrode catalyst on H_2-Br_2 flow battery performance, XC-72 or graphene on Toray 090 plain 83
Figure A.1: HBr/Br_2 pump calibration chart for the preliminary studies (sections 3.2.4-5) 96
Figure A.2: HBr/Br_2 pump calibration chart for the case studies (sections 3.3.2-8) 98
Figure A.3: H_2 rotameter calibration chart 99

List of Tables

Table 1.1: The feasibility of several EES technologies[24] 21

Table A.1: HBr/Br_2 calibration data for the preliminary studies (sections 3.2.4-5). 96

Table A.2: HBr/Br_2 pump calibration data for the case studies (sections 3.3.2-8), all three trials97

Table A.3: HBr/Br_2 pump calibration data for the case studies (sections 3.3.2-8), average of three trials..... 97

Table A.4: H_2 rotameter calibration data 98

Table B.1: H_2-Br_2 experimental data presented in Figure 3.4 101

Table B.2: H_2-Air experimental data presented in Figure 3.4 102

Table B.3: H_2-Br_2 experimental data presented in Figure 3.5 103

Table C.1: H_2-Br_2 flow battery data, base case conditions (Figures 3.9, 3.10, 3.12, 3.15, 3.16, 3.17, 3.18) 106

Table C.2: H_2-Br_2 flow battery data from Figures 3.9 and 3.10, 1 M Br_2 107

Table C.3: H_2-Br_2 flow battery data from Figures 3.9 and 3.10, 0.7 M Br_2 108

Table C.4: H_2-Br_2 flow battery data from Figure 3.12, serpentine flow field 109

Table C.5: H_2-Br_2 flow battery data from Figure 3.13, 0.5 mL/min..... 109

Table C.6: H_2-Br_2 flow battery data from Figure 3.13, 0.9 mL/min..... 110

Table C.7: H_2-Br_2 flow battery data from Figure 3.13, 1.4 mL/min..... 110

Table C.8: H_2-Br_2 flow battery data from Figure 3.13, 1.6 mL/min..... 111

Table C.9: H_2-Br_2 flow battery data from Figure 3.14, 0.5 mL/min..... 112

Table C.10: H_2-Br_2 flow battery data from Figure 3.14, 0.9 mL/min..... 112

Table C.11: H_2-Br_2 flow battery data from Figure 3.14, 1.4 mL/min..... 113

Table C.12: H_2-Br_2 flow battery data from Figure 3.14, 1.6 mL/min..... 113

Table C.13: H_2-Br_2 flow battery data from Figure 3.15, 35 ˚C 114

Table C.14: H_2-Br_2 flow battery data from Figure 3.15, 45 ˚C 115

Table C.15: H_2-Br_2 flow battery data from Figure 3.16, 2200 mL/min..... 116

Table C.16: H_2-Br_2 flow battery data from Figure 3.17, 1 psig..... 117

Table C.17: H_2-Br_2 flow battery data from Figure 3.17, 5 psig..... 118

Table C.18: H_2-Br_2 flow battery data from Figures 3.18 through 3.21, Nafion 115 and 0.5 mg/cm^2 Pt/C..... 119

Table C.19: H_2-Br_2 flow battery data from Figure 3.19, SGL 10 AA without catalyst..... 120

Table C.20: H_2-Br_2 flow battery data from Figures 3.19 through 3.21, 2.1 mg/cm^2 XC-72 carbon on Toray 090 plain..... 121

Table C.21: H_2-Br_2 flow battery data from Figures 3.20 and 3.21, 6.6 mg/cm^2 XC-72 carbon on Toray 090 plain..... 122

Table C.22: H_2-Br_2 flow battery data from Figure 3.21, 1.6 mg/cm^2 graphene on Toray 090 plain..... 123

Nomenclature

E	electrochemical potential
E°	standard electrochemical potential
$K_{equilibrium}$	chemical equilibrium constant
R_{gas}	universal gas constant
T	temperature (K)
F	Faraday constant (96487 C/mol)
a_{Br_2}	activity of bromine
a_{H^+}	activity of hydronium ion
a_{Br^-}	activity of bromide
p_{H_2}	partial pressure of hydrogen gas
ΔS	change in entropy
V	voltage
I	current
R	resistance

Chapter 1: Importance of Electrical Energy Storage

1.1: Improving Efficiency and Reliability of Non-Intermittent Sources

Non-intermittent energy sources (utilities which can be started and shut down on demand, albeit with a delay) include hydroelectric, nuclear, coal-fired, and natural gas. Energy use follows a distinct pattern through the day, shown by the curve in Figure 1.1. It is a minimum in the early morning (when most people are sleeping), continues to rise throughout the day, and has one peak in the early afternoon and one peak during the late evening. Electricity demand is met through a combination of base units (those units running 365 days a year, 7 days a week, 24 hours a day) and peak units which are operated only during periods of high demand. These peak units are needed because electricity is usually not stored; only 2.5% of the electrical base load is stored in the United States.[1]

Figure 1.1 illustrates how electricity storage reduces overall generation. During low demand (from 0 to around 10 hours), electricity can be stored and dispatched later during periods of high demand, denoted by the shaded areas. Peak shaving, the top chart in Figure 1.1, is storing enough electricity to reduce the peak demand, although not all the excess electricity is stored, thus necessitating the use of some peak units. Load leveling, the bottom chart in Figure 1.1, is storing enough energy to reduce the electrical generating capacity to an average demand only (the straight line). Peak shaving and load leveling would reduce, or eliminate, respectively, the use of peaking units, which are typically the more inefficient and higher polluting coal-fired units, or the more rapidly responsive diesel generators. Furthermore, the base load would be reduced. Van der Linden estimates a plant could operate at 40% less capacity if energy storage is used.[1]

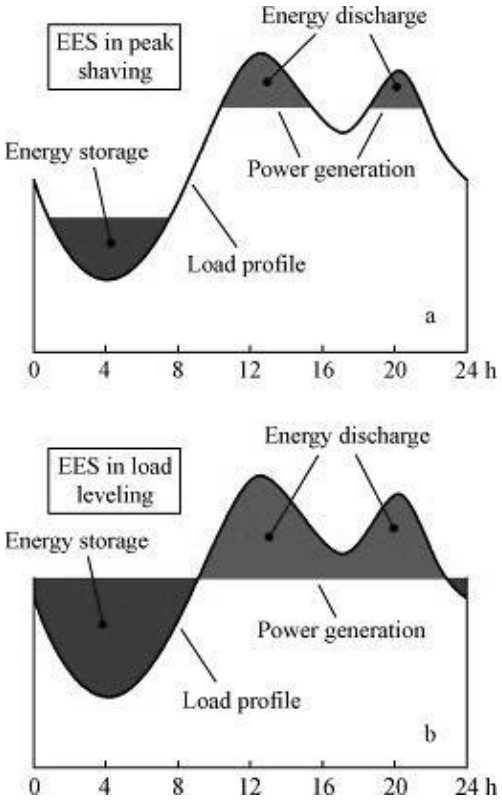

Figure 1.1: Electrical energy storage used for peak shaving and load leveling[2]

Efficiency will become even more important as worldwide electrical generating capacity continues to grow. World population is presently about six billion and is expected to reach nine billion around 2050. In addition, the global gross domestic product (closely linked with electricity generation) is expected to be two to three times larger in 2050.[3] Accordingly, the U.S. Energy Information Administration (EIA) estimates world-wide electricity generation, illustrated in Figure 1.2, will have increased 84% by 2035.[4]

Coal-fired power plants are the largest source of electricity generation, accounting for 48% of total generation in the U.S. in 2008, although use is projected to decline to 43% in 2035.[4] World-wide, however, coal is likely to be used increasingly and for a long period because of the vast reserves that are still available (a few hundred years), and the relatively even distribution of this energy source across the world, including China and India, which have both growing

populations and rising economic activity.[3] EIA estimates that world-wide coal use will grow from 139 quadrillion Btu to 209 quadrillion Btu in 2035, with little to no growth in the U.S., several European countries, Australia, Japan and South Korea, and substantial growth occurring in other countries, especially China and India.[4] These estimates are based on current policy, although a binding international policy regarding greenhouse gases is not expected in the near future.

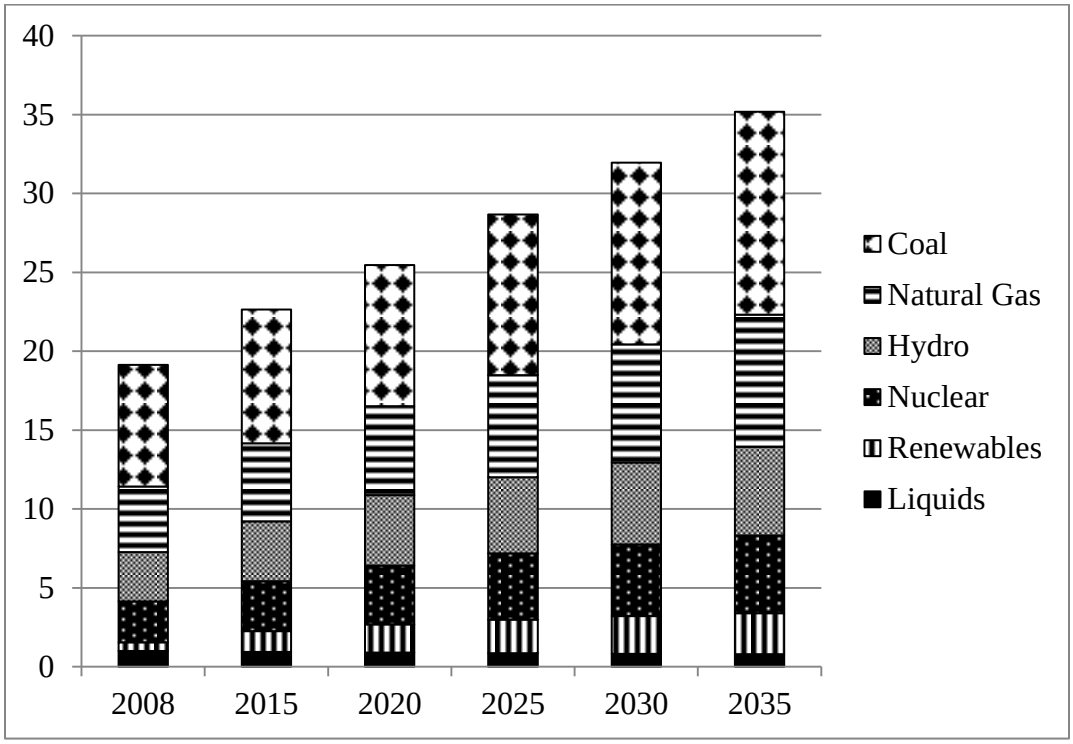

Figure 1.2: World net electricity generation in trillion kilowatt hours (created from data provided by the EIA)[4]

These energy challenges may seem overwhelming, but increasing efficiency can result in large energy and cost savings, as well as reduction in pollution from fossil fuel-fired utilities. Although developed countries use more energy than developing countries on a per capita basis, they use less energy to produce $1US of GDP (1 to 3 kWh of energy instead of 3 to 10 kWh of

energy). This is due to efficiencies in energy generation and use (such as better insulation of buildings).[3]

Carbon sequestration is being suggested as a way to curb anthropogenic climate change, but the cost is expected to be 2-3cents/kWh, which would double the cost of fossil-fuel generation (at about 3 cents/kWh).[3] Furthermore, this does not actually increase efficiency of fossil-fuel energy use, which also releases several other pollutants.

1.2: Implementation of Solar and Wind Power

While some renewable electricity sources such as geothermal and hydroelectric are reliable like fossil fuel-fired and nuclear utilities in that power can be produced when needed, wind and solar power are intermittent and unpredictable. Wind energy is the lowest cost and most widely used renewable energy source.[5] Onshore and inland wind turbines produce electricity about 20% of the time, but efforts to develop offshore wind turbines could increase that to between 30% and 40%.[3] Renewable energy is projected to be the fastest growing form of electricity generation, from 19% of total electricity generated in 2008 to 23% in 2035 (in the U.S. from 9.7% to 14.3%), although coal will remain the largest electricity source for decades.[4] The wind capacity in the U.S. in 2006 was 9200 MW and is expected to reach 30 GW by 2020.[1]

Wind energy is generally lauded as a way to generate power without fossil fuel combustion emissions, but because natural gas-fired turbines or generators are commonly used to provide back-up power when electricity is needed but not provided by wind, the emissions reductions are not equal to the amount an equivalent sized (in MW) fossil fuel-fired utility would emit. Further, as these back up turbines or generators are cycled more frequently (the power output is ramped up and down more frequently due to availability or unavailability of

wind) than a base load unit, they are less efficient than a base load unit with a constant power output. This works similarly to the efficiency of fuel use in a car when it is accelerated or decelerated frequently compared to a constant speed. Because of the reluctance of many utilities to share data, it is not clear how much (or how little) wind power decreases fossil fuel combustion emissions, but it seems that the emissions avoidance decreases as the wind capacity grows.[6] As more wind and solar power is integrated into the electrical grid, energy storage becomes increasingly important to maintain power reliability while avoiding the use of inefficient back up turbines or generators.

1.3: Electrical Energy Storage Technologies

Electrical energy storage can be stored directly as electricity (capacitors, supercapacitors, superconducting magnetic energy storage), stored mechanically in the form of kinetic energy (flywheels) or potential energy (pumped hydro storage and compressed air energy storage), or stored chemically (secondary batteries, flow batteries and fuel cells). Other efforts to improve efficiencies are thermal storage, which can be used to reduce heating and cooling costs. Energy storage is either energy related (peak shaving and load leveling) or power related (stabilizing frequency and voltage). Energy related applications require long durations (hours) and power related applications require durations of only seconds to minutes.

1.3.1: Stored Electrically

1.3.1.1: Capacitors & Supercapacitors

A simplest capacitor consists of two conductive plates separated by a nonconductive dielectric. During charge, a voltage difference is applied across the plates, forcing one plate to

become positively charged and the other to become negatively charged. When the external source is removed, the capacitor discharges and a current is produced as the electrons flow towards the positively charged plate. Since energy is stored via charge rearrangement, the response times are very fast. The amount of energy stored is increased using carbon electrodes with high surface area and/or storing charge in electrolyte solution between the plates (known as ultra or supercapacitors). Introducing a redox couple by catalyzing the electrodes or combining them with a redox electrode can further increase the capacity but slow the response time because charge arrangement has a response time of 10^{-8} s, while redox reactions typically have response times between 10^{-2} and 10^{-4} s.[7]

While capacitors have an advantage of quick response time, even ultracapacitors and supercapacitors can only reach capacities of 10-100s kW, making them unsuitable for the storage levels needed to reduce peak power or store renewable energy. Because of their characteristics of quick response time, low energy density, and long cycle life, they are most suitable to provide power during sudden interruptions or during voltage sag before another power source can be started. The largest units being developed but not demonstrated have energy densities over $20 kWh/m^3$.[2]

1.3.1.2 Superconducting Magnetic Energy Storage (SMES)

Superconducting magnetic energy storage (SMES) consists of a superconducting coil through which direct current flows, producing a magnetic energy field. To be superconducting, the coil must be kept at cryogenic temperatures, but systems operating at temperatures up to 77 K have been developed. High efficiencies are achieved because of low resistivity, and systems are typically in the multi-MW range. Like capacitors, SMES has a quick response time and is

generally used for power quality enhancement such as dampening oscillations, providing stable and balanced voltage, and as spinning reserve (continuing power until a back-up source can be started).[8] Also like capacitors, they can sustain several charge-discharge cycles. They suffer from high cost, and cannot be used for applications requiring longer than power duration of seconds to at most minutes.[2]

1.3.2 Stored Mechanically

1.3.2.1 Pumped Hydro Storage (PHS)

Pumped hydro storage (PHS) uses excess electricity to pump water from one lower reservoir to a higher reservoir, storing the electrical energy as potential energy. A schematic of PHS is illustrated in Figure 1.3 below. When electricity is needed, the water at the upper reservoir is released and flows through a turbine to generate power. The energy capacity depends on the height difference between and the volume of the reservoirs.[2,9]

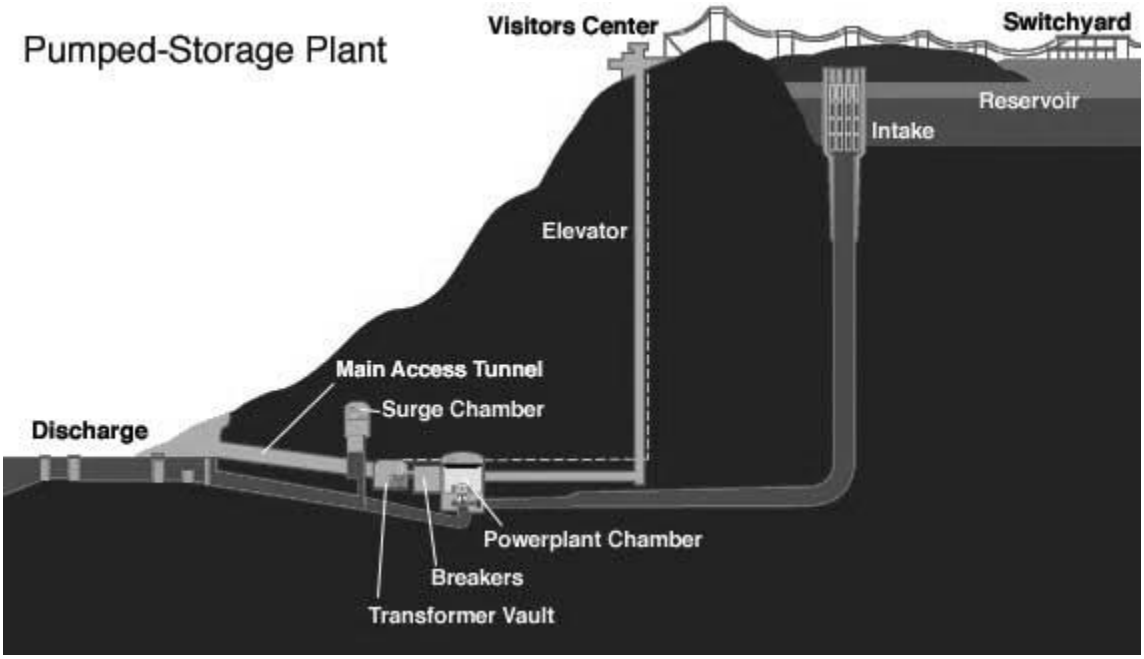

Figure 1.3: Schematic of pumped hydro storage system for energy storage[10]

PHS is the most widely used energy storage system, with about 3% of the world-wide generation being stored this way. It typically has a very large capacity, between 100 MW-3000 MW, and a round-trip efficiency of about 75%.[2] These characteristics, as well as being able to provide power for long durations, allow the system to be used for peak shaving, load following, and as reserve. The main disadvantage with PHS is the terrain requirement. Additionally, since PHS is generally located in an isolated, mountainous region, there may be more transmission losses than storage systems which can be built close to load centers.[9] Unless the PHS is located in an underground cavern, for which costs are higher, there is a local environmental impact as with any dam.[5]

1.3.2.2 Compressed Air Energy Storage (CAES)

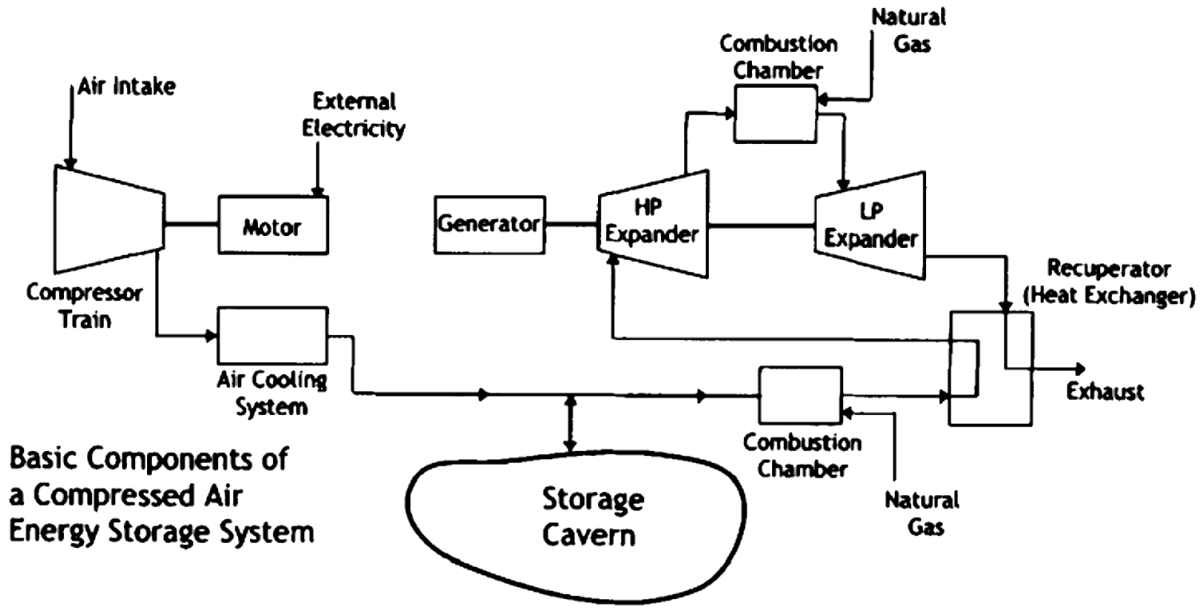

Figure 1.4: Compressed air energy storage system[9]

In compressed air energy storage (CAES), shown in Figure 1.4 above, air is compressed during charge or non-peak hours into a large cavern (underground rock cavern, salt cavern, or

porous reservoir). When this electrical energy is needed, the compressed air follows this process: heating, expansion through a high pressure turbine, mixing with fuel and combustion, then expansion through a low pressure turbine, with both turbines spinning a generator.[2,9]

Due to the combustion step, CAES does require natural gas, although renewable energy can power the compressor.[9] CAES has similar characteristics to PHS: low capital cost per unit energy, similar efficiency (~70%), high capacity (50-300 MW), a long life span, and an ability to discharge for hours. Also similar to PHS, it is limited by terrain requirements and is likely to be built far from load centers, and thus have higher transmission losses.[2,9] There are presently only two operating CAES. Huntorf, Germany has been operating a 290 MW facility (which can discharge at this power for 2 hours) since 1978, and McIntosh, Alabama Electric Cooperative has been operating a 110 MW facility since 1991 (which is much larger and can operate for 26 hours).[2]

1.3.2.3 Flywheels

Flywheels store electrical energy as inertial energy, using power to spin a wheel. To maintain the energy of the spinning wheel, it is operated in vacuum to minimize wind resistance. This rotational energy can be quickly released by the wheel, which is decelerated to generate electricity. The capacity is in the MW range, and the response time is within minutes.[1] Flywheels have low energy densities but very high efficiencies (90-95%).[2] Similar to capacitors and SMES, their characteristics make them suitable for improving and providing power stability and quality. This technology is low cost (in terms of cycle life) and developed. Beacon Power manufacturers flywheels in single MW sizes that can be connected for up to several MW and several minutes worth of discharge.[1]

1.3.3 Stored Chemically

Electrical energy can be stored chemically in electrochemical devices such as secondary batteries, flow batteries, and hybrid flow batteries. These devices use electrical energy to create chemical products via redox reactions, and these chemical species can be consumed to provide electrical output. In all these devices, reactions take place at the interface between the electrode and electrolyte, with a separator between two electrodes. The separator must be ionically conductive but not electronically conductive, or else there would be a short circuit and the electrons would not travel externally to provide useful work.

1.3.3.1 Secondary Batteries

In a secondary battery, the fuel is stored internally and at least one of the reactants is stored as the solid electrode. A schematic of a zinc-copper battery is shown in Figure 1.5 below.

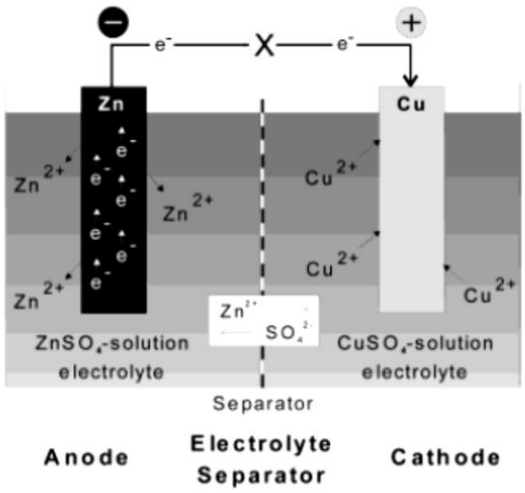

Figure 1.5: Secondary battery[7]

Since the electrodes are both the site of the energy conversion and the fuel, the electrodes are consumed and replenished during cycling. This can cause significant structural and chemical changes (such as changes in the electrode surface area or conductivity, or dendrite formation),

especially during periods of rapid charge or discharge. Also, the energy density (determined by the amount of fuel or chemicals to be consumed) and power density (determined by the size of the electrodes) are not decoupled as the electrode size determines both the energy and power density. This is a disadvantage for large scale electrical energy storage because identical components must be added to increase the energy capacity, but this adds resistances due to increasing the number of internal components, thus inhibiting a secondary battery from achieving its theoretical power density.[11]

1.3.3.1.1 Developed Secondary Batteries

Developed secondary battery technologies include the lead-acid, nickel-cadmium, nickel metal-hydride, and sodium-sulfur batteries. Although lead-acid batteries have been used for electrical energy storage in the range of 500 kW to 20MW and 500 kWh to 40 MWh, there are problems related to its electrodes which make it difficult to scale-up. Pure lead is not mechanically strong enough for large electrodes. Other elements can be added to create lead-alloy electrodes with improved strength and resistance to corrosion, but can introduce other problems such as poisoning.[12]

Nickel-cadmium batteries have higher energy density than lead-acid batteries. However, they are still not widely used for electrical energy storage because they suffer from voltage depression (in which a battery does not recharge to its full capacity after being partially discharged several times), higher costs than the lead-acid system, and the possibility of thermal runaway if the battery is charged at high rates. Environmental concerns also exist due to the heavy and toxic cadmium. The largest nickel-cadmium battery is a 40 MW unit built by Saft Batteries in Alaska for power applications. Nickel metal-hydride batteries replace cadmium with

a metal hydride, which improves the specific energy, eliminates voltage depression, and widens the operating temperature range. These systems have also been used for power applications.[12]

The sodium sulfur battery uses molten sulfur as the cathode and molten sodium as the anode, requiring high operating temperatures (300-350 ˚C) and a ceramic separator that conducts sodium ions (typically β-alumina). This system has high efficiency, but fire hazards due to the high temperatures and exothermic reaction during discharge. NGK Insulators Ltd. (a Japanese company) provides sodium sulfur batteries from 1 to 65 MW for renewable energy storage.[12]

1.3.3.1.2 Developing Secondary Batteries

Other batteries such as lithium-ion and sodium metal chloride are being developed for electrical energy storage applications, but like the developed technologies, have scale-up problems. Li-ion batteries also have safety issues and sodium metal chloride batteries have trouble obtaining high cycle lifetimes. Research on Li-ion technologies has focused on improving safety and enhancing energy capacity and cycle life. Research on sodium metal chloride batteries has focused on how the composition of the cathode transition metal affects cycle life and energy and power density.[12]

1.3.3.2 Flow Batteries

NASA began researching redox flow batteries in the mid-1970s in response to the energy crisis and the utility industry's economic problems, and as a method for storing solar and wind power.[13,14] Although iron-chromium was the initial chemistry used, L.H. Thaller's patent (as an employee of NASA) on redox flow batteries generalizes the concept to include any redox couple.[13] A diagram of a flow battery is shown in Figure 1.6.

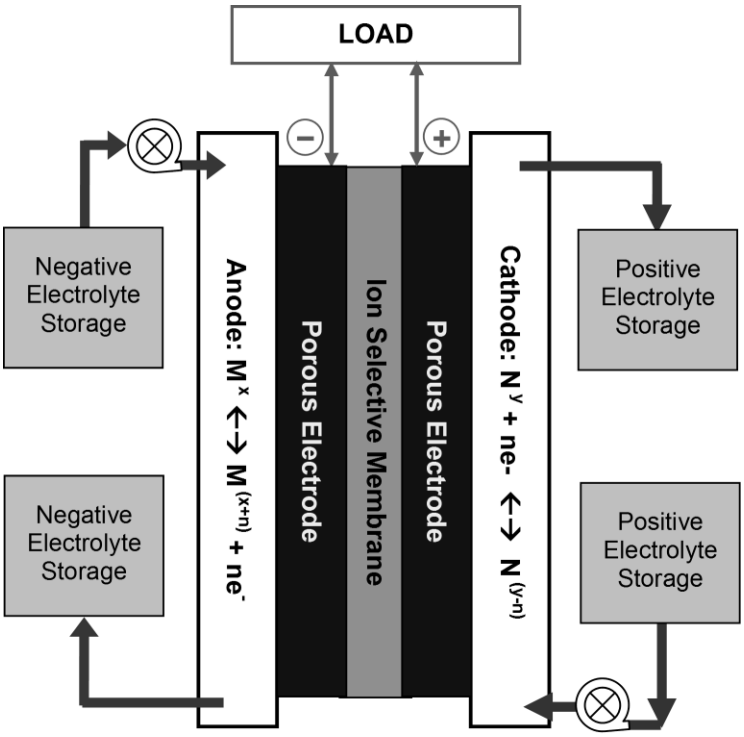

Figure 1.6: Diagram of a redox flow battery[11]

Unlike a secondary battery, the reactants are stored externally, and are pumped through the power conversion device during operation, minimizing self-discharge. During periods of high demand, the reactants in the negative electrolyte storage are pumped through the porous anode and are oxidized at a surface within the electrode, creating a positively charged species and releasing electrons. These electrons travel through an external circuit to produce electrical output and then reach the cathode where they reduce the reactants in the positive electrolyte, creating a negatively charged ion. The membrane allows only the negatively or positively charged ion to cross between the electrodes, termed an anion-exchange membrane or cation-exchange membrane, respectively. During periods of low demand, electrical input to the device forces the opposite reactions to occur at each electrode.

Since the electrodes are inert during operation and act as the reaction site only and not also as a fuel, high charge and discharge rates do not affect the electrode structure and longer

cycle life than a secondary battery should be achieved. Another advantage of a flow battery is that the energy density (determined by the reactant density and solubility) is separated from the power density (determined by the size of the electrodes). This is analogous to fuel tank size and engine size, respectively. Thus, flow batteries have scale-up and durability advantages over secondary batteries. A flow battery can be thought of as a reversible fuel cell (also called regenerative fuel cell), but many fuel cell chemistries are not reversible enough to be an efficient flow battery (such as the H_2-O_2 system which has a high kinetic overvoltage).[11] True flow batteries use soluble reactants for both electrodes. Hybrid flow batteries involve deposition and dissolution of one solid material.

1.3.3.2.1 Iron-Chromium

The iron-chromium redox couple, displayed below, was the first system investigated under NASA. [11,13]

$$Fe^{2+} \underset{charge}{\longleftarrow} \underset{discharge}{\longrightarrow} Fe^{3+} + e^- \qquad E° = 0.77\ V$$

$$Cr^{3+} + e^- \underset{charge}{\longleftarrow} \underset{discharge}{\longrightarrow} Cr^{2+} \qquad E° = 0.41\ V$$

Aqueous solutions include hydrochloric acid as the electrolyte. The electrodes are inexpensive carbon felt, but electrocatalysts are needed to improve the slow kinetics of the chromium reaction. An ion exchange membrane is used, but crossover is a problem.[15] Using electrolytes with both iron and chromium at both electrodes can overcome this crossover problem, but unwanted reactions can occur.[16]

1.3.3.2.2 All-Vanadium

The all-vanadium redox battery (VRB) avoids crossover problems that are common with other flow battery chemistries by using the same element for the redox reactions occurring at both electrodes. It was developed and patented by Maria Skyllas-Kazacos and other researchers at the University of New South Wales.[16] In the all-vanadium battery, sulfuric acid (H_2SO_4) is used as the electrolyte, and the following reactions occur.[11] VO_2^+ contains V^{5+} and VO^{2+} contains V^{4+}.

$$V^{2+} \underset{charge}{\longleftarrow} \underset{discharge}{\longrightarrow} V^{3+} + e^- \qquad E° = 0.26\ V$$

$$VO_2^+ + e^- \underset{charge}{\longleftarrow} \underset{discharge}{\longrightarrow} VO^{2+} \qquad E° = 1.0\ V$$

The main problems with developing this battery were the low solubility and poor stability of the ions in several solutions. V^{4+} and V^{5+} are unstable in common electrolytes, such as V^{5+} in HCl. The original invention recommends dissolving $VOSO_4$ in de-aerated and sealed H_2SO_4 and electrochemically reducing and oxidizing a portion to obtain the V^{2+}/V^{3+} and V^{4+}/V^{5+} solution, respectively.[16] Graphite electrodes are suitable and several membranes are used.[17]

If crossover does occur, some efficiency will be lost, but performance of the battery will not be greatly affected, and the solutions can be purified by electrochemical treatment.[16] The range of solubility is small, with the concentration in sulfuric acid being less than 2 M vanadium ions for a wide operating temperature range, and less than 3 M vanadium ions for a temperature range of 15 ˚C to 40 ˚C.[18] However, this technology is considered for a large stationary application, and so the energy density requirements are not as stringent as for mobile or vehicle applications. The all-vanadium redox battery is the most developed of all the flow batteries, but cost reduction is needed for wider implementation. The largest installation is a 4MW/6MWhr

system connected to a wind farm in Japan. Current research on the all-vanadium system has focused on reducing the cost of the membrane (the most expensive component).[19]

1.3.3.2.3 Vanadium-Polyhalide

To overcome the solubility limits of the all-vanadium system, it was proposed to use VCl_2/VCl_3 for the V^{2+}/V^{3+} half-cell, and replace the V^{4+}/V^{5+} half-cell with the $Br^-/ClBr_2^-$ couple (formed by a solution of NaBr/HCl).[18] The following reactions give an overall standard cell potential of about 1.3 V.[11]

$$VCl_2 + Cl^- \underset{charge}{\longleftarrow} \underset{discharge}{\longrightarrow} VCl_3 + e^-$$

$$ClBr_2^- + 2e^- \underset{charge}{\longleftarrow} \underset{discharge}{\longrightarrow} 2Br^- + Cl^-$$

This system enhances solubility and increases energy density from the traditional vanadium battery. Graphite electrodes and Nafion membranes are used in this flow battery.[18]

A related system is the vanadium-bromide system, in which the same solution is used in both cells (mixture of V and Br) to overcome crossover problems. Bromine-complexing agents reduce the amount of vapor bromine, but their effects on charge-discharge cycles have not yet been extensively investigated.[17, 19]

1.3.3.2.4 Bromine-Polysulfide

In the bromine polysulfide battery, the following two reactions which occur in the bromine polysulfide battery produce a standard electrochemical potential of 1.5 V.[11]

$$2S_2^{2-} \underset{charge}{\longleftarrow} \underset{discharge}{\longrightarrow} S_4^{2-} + 2e^-$$

$$Br_2 + 2e^- \underset{charge}{\longleftarrow} \underset{discharge}{\longrightarrow} 2Br^-$$

The sulfur and bromine are typically complexed with sodium, but potassium forms can also be used. This enhances the solubility of the electrolytes, which is a problem in the all-vanadium redox flow battery. Bromine can be replaced with chlorine or iodine. When chlorine or iodine is used, the standard electrochemical potential is 1.8 V or 1.0 V, respectively. The membrane is conductive to Na^+ or K^+. The electrolytes are also close to neutral, simplifying the materials needed to construct the cell and the electrodes. Noble metal catalysts are not needed, unlike the iron-chromium battery.[20] Electrodes are typically carbon or nickel foam on carbon felt.[17] The biggest problem with this system is crossover, which causes sulfur precipitation and evolution of H_2S and Br_2 gases.[15]

RWE Innogy built a 1 MW pilot plant in 1997, and began building a 12 MW/120 MWhr plant**.** The cost was more expensive than expected mostly due to tank and electrode structural problems. The project was halted in 2003 when RWE decided to sell the technology.[21] Development has ceased since the technology was sold to VRB Power Systems Inc.[17]

1.3.3.2.5 Hydrogen-Oxidant

In this type of flow battery, hydrogen gas is oxidized during discharge, and an oxidant, which can be in liquid or gas form (depending on the species and the temperature), is reduced during discharge. The oxidant is represented by X in the following reactions.

$$H_2 \underset{charge}{\longleftarrow} \underset{discharge}{\longrightarrow} 2H^+ + 2e^-$$

$$X_2 + 2e^- \underset{charge}{\longleftarrow} \underset{discharge}{\longrightarrow} 2X^-$$

The standard electrochemical potential for the reduction reaction of the oxidant gives the overall battery voltage (since the hydrogen reaction standard electrochemical potential is 0 V).

Oxidants include oxygen and the halogens (most commonly bromine, iodine, and chlorine). The oxidant being in the gas phase improves mass transfer compared to the all-liquid systems, although the energy density is reduced.[15] Oxygen reduction is known to require a large overpotential, and the exchange current density is much lower than for the reduction of bromine, chlorine or iodine.[22] The hydrogen-oxygen system is advantageous in a fuel cell for transportation applications because the oxygen can be obtained from air and only one storage system is needed (for the hydrogen). For a large-scale electrical energy storage application, high electric-to-electric efficiency is more important than volume required for the reactants.

The hydrogen-bromine, hydrogen-chlorine and hydrogen-iodine systems overcome the kinetic limitations of the hydrogen-oxygen system, but at the expense of creating a harsh environment for materials. The halogen acid (HBr, HCl, HI) is both the electrolyte and the product during discharge in a hydrogen-halogen flow battery.[23] The solubility of the halogens in aqueous solutions is low, but is enhanced by complexation, represented by the following equation.

$$X_2 + X^- \rightleftharpoons X_3^-$$

At room temperatures, the equilibrium constants are approximately 630 for iodine, 16 for bromine, and only 0.2 for chlorine. The low solubility for chlorine can be overcome using a clathrate. The alternative would be a gas-phase system, but this would be more difficult to store and pump, and would be harsher on the materials. The reversible potential is approximately 1.4 V for chlorine, 1.1 V for bromine, and 0.6 V for iodine. The bromine system has the most advantageous reversible potential, as it can avoid oxygen evolution during recharge by avoiding the electrolysis of water ($E^\circ \sim 1.2$ V), but is higher than the iodine system which would need to generate a larger current to obtain the same power output. The heat evolved during discharge is

highest for HCl, second highest for HBr, and lowest for HI over a wide range of acid concentrations. Overall, Balko determined the bromine system was most suitable (compared to iodine and chlorine) for a battery due to bromine being a liquid at ambient temperature and pressure and the ability to avoid oxygen evolution.[23]

1.3.3.3 Hybrid Flow Batteries

Hybrid flow batteries also use an externally stored electrolyte, but the reaction at one of the electrodes involves dissolving or plating of a solid material. Thus, it incurs disadvantages of a secondary battery such as not being able to completely decouple the power and energy densities and the inability to control how the solid structure is formed or dissolved.[15, 17]

The zinc-bromine system uses aqueous solutions of zinc bromide, and at one electrode, zinc metal is plated out or dissolved. Other zinc hybrid systems include zinc-cerium and zinc-chlorine, but all suffer from dendrite formation, which can cause electrical shorting. The soluble lead-acid and iron hybrid flow batteries involve solid formation and dissolution of lead and iron, respectively, and similarly to the zinc systems, their main disadvantage is maintaining uniformity of the solid materials.[15, 17]

1.3.4 Stored Thermally

Thermal energy storage uses electricity during hours when it is not in high demand to cool or heat a substance. During peak demand, this substance can be used for heating or cooling or to generate electricity using a heat pump. Electricity use for air conditioning can be reduced by using electricity during off-peak hours to generate ice, and then using this ice and a heat exchanger to cool the building during peak hours. If instead of ice, cryogen is generated during

off-peak hours, electricity can be produced during peak hours from the heated cryogen in a cryogenic heat engine. The previous two examples store energy at low temperatures. High temperature thermal storage includes molten salt, ionic liquids, concrete or ceramics. Phase change materials result in higher energy storage densities due to latent heat rather than sensible heat being stored. The overall round trip efficiency of thermal energy storage is lower than electrical energy storage technologies, between 30% and 60%.[2] For this reason, and because of the ability to provide heating and cooling instead of electricity, thermal energy storage is more suitable for residential or commercial buildings than large-scale applications.

1.3.5 Comparing Electrical Energy Storage Technologies

Electrical energy storage technologies can be summarized into two main applications, power and energy. Power applications require high power for short duration, such as frequency and voltage regulation and uninterruptible power supply. Energy applications require moderate to low power for a long duration, such as peak shaving or load leveling. Table 1.1 is obtained from the Electricity Storage Association and summarizes the feasibility of several EES technologies (thermal energy is not included) in terms of these two applications. No circle indicates it is neither feasible nor economical, an open circle indicates it is feasible but not economical or practical for another reason, a half circle indicates it is reasonable, and a filled circle indicates it is fully capable.

Table 1.1: The feasibility of several EES technologies[24]

Storage Technologies	Main Advantages (relative)	Disadvantages (Relative)	Power Application	Energy Application
Pumped Storage	High Capacity, Low Cost	Special Site Requirement		●
CAES	High Capacity, Low Cost	Special Site Requirement, Need Gas Fuel		●
Flow Batteries: PSB VRB ZnBr	High Capacity, Independent Power and Energy Ratings	Low Energy Density	◑	●
Metal-Air	Very High Energy Density	Electric Charging is Difficult		●
NaS	High Power & Energy Densities, High Efficiency	Production Cost, Safety Concerns (addressed in design)	●	●
Li-ion	High Power & Energy Densities, High Efficiency	High Production Cost, Requires Special Charging Circuit	●	○
Ni-Cd	High Power & Energy Densities, Efficiency		●	◑
Other Advanced Batteries	High Power & Energy Densities, High Efficiency	High Production Cost	●	○
Lead-Acid	Low Capital Cost	Limited Cycle Life when Deeply Discharged	●	○
Flywheels	High Power	Low Energy density	●	○
SMES, DSMES	High Power	Low Energy Density, High Production Cost	●	
E.C. Capacitors	Long Cycle Life, High Efficiency	Low Energy Density	●	◑

The high power and short duration characteristics of capacitors, flywheels and superconducting magnetic energy storage (SMES) make them suitable for power, but not energy, applications. Supercapacitors and ultracapacitors may be suitable for energy applications as well, although to date they have not reached the energy density needed for large-scale storage. Compressed air energy storage (CAES) and pumped hydro are used for energy, but not power

applications. Flow batteries and a few secondary batteries are most suitable for energy applications but are also reasonable for power applications.

Cost can be evaluated in several different ways. Figure 1.7 below compares capital cost in terms of power and energy. This does not account for operating costs, and it gives no indication of cycle life. While the metal-air battery shows the lowest cost for energy applications, they have a low cycle life. CAES and PHS have lower capital costs than the flow battery, but are again limited by terrain requirements. This data is from 2002; changes in technologies or breakthroughs in research may have further lowered the costs of flow batteries.

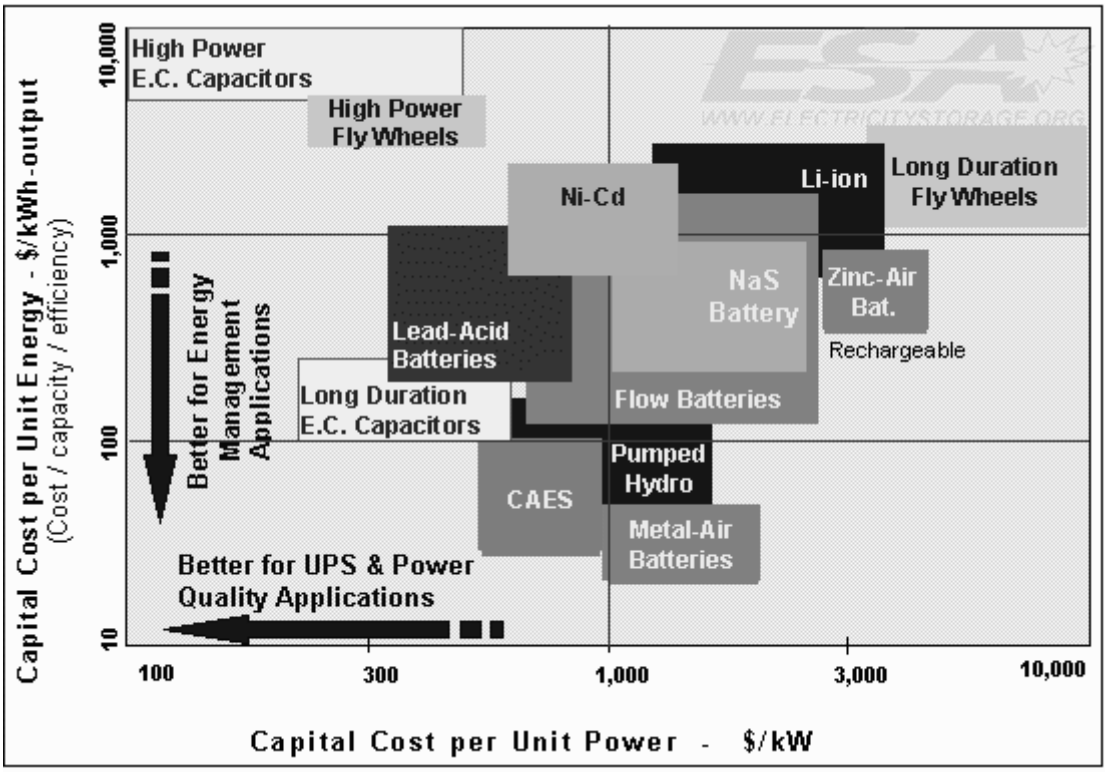

Figure 1.7: Capital cost per power and per energy of several EES technologies[25]

Chapter 2: Overview of the Hydrogen-Bromine Flow Battery

2.1: H_2-Br_2 Flow Battery Operation

Figure 2.1 summarizes how a hydrogen-bromine flow battery operates. The electrodes consist of a porous carbon substrate on which catalysts can be finely dispersed. The separator is a cation-exchange membrane, typically Nafion. The flow fields must be electronically conductive to allow electrons to pass from the electrodes to the current collectors, and are usually carbon-based because of their corrosion resistance, conductivity, durability, and low cost. The current collectors are typically metal, as they must also be electronically conductive, and serve as the link between the battery and the power load or source. The membrane must be ionically conductive to allow proton transport. The membrane cannot be electronically conductive, or else a short circuit between the two electrodes would occur, dissipating all potential energy as waste heat and possibly damaging the cell materials. The interfaces between the electrodes and the membrane serve as the link between the internal ionic pathway (within the membrane) and the external electronic pathway (through the catalysts and substrates).

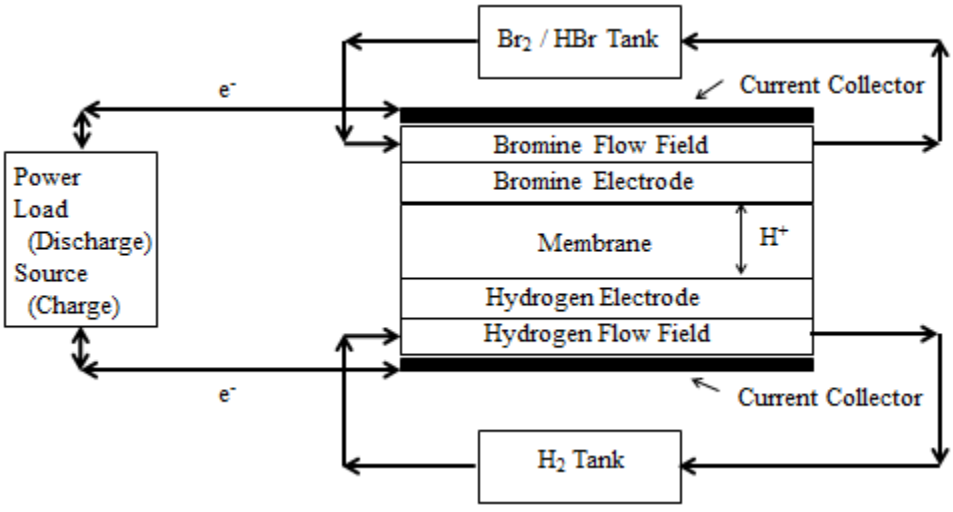

Figure 2.1: Hydrogen-bromine flow battery operation

The hydrogen (a gas) and HBr/Br_2 aqueous solution (a liquid at room temperature and pressure) are continuously pumped through each flow field during operation, and the direction the reactants are flowing does not influence the direction of the reactions. In other words, the solution and gas streams can be continuously pumped in the same direction regardless of whether the battery is charging or discharging. Whether the battery is charging or discharging is determined by the difference of the applied voltage to the open circuit potential.

The open circuit potential is the potential measured between the current collectors when no voltage is applied, as the hydrogen and HBr/Br_2 aqueous solution are being pumped through each of their respective flow fields. The standard electrochemical potential (E˚) is the open circuit potential of a redox couple at standard conditions (25 ˚C, concentration of 1 M for aqueous species, activity of 1 for pure species, and 1 atm pressure for gaseous species). The open circuit potential can be adjusted from standard concentration conditions by the following equation where R_{gas} is the universal gas constant, T is the temperature, F is the Faraday constant, p_{H_2} is the partial pressure of hydrogen, and a_{Br_2}, a_{H^+}, and a_{Br^-} are the activities of the species.

$$E = E° + \frac{R_{gas}T}{2F} ln\left[\frac{a_{Br_2}p_{H_2}}{(a_{H^+})^2(a_{Br^-})^2}\right]$$

To account for temperature changes, the following equation must be used.

$$\left(\frac{\partial E}{\partial T}\right)_P = \frac{\Delta S}{2F}$$

At periods of high demand, when electricity is needed, the voltage applied across the battery terminals is less than the open circuit potential, enabling the transfer of electrical energy out of the battery to power the electrical load. At the anode, hydrogen is oxidized at the catalyst surface within the electrode, producing hydronium ions and electrons.

$$H_2 \underset{charge}{\longleftarrow} \underset{discharge}{\longrightarrow} 2H^+ + 2e^- \qquad E° = 0 \text{ V}$$

The hydronium ions migrate to the bromine electrode through the membrane. The electrons travel from the catalyst site through the carbon support, flow field and current collector to an external circuit, providing electrical work. The electrons continue to the current collector on the bromine side, through the flow field and carbon electrode substrate to the catalyst site, where they reduce bromine to produce bromide.

$$Br_2 + 2e^- \underset{charge}{\longleftarrow} \underset{discharge}{\longrightarrow} 2Br^- \quad E° = 1.09 \text{ V}$$

The bromide ions combine with the hydronium ions transported through the membrane to produce hydrobromic acid. Overall, during discharge, the voltage applied to the battery is less than the open circuit potential, and hydrogen and bromine create hydrobromic acid and an electrical output, as shown in the reaction below, left to right. During charge, the applied voltage across the battery terminals is higher than the open circuit potential, and this electrical energy input forces the reactions shown above and below to occur from right to left, converting hydrobromic acid to hydrogen and bromine.

$$H_2 + Br_2 \underset{charge}{\longleftarrow} \underset{discharge}{\longrightarrow} 2HBr + electrical\ energy \qquad E° = 1.09 \text{ V}$$

As denoted by the diagram, this is a closed system in which only one tank for each electrode is needed. Thus, the concentrations will be continuously changing. The amount of hydrogen in the tank will be continuously depleted during discharge or replenished during charge, but no other species should exist in the tank. It is likely that there will be some crossover of water, bromine, or bromide, so a water trap can be used to remove liquid from the hydrogen stream to maintain single phase flow. The HBr/Br_2 aqueous solution will become enriched in HBr and depleted in Br_2 during discharge, and enriched in Br_2 and depleted in HBr during

charge. Only a little amount of each species is required to establish equilibrium and obtain a voltage. However, there are some solubility concerns with having too high a Br_2 to HBr ratio, as discussed in section 2.3.1. Therefore, since there will be no net consumption of any of the species (although there will be some inefficiencies) as long as the battery is discharged the same amount as it is charged, this should be a closed, contained, and isolated system. The storage tanks can be mechanically replaced if impurities are present such as the carbon within the substrates or flow field blocks being corroded into the HBr/Br_2 solution or if bromine or bromide crosses over to the hydrogen gas stream.

The change in entropy for charging is 4.4 kcal/mol HBr. Thus, the electrolyte is cooled during charge and heated during discharge.[26] Bromine is a liquid at room temperature (the boiling point is 59°C), but it does have a vapor pressure at room temperature. The hydrobromic acid not only acts as the electrolyte, but helps solubilize bromine by the following reactions.

$$Br_2 + Br^- \leftrightarrow Br_3^- \quad K_{equilibrium} = 16$$

$$2Br_2 + Br^- \leftrightarrow Br_5^- \; K_{equilibrium} = 40$$

While it has been assumed that bromine is the species reacting at the electrode, the following reaction could also be occurring.

$$Br_3^- + 2e^- \underset{charge}{\longleftarrow} \underset{discharge}{\longrightarrow} 3Br^- \quad E° = 1.06 \text{ V}$$

The cation-exchange membrane acts as a physical separator between the electrodes to prevent a short-circuit of the two electrodes, and allows hydronium ion migration to complete charge and discharge reactions while minimizing crossover of hydrogen to the bromine side and crossover of bromide ions and bromine to the hydrogen electrode. However, no membrane is 100% efficient, and bromine is known to permeate Nafion.[27] If bromine crosses over to the hydrogen electrode during operation, it will be reduced to bromide, which is known to adsorb

onto platinum and decrease the bond energy of hydrogen adsorption, poisoning the electrode.[28,29] It could also react with the hydrogen directly, resulting in self-discharge. It is expected that crossover of bromine or bromide is more likely during discharge when the hydronium ion is transported from the bromine electrode to the hydrogen electrode, carrying water (possibly with bromine and/or bromide). Hydrogen is a small molecule and will also likely crossover to the bromine electrode, lowering the open circuit potential and possibly reacting with bromine directly, but bromide or bromine crossover to the hydrogen electrode is much more detrimental to the ability to maintain cell performance due to its poisoning effect.

Other challenges with this system include the high corrosivity of bromine and hydrobromic acid. Materials which are resistant to corrosion of this system are typically expensive, such as platinum, iridium, tantalum, and Teflon.[30]

2.2: History of the H_2-Br_2 Flow Battery

The first major study on the hydrogen bromine fuel cell was conducted by Werner and Glass.[30] G.H. Schuetz extensively studied electrolysis of HBr in the late 1970s, with the motivation of producing hydrogen at a lower voltage than is required to electrolyze water.[31-33] NASA began researching redox flow batteries in the mid-1970s in response to the energy crisis, the utility industry's economic problems, and as a method for storing solar and wind power.[13-14] Although the iron-chromium battery was initially focused on, L.H. Thaller's patent (as an employee of NASA) on redox flow batteries generalizes the concept to include any redox couple.[13]

NASA began focusing on the hydrogen bromine flow battery in the mid to late 1980s.[27,34] Texas Instruments began developing a solar energy system for residential applications in the

early 1980s in which HBr is electrolyzed directly by the sun and the hydrogen and bromine are recombined in a fuel cell to provide electricity.[35-37] All the halogen acids have high conductivity, low cost, are light transmissive, and the electrolysis reactions are highly reversible with low kinetic voltage losses. HBr was chosen as the most promising because it has the highest performance with a voltage low enough for a pair of silicon cells to be able to dissociate the acid.[35] Interest in the H_2-Br_2 fuel cell and flow battery has recently been renewed, most likely due to growth in renewable energy and the aging utility fleet.[38-39]

2.3: Literature Review

In this literature review, properties of the solution, catalyst, and membrane materials for the H_2-Br_2 system will be discussed first. Materials used for flow fields, electrode substrates, and current collectors are not extensively studied, as they were not discussed in any of the hydrogen-bromine fuel cell/flow battery studies reviewed for this section. Flow fields and electrode substrates for these studies were typically carbon-based, as they are electronically conductive and durable for this system. During the preliminary studies for this thesis, a carbon-type flow field was found to not be stable in the aqueous HBr/Br_2 solution, as will be discussed later. The current collectors are typically a metal, and as it should not encounter the HBr/Br_2 solution, corrosion is not typically an issue. However, during the experimental studies for this thesis, it was found that some solution will permeate the slightly porous flow fields and corrode the stainless steel collectors. Some information is presented on metals which corrode in HBr or Br_2. The review will conclude with both experimental and simulation studies on H_2-Br_2 fuel cells and flow batteries.

2.3.1: Properties of HBr-H_2O-Br_2 Solution

Werner and Glass tested several possible solubilizers for bromine, including hydrobromic acid, hydrochloric acid and several bromine salts. Hydrobromic acid was determined to be the best solubilizer due to both solution conductivity and avoidance of precipitation formation.[30] Although this was not mentioned, it also maintains the simplicity of the system and prevents other unwanted reactions which could decrease the efficiency of the system. The specific conductance of HBr decreased with increasing HBr/H_2O ratio due to decreasing ionization, and increased with temperature. Looking at both the specific conductance of HBr and the conductivity of different composition HBr-H_2O-Br_2 systems, it was determined that bromine content decreased the conductivity of the solution without decreasing the specific conductance of HBr, thus serving as an inert diluent. It was postulated that complexation with bromide may be the reason bromine has a small effect on properties of the solution.[30]

Since HBr enhances the solubility of Br_2 in the aqueous phase by complexation, a small ratio of HBr to Br_2 can result in a second phase forming. Baldwin found that when a cell was charged to 5% HBr from 45% HBr, the bromine concentration in the aqueous phase kept increasing linearly until 86% state-of-charge, when the bromine concentration began to decrease linearly. This was due to formation of a second phase consisting of only bromine.[27]

Complexing agents have been used to further increase the solubility of bromine in solution, lowering its vapor pressure and release. Although the solution in the flow battery should be contained in a closed system, enhanced solubility of bromine would be highly beneficial in the event of a spill or leak or for maintenance activities. Polyethylene glycol (PEG) was used as a complexing agent, but performance was reduced possibly because of slower release of bromine from the PEG-complex. Problems with dispersion arose due to oil formation

and separation, but could be minimized with low bromine concentrations. Fluorad surfactants would disperse the complex when the system was mixed, but were not evaluated for fuel cell performance.[34]

2.3.2: Open Circuit Potential

The open circuit potential decreases with increasing temperature, with the largest difference being 150 mV between 295 K and 343 K at 23.8 wt% HBr. HBr concentration has a larger effect, with a 200 mV decrease from 40% to 60% by weight.[32] These trends agree with Glass and Werner's work.[30] Increasing bromine concentration increases open circuit potential by about 0.7 mV/% Br_2.[32]

2.3.3: Electrode Catalyst Materials

2.3.3.1: Both Electrodes of the Same Material

G.H. Schuetz found using graphite for both electrodes, with different treatments, resulted in low performance. Platinum electrodes resulted in the best performance (in terms of current and reproducibility), iridium second, and the other metals tested (tantalum, zirconium and their alloys) did not perform well. Molybdenum gave high current densities, but bromides were formed. Platinum performance differed with treatment methods, with platinizing both electrodes providing the best performance, probably due to the higher surface area.[31]

2.3.3.2: Hydrogen Electrode

Zirconium, niobium, tantalum, molybdenum, tungsten, iridium, and platinum catalysts were tested for the hydrogen electrode during electrolysis, and had improving performance in

that order.[32] Kosek and LaConti developed platinum alloy hydrogen electrodes.[40] Electrodes with ranging heat treatment temperatures and platinum to base metal ratios were studied using floating half-cell oxidation studies to determine polarization losses, cyclic voltammetry to measure hydrogen adsorption, and corrosion tests. The non-heated electrodes had lower polarization losses for hydrogen oxidation when bromide was present and lower changes in hydrogen adsorption, although the authors cautioned the sample size was not large enough to validate a consistent trend. The alloys with higher ratios of platinum also showed smaller changes in hydrogen adsorption after bromide was introduced. Heat-treated electrodes showed a higher resistance to corrosion (in a solution of 1M KBr/2M H_2SO_4), but fortunately this sort of environment is not likely at the hydrogen electrode. In summary, a platinum-rich non heat-treated alloy as the hydrogen electrode was recommended.[40]

Hydrogen half-cell lifetime studies using platinum black with a mixture of Teflon bonded to gas diffusion electrodes were performed in 6.9M HBr/1M Br_2. By looking at the polarization slope in the kinetically controlled region and the limiting current, it was determined the hydrogen half-cell performance decayed due to mostly flooding, but also poisoning. The authors recommend increasing Teflon content and sintering temperature (which enhances the flow of Teflon) to make the catalyst more hydrophobic, although these will give lower currents due to increased resistance.[37]

2.3.3.3: Bromine Electrode

Tantalum is the most resistant to bromine corrosion, but has high kinetic polarization losses. Platinum does corrode some in a bromine environment, but it's slow unless the bromine concentration is high. The linear relationship between current density and voltage using

platinum electrodes in HBr/Br_2 solution indicates the reaction is reversible. Electrographite was also found to resist corrosion in the HBr/Br_2 environment and gave high performance. Several different graphite types gave similar performance as platinum, with a linear current density to voltage relationship. The polarization losses were higher at the lower current densities, although the slopes ($\Delta V/\Delta I$) were similar to platinum at the higher current densities.[32] Other studies showed similar trends, with platinum performing the best, the other noble metals giving similar, but reduced performance, and graphite giving adequate, but even more reduced performance. A ruthenium-iridium catalyst gave lower performance than platinum, but better stability in terms of halide poisoning.[34]

2.3.4: Membrane

2.3.4.1: Structure of the Nafion Membrane

A Nafion membrane consists of a tetrafluoroethylene (Teflon) backbone with extended chains of sulfonate ion exchange groups, as shown in Figure 2.2 below. The backbone is hydrophobic while the exchange groups are hydrophilic. This allows the separator to be inert and resistant to degradation by halogens or acids while containing a conductive pathway for protons.

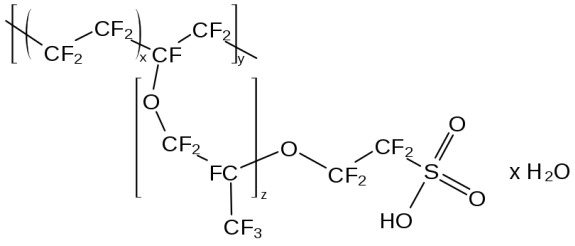

Figure 2.2: Structure of Nafion membrane[41]

Although the structure of the ionic pathway is not certain, one model is presented in Figure 2.3 below. The ion-exchange sites separate into spherical inverted micellar structures connected by short narrow channels and are the interface of the hydrophilic region within the spheres and the hydrophobic fluorocarbon backbone.[42] Hydration is essential to open up the channels within the membrane for ionic transport, although this also enhances permeation of uncharged species.

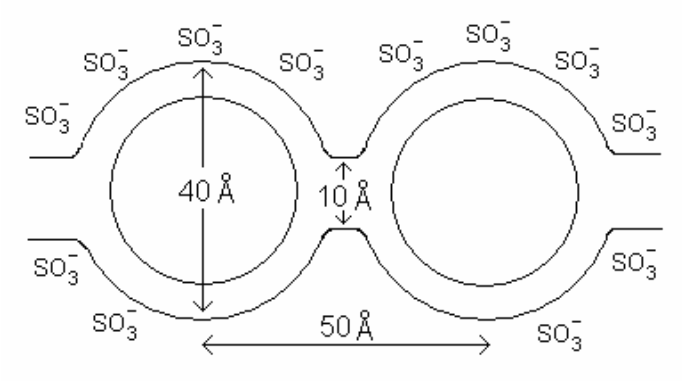

Figure 2.3: Cluster-Network model in Nafion membrane[43]

2.3.4.2: Properties of Nafion Membrane in an HBr Environment

The hydrobromic acid concentration within a Nafion membrane after attaining equilibrium increases with increasing external concentration and is slightly less than the external solution concentration (approximately 8 wt% HBr in the membrane for an external 12 wt% HBr concentration). The amount of electrolyte absorbed though, decreases with external solution concentration.[26] This is probably due to dehydration of the membrane with increasing acid concentration.[27]

Membrane conductivity between 2M and 7.5M HBr showed a maximum at 3M HBr, decreasing below and above this value. This is probably because increasing the HBr

concentration affects the conductivity in competing ways by both increasing the H^+ concentration and decreasing the water content within the membrane.[27] Increasing electrolyte concentration can also enhance ion association and increase solution viscosity within the membrane, which also hinders transport.[45] Nafion membrane conductivity also increases with increasing temperature.[27] Similar trends were observed in hydrochloric acid systems.[44]

2.3.4.3: Transport of Bromine Within Nafion

It was suggested that complexation not only enhances solubility of bromine within the aqueous solution, but could also hinder the transport of bromine across the membrane, as the cation exchange membrane should mostly reject the bromide ion.[44] Also because of complexation, it was expected that elemental bromine (Br_2) rather than tribromide (Br_3^-) crosses the membrane due to the likely low concentration of bromide ion concentration within the membrane.[45] However, as mentioned in the section before, uptake of hydrobromic acid within the membrane is substantial at equilibrium.[26] It is unknown whether the equilibrium constant changes within the membrane.

NASA did an extensive study on changes in transport of bromine in aqueous HBr/Br_2 solution with Nafion membranes.[26] No attempt was made to differentiate between Br_2 and Br_3^-, and this assumption was validated by how the simple Fick diffusion models fit the experimental data. Bromine diffusivity reached a maximum around 3M HBr, and decreased on either side of this.[27] The decrease in diffusivity at lower HBr concentrations was unexpected, as previous reports had shown bromine diffusivity in Nafion decreasing with increasing HBr concentration.[44] This is the expected behavior due to dehydration of the membrane with increasing acid concentration.

Bromine permeability increased with increasing bromine concentration and decreased with increasing HBr concentration (concentrations between 2M and 7.4M HBr) due to the decrease in hydration of the membrane. Bromine permeation increased with temperature, which can be attributed to the change in diffusivity only. The apparent activation energy for bromine permeation remained similar over the HBr concentration range (2 to 7.5 M). The reason the apparent activation energy for permeation, a combination of the apparent activation energy for diffusion and the apparent heat of solution for bromine dissolution in the membrane phase, did not significantly change over the concentration range is probably due to competing effects. Increasing HBr concentration will both dehydrate the membrane and better solubilize the bromine.[27]

F.G. Will determined bromine diffusivity through several different Nafion membranes of ranging equivalent weights and thicknesses in $ZnBr_2$ and NaBr solutions.[45] Diffusivity decreased with increasing equivalent weight (weight of Nafion per mole of sulfonic acid group), also because of decreased hydration. Increasing cation charge increased diffusivity probably because of the decrease in cation size. Diffusivity decreased with increasing electrolyte concentration, which the author attributes to increasing viscosity from ion association within the membrane.[45]

2.3.4.4: Alternate Membrane Performance

Glass and Werner tested a hydrogen-bromine fuel cell using a sulfonated polystyrene membrane with low water content (less than 33 wt%). It extended cell life by reducing bromine crossover, but suffered from higher resistance. While the hydrogen bromine fuel cell has the advantage of low polarization losses over the hydrogen oxygen system, the internal resistance is

higher.[30] In summary, a well-hydrated membrane lowers cell resistance, but increases the permeation of bromine, which will be reduced to bromide at the hydrogen electrode, a poison for the platinum catalyst.

2.3.5: Catalyst/Membrane Interface

The interaction between the catalyst and membrane is important to understand, as it is the interface between the ionic and the electronic pathway. In this system, it is the point where H^+ combines with or is split from the electrons and where Br^- produces electrons or Br_2 combines with the electrons to produce Br^-.

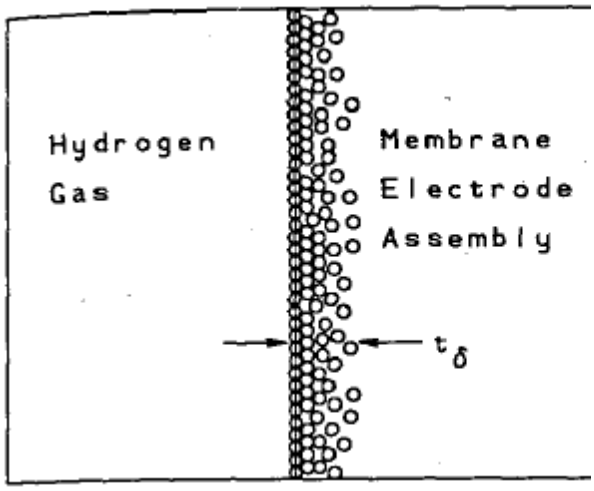

Figure 2.4: Electrode-membrane interface at hydrogen electrode[46]

Savinell and Fritts developed a model to look at the catalyst-membrane interface at the hydrogen electrode.[46] Macro-homogeneous porous electrode theory was used, in which one phase is the polymer (Nafion) and the other phase contains the platinum catalyst particles. Hot pressing the Nafion membrane to a catalyst/Nafion mixture will result in closely packed particles at the electrode-membrane interface that becomes more loosely packed further into the

membrane, as illustrated in Figure 2.4. This figure is representative of both sides of the membrane electrode assembly used in the experiments presented in this thesis. The spheres represent platinum particles.

A linear catalyst distribution was assumed. During discharge, the local current density and dissolved hydrogen concentration are largest at the interface of the MEA with the gas phase and decrease rapidly through the region of the membrane containing catalyst particles. Since hydrogen gas is the reactant during discharge, this indicates "that the reaction is limited by the diffusion of dissolved hydrogen into the dense catalyst region"[46].

During charge, the current density is minimum near (but not flush with) the gas phase interface, and increases about 50% throughout the catalyst-containing region. The hydrogen concentration increases 300% by the end of the catalyst zone from a minimum at the interface. This is because during charge, the H^+ coming from the bromine electrode and travelling through the membrane reaches an electron deep within the catalyst zone, and creates hydrogen gas. The hydrogen gas can get built up within the catalyst zone because of difficulty transporting through the dense catalyst region out of the membrane electrode assembly. The authors warn this indicates a hydrogen build-up at the edge of the catalyst zone, and may indicate a need to charge at slower rates to prevent membrane rupture.[46]

Current density was slightly higher during discharge for a uniform rather than linear platinum distribution due to the less dense packing near the interface (which can inhibit transport), although the difference was small. Optimum performance was achieved when the catalyst and polymer contents were equal; higher polymer amounts hinder kinetics and higher catalyst amounts showed diffusion limitations. Of particle sizes between 50 Å and 200 Å, 50 Å achieved the best performance because of increased surface area. Of catalyst loadings between

0.5 mg/cm^2 and 4 mg/cm^2, 1 mg/cm^2 achieved the highest current densities because of more uniform current distribution than the higher loadings.[46]

2.3.6: Overall Cell Performance

2.3.6.1: Experimental Studies

For the experimental liquid-phase studies conducted by the groups at Tel-Aviv University and Texas Instruments, only fuel cell performance was investigated (discharge only).[37,38] As mentioned before, it is expected that crossover may be enhanced during charging, due to water transport from the bromine electrode to the hydrogen electrode. Thus, while the fuel cell constructed by Texas Instruments was able to maintain a relatively long lifetime without degradation, as discussed later, lifetime was a serious problem in the experimental studies conducted for this thesis.[37] Unlike these experimental studies, both charge and discharge performance was investigated for this thesis, and it is expected that cycling between the two would result in faster performance degradation, although to date this has not been studied.

2.3.6.1.1: Fuel Cell Lifetime Study

Texas Instruments (in developing their solar energy system for residential applications) performed lifetime studies on both hydrogen half cells and hydrogen-bromine fuel cells in 6.9M HBr/1M Br_2.[37] Bromine electrodes were porous graphite. Gas-diffusion hydrogen electrodes used platinum black as the catalyst and contained Teflon, with a silicon carbide (SiC) layer for the fuel cell tests. Not all membrane types tested were given (probably for proprietary reasons, especially since the membrane is crucial in extending lifetime of the cell), but earlier papers described it as a cation exchange membrane.[35] The membrane had to provide adequate

electrolyte wetting of the SiC layer to provide ionic transport to and from the hydrogen electrode, since dry hydrogen was used.[37] Without knowing all the membrane types tested, it is unclear why this SiC layer was needed, although the one membrane type mentioned was a styrene-based sulfonic acid membrane, which may have a lower water content than Nafion.

Similarly to the hydrogen half-cell testing discussed in section 2.3.3.2 above, the anodes in fuel cell testing that were more hydrophobic provided a longer lifespan but lower limiting current. A membrane "with essentially zero electrolyte transport properties" could not obtain stable performance when the current density was higher than 450 mA/cm^2 due to drying of the anode.[37]

There was a 30% decrease in peak power and current densities scaling up from a 1 in^2 to a 10 in^2 fuel cell, but the flow rates were not scaled proportionally, and the residence time was lower for the 10 in^2 fuel cell. A net loss of platinum catalyst was observed. Since any bromine which crosses to the hydrogen electrode should be immediately reduced (the voltage at the hydrogen electrode should be less than the reversible potential of bromine), it was suggested there must have been "an inadvertent brief pulsing of the anode to a high positive potential", creating bromine, which could dissolve the platinum.[37] The authors say after optimization, a fuel cell was run greater than 10,000 hours "without significant degradation"[37]. The type of membrane and hydrophobicity of the hydrogen electrode were identified as the two most important variables for extending hydrogen-bromine fuel cell life.[37] Again, the membrane type which gives the maximum lifetime is not given, and the cell was discharged only instead of being cycled between charge and discharge. While not employed in these studies, earlier discussions of the solar energy system recommended flushing sulfuric acid between the hydrogen electrode and membrane to minimize bromine transport to the hydrogen electrode.[35]

2.3.6.1.2: Temperature, Concentration, Flow Rate and Catalyst Studies

Livshits, Ulus and Peled presented data using a 5 cm^2 fuel cell constructed of graphite blocks with serpentine flow fields, 60% Pt-Ru or Pt with XC72 on un-Teflonated Toray paper for the bromine electrode, 30% Pt with XC72 on E-TEK for the hydrogen electrode, 0-2 atm gauge un-humidified hydrogen at 2 or 10 stoichiometric flow rate, and 200 mL/min recirculation of 0.3-0.9 M Br_2 with 1 or 5 M HBr.[38] Bromine electrode loading was 1.5 mg Pt/cm^2 and hydrogen electrode loading was 1 mg Pt/cm^2. The membrane was a nanoporous proton-conducting membrane (NP-PCM) consisting of 30% poly-vinylidene-difluoride (PVDF) and 10% SiO_2 by volume (the rest of the volume being the open pores).

The membrane was developed by the research group for use in the direct methanol fuel cell and has a high water permeability to decrease cathode flooding by allowing the water to permeate back to the anode. This higher water permeability (compared to Nafion) is advantageous in terms of being able to use dry hydrogen because of the enhanced wetting of the anode, but is disadvantageous in terms of enhanced bromine and bromide crossover. To prevent this, hydrogen was not recirculated, but continuously flushed the anode. The anode was also flushed with hydrogen before introducing the HBr/Br_2 solution to the cathode.[38]

Increasing temperature and bromine concentration simultaneously lowered the open circuit voltage (bromine concentration probably has a smaller effect than temperature), but decreased mass transport limitations and increased the maximum power density. The maximum power densities were more than twice that of hydrogen/air fuel cells "operating under similar conditions" [38]. The Pt cathode catalyst gave slightly higher OCVs (although the OCVs should be the same regardless of catalyst type), and higher maximum power densities compared to the Pt-Ru cathode catalyst for temperatures 50 ˚C and below. The difference in performance was

negligible at the highest temperature (80 ˚C).[38] It is unclear why it was decided to go past the boiling point of bromine (59 ˚C), but perhaps having more HBr than Br_2 (1M HBr was the lowest while 0.9M Br_2 was the highest) helps keep the bromine in the liquid phase. It is likely that both vapor and liquid phases are present, but vapor liquid equilibrium data at this temperature range is unavailable.

Increasing the hydrogen flow from 2 to 10 stoichiometric increased the power densities at 25 ˚C and 50 ˚C. At 80 ˚C, however, increasing the stoichiometric flow of hydrogen did not change the maximum power density, probably due to drying of the membrane. Increasing the HBr concentration from 1 M to 5 M lowered the OCV and maximum cell power, which the authors attribute to platinum catalyst poisoning.[38] As mentioned in the membrane section, while increasing external acid concentration will increase the concentration of acid (containing bromide) within the membrane, increasing the HBr concentration may also hinder bromine transport by dehydrating the membrane.[26-27] An alternative explanation is that an increase in HBr concentration will hinder discharge since it is a product, according to Chatelier's principle.

2.3.6.2: Simulation Studies

2.3.6.2.1: Liquid Phase Flow Battery: Heat Effects

Yeo and Chin used heat and material balances to simulate a 2 MW battery operating for 10 hours of charge starting at 50 ˚C followed by 10 hours of discharge, with HBr concentration between 7 and 35 wt%, pressure of 10 atm, and temperature limits between 15 ˚C and 50 ˚C. The temperature decreased during charge, with more rapid decreases occurring for lower current densities. The temperature increased during discharge more rapidly than the temperature change during charge, and cooling was required to keep the temperature below 50 ˚C. This behavior is

similar to the HCl system, although the temperature change is less rapid. Overall electric-to-electric efficiency decreased with increasing current densities and increasing hydrobromic acid beginning concentration. Varying the pressure between 1 and 40 atm and the maximum temperature between 30 ˚C and 90 ˚C had little effect on overall electric-to-electric efficiency.[26]

2.3.6.2.2: Liquid Phase Fuel Cell

Savinell and Fritts developed a model for a hydrogen-bromine fuel cell, in which a planar model is used for the hydrogen electrode and macroscopic homogeneous porous electrode theory is used for the bromine electrode.[47] It is assumed that the reacting protons are obtained from the free acid phase instead of the sulfonate groups within the membrane. Changing the bromide ion mass transfer coefficient demonstrated a negligible effect on performance, indicating mass transfer of this species is not a limiting factor. Changing the exchange current density for the bromine electrode from 1 mA/cm^2 to 1000 mA/cm^2 improved the average current density from about 425 mA/cm^2 to approximately 610 mA/cm^2, suggesting the kinetics of this system are also not limiting unless a very substantial change is made. Increasing the exchange current density for the hydrogen electrode above 0.3 mA/cm^2 did not substantially improve average current density, but decreasing it to below this value decreased the average current density significantly. This indicates that poisoning of the hydrogen electrode would be extremely detrimental even though increasing the kinetic activity beyond a certain level does not dramatically improve performance.[47]

Membrane transport was the most important factor in this study, as demonstrated by the reduction in performance when resistivity was increased. Savinell and Fritts recommended that how transport occurs in the membrane should be further studied, especially considering that an

assumption was made that the protons taking part in reactions were obtained from the free acid phase, in which diffusion and migration are both occurring. When the protons are moving along the sulfonate groups (ion exchange sites), only migration is occurring. It is more likely that transport is a combination of these two processes, and the mechanism may change with changes in current density.[47]

Scale-up effects were also investigated. Increasing the axial cell length decreased the overall current. Increasing the porous electrode thickness above 1.8 mm while maintaining the same velocity only slightly improved the current density, but the conversion per pass decreased. This is because a larger volumetric flow rate is used if the velocity is maintained constant. If volumetric flow rate is held constant while the electrode thickness is increased from about 0.1 cm to 0.65 cm, current density will decrease from approximately 570 mA/cm^2 to 530 mA/cm^2 and conversion per pass will decrease from approximately 0.194 to 0.182 because of the lower velocity which inhibits mass transport.[47]

2.3.6.2.3: Gas Phase Flow Battery

Zhang and Weidner simulated a gas phase hydrogen-bromine flow battery. It was verified to experimental data for both charge and discharge at 1 atm, 80 ˚C with a Nafion 212 membrane with 2.0 mg/cm^2 Pt black on both sides, a flow rate of 1.98×10^{-2} mol/s cm^2 HBr and varying HBr to Br_2 ratio. A major assumption in the model was no crossover of bromide or bromine across the membrane.[39] Although higher current densities are achieved in the gas phase, the open circuit voltage is also lower (E°=0.58 V), so the power densities are likely to be lower for discharge (which is detrimental for the energy storage application) and charge (which is

beneficial). Better charge and discharge performance was obtained with higher and lower ratios, respectively, of hydrobromic acid to bromine.[39]

A major issue with the all gas phase system is condensation of water. Although condensation increases the membrane conductivity, it should be avoided due to this formation of a liquid barrier inhibiting mass transfer of the gas phase into the liquid phase to reach the catalyst layer. Condensation is more likely to occur on the bromine electrode due to vapor-liquid-equilibrium data presented for HBr-H_2O and H_2-H_2O systems (bromine has a negligible effect on water condensation). Only 0.052 mole fraction of water in the vapor phase is needed for condensation in the HBr-H_2O system, compared to 0.44 mole fraction of water in the vapor phase for the H_2-H_2O system. Condensation is more detrimental and more likely to occur during discharge since HBr is more soluble in water than Br_2 and water is being transported from the hydrogen electrode to the bromine electrode.[39] It should be reminded that crossover of bromine or bromide was neglected, and the possibility of bromide poisoning the hydrogen electrode was not explored in this study.

It is unclear why this group has reported gas-phase performance data for the H_2-Br_2 system at 80 ˚C, while another group has reported liquid-phase performance data (both experimental).[38-39] While a higher HBr amount would solubilize more of the Br_2, the ratios between the two studies were similar. It is possible there are two phases in the storage vessel at this temperature, but it's unclear why one would report a gas-phase open circuit potential near 0.58 V and the other reports a liquid-phase open circuit potential near 1 V, unless their pumping system was such that only gas or only liquid was pumped through.[38-39]

2.4: Advantages of the Hydrogen Bromine Flow Battery

The kinetics for hydrogen and bromine are very fast. Hydrogen oxidation and evolution require expensive catalysts (typically noble metals), but bromine reduction and evolution are fast on graphite, which is abundant and relatively cheap (depending on the form).[22] Due to the fast kinetics, as indicated in many of the studies referenced, most of the resistance in the cell is due to mass transfer limitations, especially resistance of ionic transport within the membrane.[37,47]

Since bromine is a liquid at room temperature, the molar density is much higher than for a gas oxidant, such as oxygen. Thus, high-pressure storage systems would be required for the hydrogen side only. The all gas phase hydrogen-bromine flow battery can increase current through increasing mass transfer.[39] There is not expected to be a significant advantage in terms of power density since the open circuit potential is lower, and materials problems (due to corrosivity) and safety problems (due to the gaseous bromine) will be larger than for the liquid system.

As with any flow battery, the electrodes are inert and act as the site for energy conversion only. The reactants are stored externally and are pumped through the power conversion device. This is a distinct advantage over secondary batteries, in which the electrodes are both the fuel and the energy conversion site. The electrodes in secondary batteries are consumed during discharge and replenished during charge, thus the electrodes can undergo significant physical and chemical changes. Not only do inert electrodes allow flow batteries to be more durable and have a longer cycling lifetime, but they allow the power density (determined by the electrodes) to be separated from the energy density (determined by the reactant density and storage tank size). The reactants can also be easily replaced. Inert electrodes also enable the flow battery to be discharged and charged at high rates.[11]

Although this thesis focuses on the flow battery application, using hydrogen and bromine to electrochemically produce hydrobromic acid would be much more efficient than the current thermal production route. The widely used route of producing hydrobromic acid requires both very high temperatures and energy to cool the reactor. Producing it electrochemically would not only be more efficient, but power would be generated simultaneously.[38]

2.5: Disadvantages of the Hydrogen Bromine Flow Battery

While bromine as a powerful oxidizer allows the reduction and evolution reactions to be very fast on even an inexpensive material such as graphite, this also makes it extremely corrosive to most materials. Unfortunately, materials resistant to bromine corrosion also tend to be expensive (such as Teflon, tantalum, platinum, iridium). This is also true for hydrobromic acid, which is highly corrosive. HBr and Br_2 are also toxic. Both cause burns and damage to the mucous membranes. Hydrogen is potentially explosive. For the application of energy storage, however, this system is contained in a closed, isolated system, possibly far from heavily populated areas. A hydrogen-bromine storage system should not be any more dangerous than many chemical plants, including the very similar chlor-alkali plants. It is not recommended to use this system for transportation or residential applications.

2.6: Experimental Objectives

Electrical energy storage is essential for wide implementation of intermittent renewable energy sources such as solar and wind, but can also be used to improve the efficiency of the existing utility grid by reducing or eliminating the need of inefficient peak units. Flow batteries have the energy and power densities needed for large-scale electrical energy storage and do not

have the terrain requirements of compressed air energy storage and pumped hydro storage. Fuel cells and flow batteries have an inherent advantage over secondary batteries due to the ability to decouple the power and energy density.

Earlier attempts (mostly in the late 1970s and early 1980s) by NASA and Texas Instruments to develop the hydrogen-bromine fuel cell were largely abandoned, likely due to the high cost platinum-based catalysts and Nafion membranes and the abundance of low-cost fossil fuel-fired electric generating capacity.[13,27,34-37] While the all-vanadium redox flow battery is well-developed, its energy density is lower than the hydrogen-bromine system due to the reactants' lower solubility and the cost of vanadium is higher than the cost of bromine.[16]

The objective of this work is to characterize the performance of the hydrogen-bromine flow battery (previous work has focused on discharge). This experimental information will be used to develop a working model and optimize the cell design. The experimental work presented in this thesis investigates the transport properties of a hydrogen-bromine flow battery for both charge and discharge by changing the following:

- Concentration of bromine
- Flow rate of the hydrogen and hydrobromic acid/bromine aqueous solution
- Flow field design (specifically interdigitated and serpentine)
- Hydrogen pressure
- Temperature
- Membrane length

Performance data using different catalysts on the bromine electrode is also presented. The information gathered is essential for identifying the limiting factors for optimal performance.

This project is part of a collaborative effort with three other universities. The University of California-Santa Barbara team is focusing on developing low-cost and durable electrocatalysts with high activity and selectivity for the hydrogen electrode. Vanderbilt University is working on developing low cost and durable membranes which are highly conductive to protons but minimize crossover of hydrogen, bromine, and bromide. The University of Texas-Arlington team will develop a method for integrating the battery to the electrical grid and identify any auxiliary components needed. Our team within The University of Kansas focuses on cell design and serves as the testing bed for the cell components.

Chapter 3: Experimental Studies

This chapter will begin with an overview of how the performance of a flow battery is analyzed. Section 3.2 will discuss observations from preliminary studies, and how these influenced experimental design decisions for the case studies presented in section 3.3. After the experimental studies are presented, the results will be summarized in section 3.4 as the basis for the recommendations to cell design and further testing presented in chapter 4.

3.1: Typical Fuel Cell/Flow Battery Behavior

Before discussing the performance of the hydrogen-bromine system in detail, some comments should be made about the characteristics of a voltage-current plot. A typical plot for the performance of a fuel cell (a flow battery during discharge) is Figure 3.1 below. The x-axis is the current density (current normalized by dividing it by the area of the electrode) in A/cm^2, and the y-axis is the voltage of the cell in V.

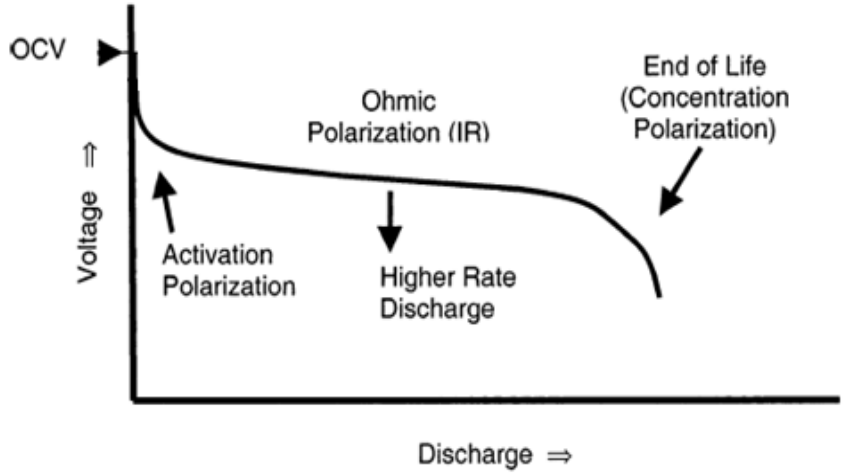

Figure 3.1: Generic voltage-current plot for a fuel cell or flow battery during discharge[7]

The open circuit potential is denoted by the arrow with label "OCV", or open circuit voltage. This is the voltage measured between the current collectors when the hydrogen gas and HBr/Br_2 aqueous solution is being pumped through the system, but there is no applied voltage and so no reactions are taking place (the current is zero or x=0). To discharge the battery and create an electrical output, the voltage applied across the battery terminals must be less than the OCV. To charge or replenish the battery, the voltage applied across the battery terminals must be greater than the OCV. (The charge curve is not shown in Figure 3.1, but is a mirror image of the discharge curve, reflected over the x-axis.) The OCV represents the maximum energy of the system, but it can never be obtained while current is flowing because of limitations that have to be overcome to produce a current. In other words, there is an energy (or voltage) penalty to produce this current. These limitations can be separated by analyzing the regions in the plot. Polarization is the voltage drop associated with its respective mechanism ($\Delta V=I*R$ where I is the current and R is the resistance).

At low currents, the nonlinear drop from the open circuit potential indicates the activation polarization, the left-most part of the curve in Figure 3.1. The steeper the drop in this region means the slower the kinetics due to low activity materials for one or both of the reactions. For fuel cells in which kinetics are slow, such as oxygen reduction in a H_2-O_2 fuel cell, there may be such a steep drop in this region that no significant current is produced until the applied voltage is around 100 mV less than the OCV.

The slope of the middle region in Figure 3.1 (when the curve is linear) equals the ohmic resistance, which contains the resistances of all internal components including the flow field blocks, current collectors, membrane and electrodes including the catalyst layer, and the contact resistances between the interfaces. The voltage drop in this region is termed the ohmic

polarization, and represents the energy penalty associated with overcoming resistances of the materials to flowing current. Thus, a cell with more ohmic resistance will have a steeper slope in this region, indicating that the voltage drop must be higher to produce a certain current, and therefore the power density (obtained by multiplying the current and the voltage) will be lower at this current. The faster the kinetics of the system, the smaller the vertical voltage drop due to activation polarization resistance and the sooner (in terms of voltage below OCV) the voltage-current curve will become linear and reach this region.

At the higher currents, at the right-most part of the curve in Figure 3.1, the slope becomes non-linear again. In this region, as the voltage is dropped, the change in current per change in voltage becomes smaller until eventually a further drop in voltage will not result in any increase in current. At this point, the transfer of reactants to the reaction site (at the surface of the electrode) cannot keep up with the reaction rate, and the system is mass-transport limited. The voltage drop in this region is the concentration polarization. For charge, the performance would be a mirror image, reflected over the x-axis, with the same activation, ohmic, and concentration polarization regions.

3.2: Preliminary Studies

3.2.1: Flow Field Block Material & Design

The dimensions of the flow fields used for the preliminary studies (sections 3.2.4-5) are presented in Figure 3.2. Interdigitated flow field design was used. The flow field blocks were made of grafoil, which consists of very thin layers of graphite compressed together. The grafoil blocks were acquired from Graphtech Materials, and the flow fields were machined into it. These flow field blocks had a short lifetime in the HBr/Br_2 environment, probably because acid

is known to expand graphite. The machined flow field channels allowed the layers under the outer surface to be exposed to the hydrobromic acid, which expanded the graphite layers causing the material to flake. The flow fields could be chipped off after several trials (approximately 2 weeks) when the cell was taken apart. Due to this observation, graphite powder blocks (in which graphite power is compressed with a binding polymer) were used for the experimental studies in sections 3.3.2-8.

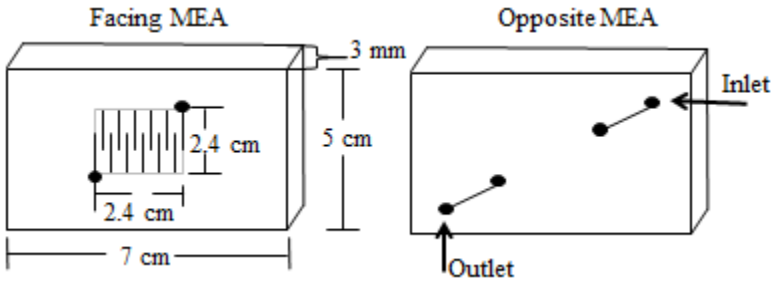

Figure 3.2: Flow field design used in preliminary studies

The thin layers of graphite in the grafoil material provide higher electronic conductivity than the graphite powder with polymer binder material. The flow fields are thin to minimize the length for electronic transport. Inlet and outlet channels were through the interface. A small grafoil sheet was used in between the flow field plate and the current collector to seal the channels at the back of the flow field plate from the current collectors. This design required gaskets to seal the space at the inlet and outlet holes between the current collectors and the flow fields. The current collectors for both the preliminary and the case studies were stainless steel.

3.2.2: Membrane Electrode Assembly

The two electrodes were bonded to either side of the membrane in a membrane electrode assembly (MEA), as represented in Figure 3.3. The soft, compressible Teflon mask seals the space between the membrane and flow field blocks. The membranes were Nafion 112. The

electrode areas were 2.5 cm x 2.5 cm (slightly larger than the flow field design), and the length and width of the MEA was the same as the flow field block (7 cm x 5 cm). The hydrogen electrode consists of 0.75 mg/cm^2 Pt/C catalyst with Teflon on SGL35BC. The bromine electrode consists of 0.75 mg/cm^2 Pt/C catalyst (without Teflon) on Toray 090 plain.

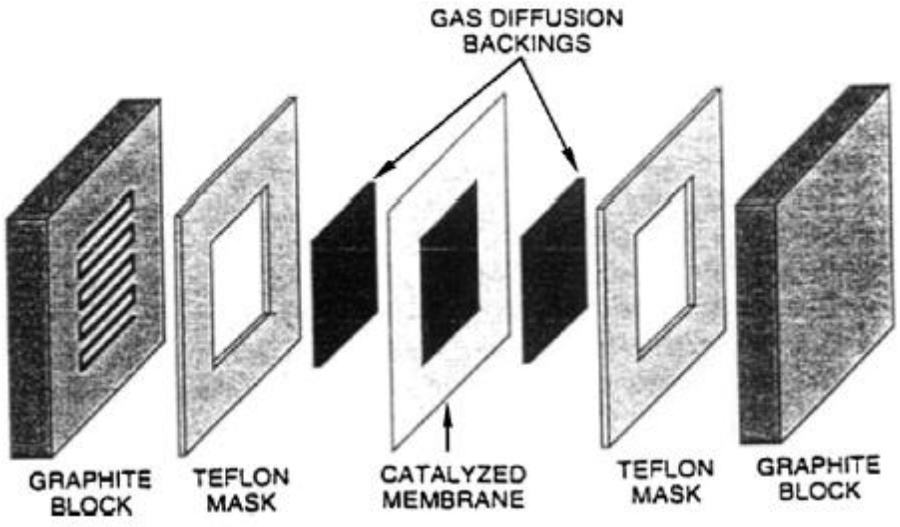

Figure 3.3: Components of an MEA[38]

The hydrogen electrode is as hydrophobic as possible so that any water that may accumulate on the hydrogen electrode (such as water transported from the bromine electrode during charge) will more easily be removed from the surface so the liquid will not inhibit gas transfer to the electrode surface. Other studies have indicated a more hydrophobic hydrogen electrode increases lifetime by reducing flooding and poisoning, at a cost of increased ohmic resistance.[37] The bromine electrode has no Teflon and the carbon substrate is easily wetted since the reactants are in the liquid phase. The MEAs were provided by TVN Systems to ensure high reproducibility.

3.2.3: Set-Up and Procedure

It was not possible to obtain a stable open circuit potential when just aqueous solution containing HBr but not $Br_2$was pumped to the bromine electrode. This is because all three species (H_2, Br_2 and HBr) are needed to establish equilibrium, as demonstrated by the Nernst equation. Thus, 2M HBr with 2M Br_2 was recirculated through the bromine electrode using a peristaltic pump. Similarly, hydrogen was recirculated through the hydrogen electrode using a pump connected to a rotameter. The set-up is the same as in Figure 3.7, except the aqueous HBr/Br_2 solution was recirculated in the preliminary studies. The details and the resulting calibration charts for both the electrolyte pump and the hydrogen rotameter are contained in Appendix A.

A potentiostat/gavalnostat by Arbin Instruments was used to collect data. The potentiostat mode was used in which the voltage was set and the given current was recorded. Data was collected over 5 minutes. Steady state had been achieved for at least 3 minutes, and the steady state values were averaged.

3.2.4: Comparison to H_2-O_2 System

The preliminary data shown in Figure 3.4 was obtained at room temperature (22 ˚C) using the MEA described in section 3.2.2, hydrogen recirculated at 2-3 psig (flowing through a water trap), and a solution of 2M HBr/2M Br_2 pumped to the bromine electrode at 1.0 A/cm^2. H_2-O_2 data with similar operating variables and the same MEA is presented as comparison. Air at ambient pressure was used and was not recirculated. The dotted straight line represents the open circuit potential of the H_2-Br_2 system. The H_2-O_2 performance may be slightly lower than usual due to the bromine electrode (acting as the O_2 electrode) not being wet-proof and because

most H_2-O_2 fuel cell performance data is obtained at higher temperatures (typically around 60 ˚C) with a humidified hydrogen stream. O_2 electrodes typically contain some Teflon because water is transported from the hydrogen electrode to the O_2 electrode, and the liquid water inhibits oxygen gas transfer to the electrode surface. H_2-O_2 fuel cells are usually operated at higher temperatures to keep the hydrogen stream and membrane hydrated. Charge data is not shown for the H_2-O_2 system, as these fuel cells are most suitable for transportation applications, and not for energy storage, for reasons discussed below.

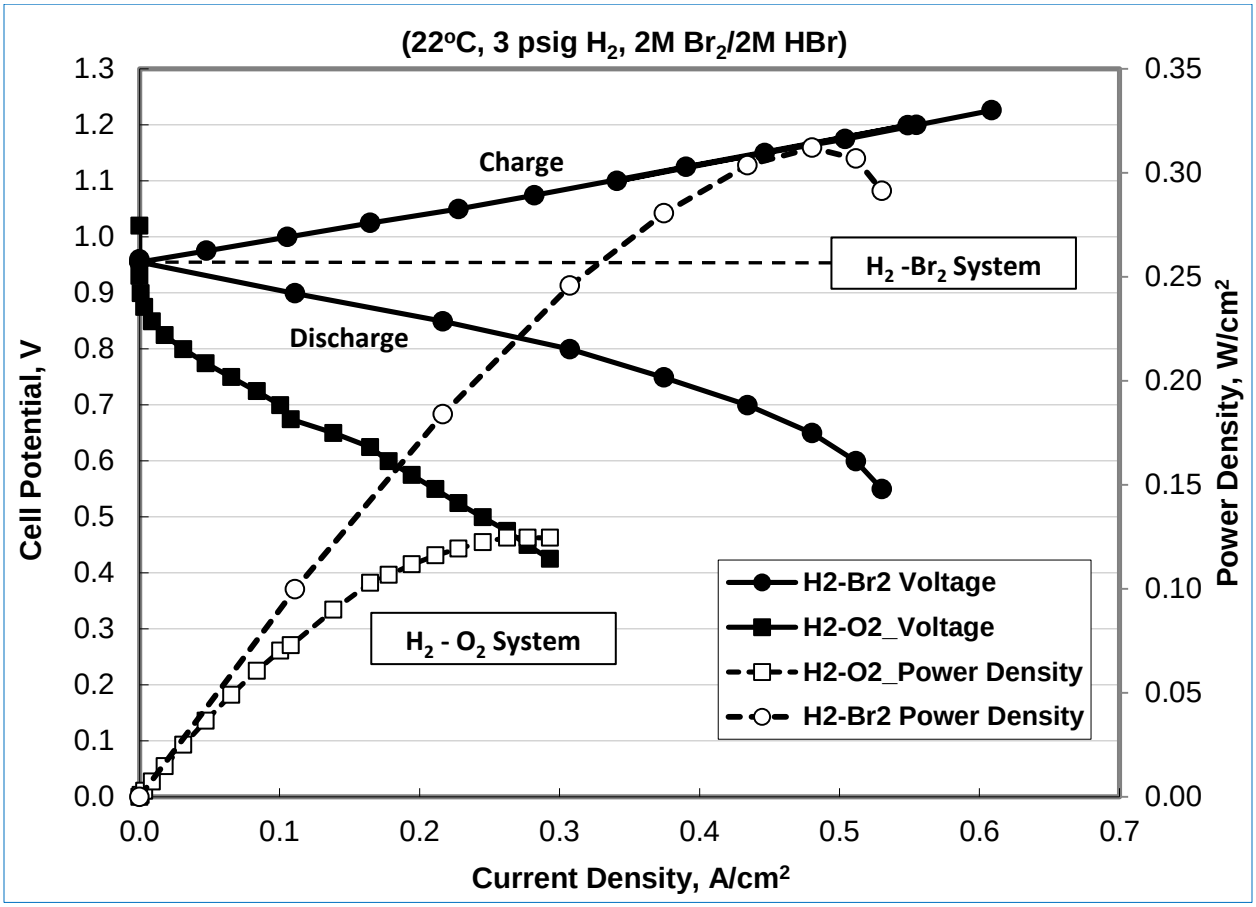

Figure 3.4: Comparison of H_2-Air fuel cell performance to H_2-Br_2 flow battery performance

The first discrepancy between the H_2-O_2 system and the H_2-Br_2 system can be seen in the kinetic region, where the current is close to 0 A/cm^2. The H_2-O_2 discharge curve (H2-

O2_Voltage) has an abrupt vertical drop from about 0.95 V to 0.825 V. Thus, there must be a voltage drop of about 0.125 V to produce even a small amount of current due to the large kinetic polarization of the oxygen reduction reaction. In contrast, the H_2-Br_2 discharge curve (H2-Br2 Voltage) has no nonlinear vertical drop. It is immediately linear, and the curve has already reached the ohmic polarization region (the linear region), indicating very fast kinetics. The comparison of the kinetics is between the reduction of bromine and the reduction of oxygen, as the same reaction is occurring at the anode (the oxidation of hydrogen) in both systems. There is also an absence of a large vertical rise for the charge reaction in the H_2-Br_2 system, indicating the reverse reaction (evolution of bromine) is also very fast, and the reactions are highly reversible.

The linear regions of the discharge curves for the H_2-Br_2 and H_2-O_2 systems are the ohmic polarization regions. The slope of the H_2-O_2 system is steeper than the H_2-Br_2 system, indicating a higher ohmic resistance. This is likely due to better hydration in the H_2-Br_2 system since the bromine electrode is constantly wetted by the aqueous electrolyte (as long as the hydrobromic acid concentration is not high enough to dehydrate the membrane).

The H_2-Br_2 system begins to become nonlinear at around 0.65 V, indicating mass transport limitations, in which the transport of the reactants from the bulk to the surface cannot keep up with the reaction rate. It is not clear whether transport limitations occur during charge in the H_2-Br_2 system at the same voltage change above open circuit potential (which would be around 1.25 V) because the charge data is limited to around 1.225 V. However, it is evident the ohmic resistance (indicated by the slope of the linear region) is smaller for charge than discharge. This may be due to the better hydration of the membrane because during discharge, the hydronium ion (carrying water) travels from the hydrogen electrode to the bromine electrode, and this may dehydrate the side of the membrane closest to the hydrogen electrode. During

charge, the hydronium ion is transported from the bromine electrode to the hydrogen electrode, carrying water with it which hydrates the membrane-hydrogen electrode interface. Carrying water from the bromine electrode will not dehydrate the membrane-bromine interface because this interface is in contact with an aqueous electrolyte.

The open squares and circles display the power densities for the H_2-O_2 and H_2-Br_2 systems, respectively, with the corresponding y-axis on the right side. The power density is obtained by multiplying the current density and the power density. Due to the absence of a large kinetic polarization and the lower ohmic resistance, the maximum power density is 0.3 W/cm^2 for the H_2-Br_2 fuel cell, which is much higher than 0.125 W/cm^2 for the H_2-O_2 fuel cell.

3.2.5: Looping Phenomena

A highly unusual and unexpected feature noticed during the preliminary studies was what will be termed "looping", and is shown in Figure 3.5. As the voltage drop is increased beyond the linear region (as the mass transport region is reached), the current should either increase slightly or stay the same. Normally in the mass transport limited region, a larger voltage drop from the open circuit potential does not increase the current because the transport of reactants to the electrode surface is not fast enough to keep up with the reaction rate. In this looping behavior, displayed in Figure 3.5, the current becomes smaller as the voltage drop is increased. Thus, a larger energy penalty (the voltage drop) results in a smaller output (the current), which should not be possible.

While this behavior was only present during discharge, this could be because charge was limited to 1.2 V. The voltage difference from open circuit to the end of discharge (0.4 V for this data) is larger than from open circuit to 1.2 V. It was thought the looping could be due to the

system being at unsteady-state, but behavior like this was observed even when staying at each voltage for ten minutes, and the currents recorded had reached a stable value. Also, for many of these cases, the behavior was reversible. The same currents were given when going from high voltage to low voltage as going from low voltage back to high voltage. It was also not due to dehydration, which was ruled out by increasing the hydrogen flow rate (the hydrogen flowed through water before reaching the cell). There were some cases in which increasing the hydrogen flow rate did slightly improve the performance, but it was not enough to eradicate the looping. The loop began at varying voltages (0.5 V to 0.775 V) and for a large range of HBr/Br_2 flow rates (1.1 mL/min to 11.2 mL/min).

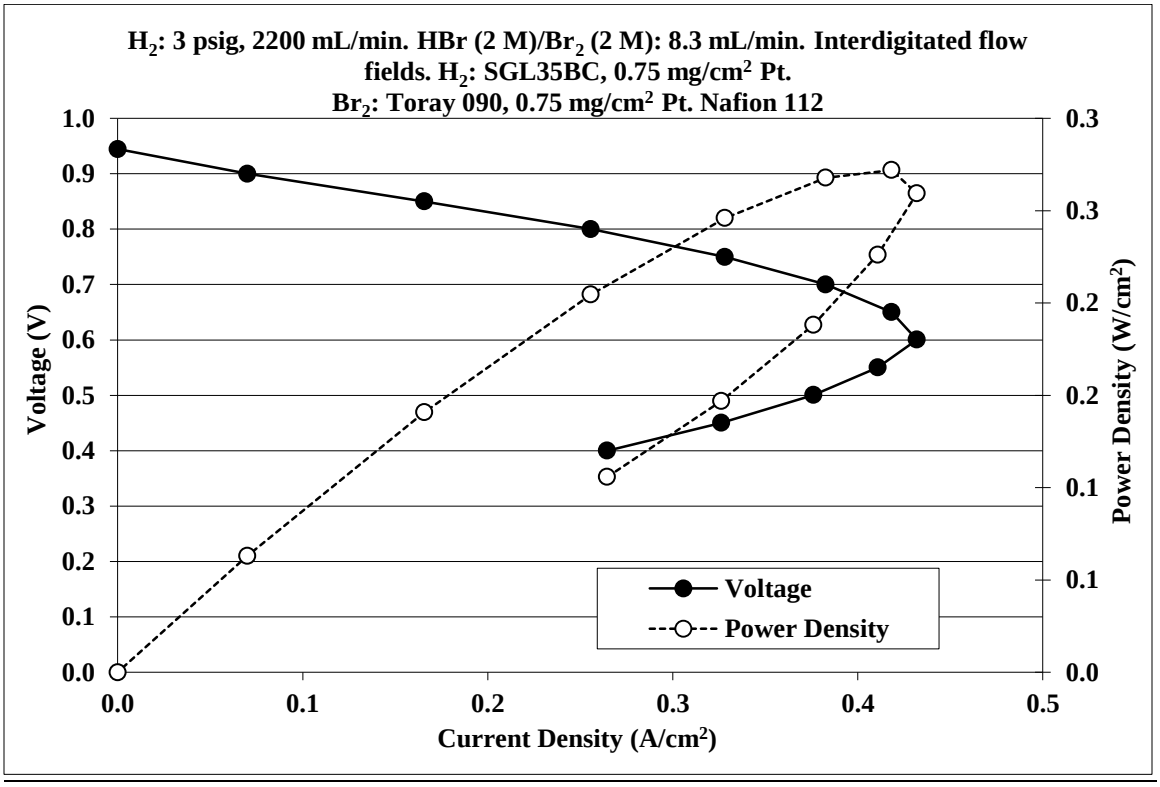

Figure 3.5: Example of looping behavior observed during preliminary studies

All the cells which resulted in looping contained MEAs that had been used in a H_2-Br_2 system, with one exception for an MEA that had been used in a H_2-Air run but not a H_2-Br_2 run.

A cell which did not exhibit looping would be cleaned and left overnight, and looping would occur during the trial on the next day. In other words, the looping never occurred suddenly during an experiment. As mentioned in section 2.1, the Nafion membrane is not completely resistant to bromine and bromide crossover, and bromide is known to poison the hydrogen electrode.[27-29] The cells were cleaned by flushing it with deionized water, but bromine or bromide may still be absorbed in the membrane or in the flow fields, and could be released overnight. Furthermore, cleaning with deionized water would better hydrate and swell the membrane, which increases permeability of all species, including bromide.

While bromide poisoning of the hydrogen electrode may be playing a role, it would be expected that the overall performance would decrease, rather than giving a lower current for a bigger voltage drop. The poisoning should be reversible, as bromine only slowly corrodes platinum, and any bromine which does crossover would be immediately reduced to bromide.[32] Thus, the catalyst surface could be cleaned by oxidizing the bromide to bromine and flushing the bromine from the hydrogen electrode.

It may also be possible that complexation is playing a role. If the bromine that is complexed within the tribromide is not released instantaneously, it could be more difficult for the reactant bromine's transport to the catalyst surface to keep up during discharge at higher currents. However, if complexation was the reason, it is not certain why looping was displayed only after the MEA had been previously used in a HBr/Br_2 environment. Also, as mentioned before, it is possible the tribromide (Br_3^-) is reacting instead of or simultaneously with bromine. Similar to the effect of poisoning, it is expected that a possible complexation effect would only show a drop of performance in the transport limited region rather than a loop back to even smaller current densities. A model which takes into account the complexation reactions could

be used to investigate these ideas by lowering the exchange current density on the hydrogen electrode (simulating bromide poisoning) and changing whether tribromide or bromine is reacting to see if looping behavior can be obtained. For the case studies presented in sections 3.3.2-8, the MEAs had to be replaced frequently to avoid looping.

3.3: Case Studies

Information learned during the preliminary studies influenced the flow fields and set-up of the experiments, as presented in section 3.3.1. Most of the case studies revealed transport information, such as temperature, electrolyte and hydrogen flow rates, and flow field design. A few studies using different catalysts and carbon substrates for the bromine electrode are also presented. The studies are divided into sections 3.3.2-8 by the operating variables that were changed (e.g. flow rate, concentration, membrane thickness, electrode, flow field design).

3.3.1: Experimental Design

3.3.1.1: Flow Field Block Material & Design

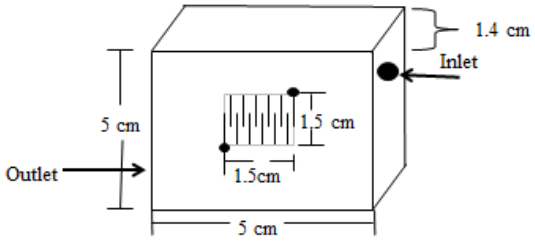

Figure 3.6: Flow field dimensions used for the case studies in sections 3.3.2-8

The flow field size used for the case studies is shown in Figure 3.6 above. The flow fields were made of graphite powder compressed with a polymer binder and treated with

polymer sealant. This was due to the incompatibility of the grafoil materials (layers of graphite pressed together) in the HBr/Br_2 environment, although the resistance was increased.

The inlet and outlet holes which connected the cell to the reactant storage were relocated to the side of the blocks rather than through the face. This eliminated the need for a gasket and the possibility of leaking in between the back of the flow field blocks and the current collectors, at the expense of increasing the thickness, and electrical resistance, of the blocks. The current collectors were made of stainless steel, and corrosion would occur upon prolonged contact with the acid, which roughens the contact surface with the carbon block, increasing the electrical resistance. The HBr/Br_2 aqueous solution could permeate the carbon block, which is why they were treated with polymer sealant. Using the compressed carbon powder with polymer sealant for the blocks and increasing the thickness increases the electrical resistance, but this design had a much higher lifetime than the previous design used in the preliminary studies. The area used to normalize the current to current density was the flow field size, 2.25 cm^2.

3.3.1.2: Membrane Electrode Assembly

The flow field size was decreased, and correspondingly the electrode areas were decreased to 1.7 cm x 1.7 cm (slightly larger than the flow field size). The catalyst loading for each electrode was lowered to 0.5 mg/cm^2. The same materials were used for the electrodes: SGL 35BC and Pt/C catalyst with Teflon for the hydrogen electrode and Toray 090 plain and Pt/C catalyst without Teflon for the bromine electrode. Nafion 112 was still used for the membrane. The MEAs were provided by TVN Systems, Inc. to obtain the highest possible reproducibility, as electrodes made in the lab would have catalyst that is hand-painted on instead of dispersed by a machine. This was especially important for these studies as many MEAs were

used in comparative studies because of the looping problem observed with MEAs that had been exposed to the HBr/Br_2 solution for an extended period of time.

3.3.1.3: Flow Battery Set-Up

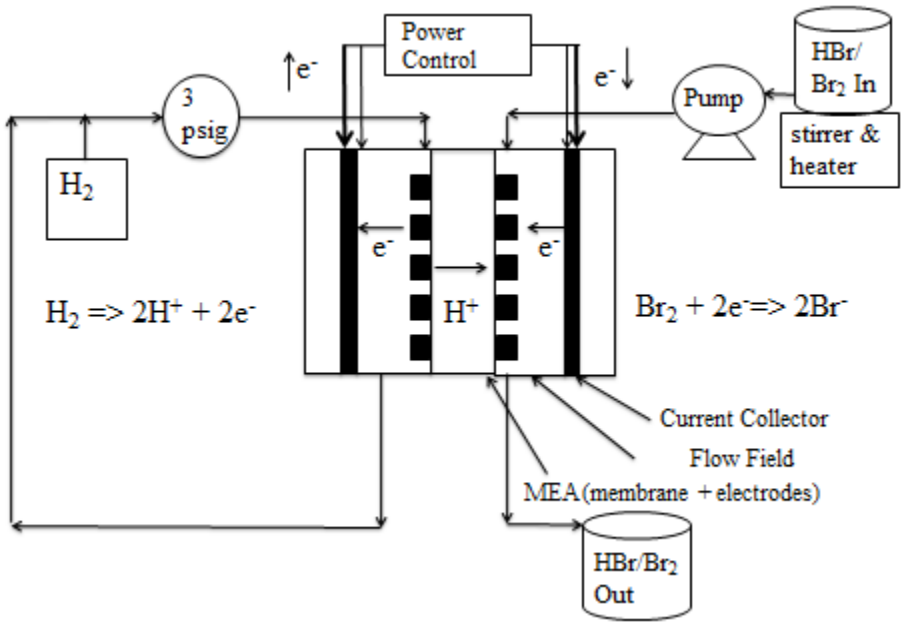

Figure 3.7: Experimental set-up to obtain hydrogen-bromine flow battery data

Figure 3.7 summarizes the experimental set-up. To begin operation, the hydrogen gas stream is recirculated through the hydrogen flow field. This, along with the use of the interdigitated flow field, allows any liquid water that is entrapped in the hydrogen electrode to be flushed from the gas stream during operation. The $HBr/Br_2/H_2O$ solution is introduced to the bromine side of the cell. For many flow batteries, there is one electrolyte storage tank which is recirculated, but for the experiments presented hereon, the HBr/Br_2 tank was not recirculated. While the currents should be small enough to not change the concentration significantly, not recirculating the electrolyte eradicates any possibility of the feed concentration changing. This

being the reason for any looping behavior could then be ruled out. Also, the open circuit potential will not be changing during each experiment (discussed in section 2.1).

An open circuit potential is established once the reactants have been introduced into the cell, and for these experiments, was around 1 V. To discharge the battery (such as during times of peak demand), a voltage is applied across the terminals that's less than the open circuit potential. At the hydrogen electrode, hydrogen is dissociated into hydronium ions and electrons. The hydronium ions migrate across the membrane towards the bromine electrode, while the electrons travel through the hydrogen flow field to the current collector, then through an external circuit to produce electrical output before reaching the current collector on the bromine side and the bromine electrode. At the surface of the bromine electrode, the electrons reduce bromine to bromide. The bromide combines with the hydronium ion that has traveled across the membrane to produce hydrobromic acid, which stays within the $HBr/Br_2/H_2O$ solution. Thus, the HBr/Br_2 outlet tank should be slightly enriched in HBr and depleted in Br_2 compared to the HBr/Br_2 inlet tank, and there will be slightly less hydrogen being recirculated. The direction the electrons and hydrogen protons travel as shown in Figure 3.7 is for discharge, and is reversed during charge.

To operate the battery in charge mode (such as during periods of low electricity demand), a voltage that's above the open circuit potential is applied across the battery terminals. This means electrical energy input to the system forces two bromide ions, dissociated in the aqueous solution from hydrobromic acid, to be combined, creating bromine and releasing electrons. The hydronium ions transport across the membrane while the electrons travel from the bromine flow field to the current collector, then through an external circuit to the hydrogen side current collector and flow field. The hydronium ions and electrons combine at the hydrogen electrode, creating hydrogen. Thus, after charge, the HBr/Br_2 outlet tank is slightly enriched in Br_2 and

depleted in HBr compared to the HBr/Br_2 inlet tank, and there will be more hydrogen being recirculated (if the temperature and volume is constant, the pressure will increase). Again, most flow battery operations consist of a single electrolyte storage tank that is recirculated, and thus the concentration would be changing during operation, with the tank being enriched in HBr and depleted of Br_2 during discharge, and enriched in Br_2 and depleted of HBr during charge.

A stir bar and magnetic stirrer were used for the electrolyte feed tank. A heater could also be used for the experiments at higher than room temperature. The electrolyte pump was re-calibrated before the case studies, and the details and data for this are included in Appendix A. A potentiostat/gavalnostat by Arbin Instruments was used to collect data, in which the voltage was set and the given current was recorded.

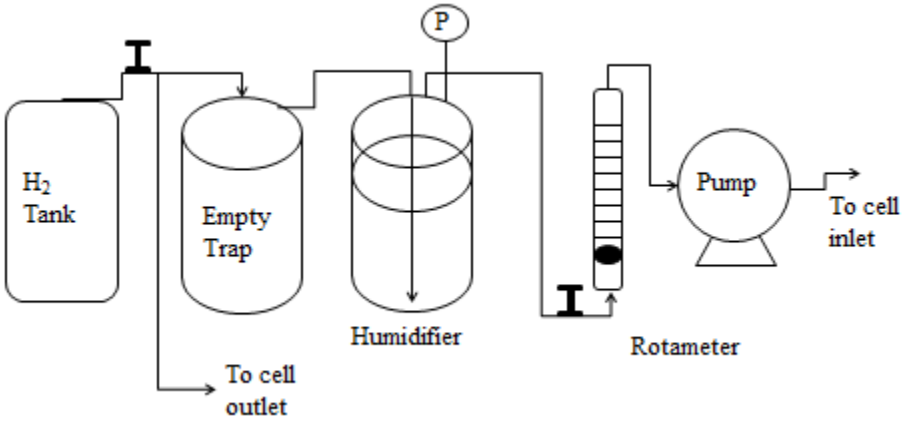

Figure 3.8: Hydrogen path connected to the flow battery

The hydrogen feed was recirculated, as detailed in Figure 3.8. The line from the hydrogen tank splits into two lines, one to the cell outlet and one to an empty cylinder. The hydrogen gas passes through the empty cylinder to a water trap with the inlet line being submerged below the liquid level, close to the bottom of the tank. The traps protect the pump and rotameter in case of HBr/Br_2 crossover. The humidifier hydrates the hydrogen to maintain hydration of the membrane. At room temperature, the vapor pressure of water is low, but the

recirculation of hydrogen should ensure the gas is saturated. It is not as important to hydrate the hydrogen feed as it is for the H_2-Air system since aqueous HBr is flowing to the bromine electrode. After the humidifier, the hydrogen gas passes through the rotameter, to the pump, and then to the cell inlet. A needle valve connected to the rotameter is used to adjust the flow rate. The rotameter calibration is included in Appendix A. A pressure gauge connected to the first cylinder (the empty trap) was used for the reported pressures.

3.3.1.4: Experimental Procedure

The flow field blocks and current collectors were first polished with regular printing paper and 1500 grade sandpaper, respectively, and cleaned with isopropyl alcohol before assembling a new cell to ensure good electrical contact. Each cell was assembled with stainless steel end-blocks and compressed to 1900 psi. The compression must be such that the Teflon gasket within the MEA completely seals the electrodes from the outside environment, but not enough to cause the flow fields to crush the electrodes. No compression of the electrodes was noticed after the cells were taken apart.

After assembling a new cell and prior to it being used for the hydrogen-bromine system, the cell was run with hydrogen recirculating to both sides. This was to clean and activate the electrodes. Since carbon is not active for hydrogen oxidation and reduction, this step was not included for the electrodes which did not contain platinum on the bromine electrode (presented in section 3.3.8). The hydrogen was recirculated at 2200 mL/min and 3 psig. The voltage would be changed by 25 mV increments from open circuit (0 V) to -150 mV, back up to open circuit by 50 mV increments, up to 150 mV by 25 mV increments, and back down to open circuit by 50 mV increments.

Before each experiment, the electrical resistance was measured by a DC ohmmeter, and if the resistance was over 0.4 kohm, there was no short-circuit and the experiment would proceed. A short-circuit occurs when there is an internal electronic pathway between the electrodes. (There should only be the external electronic pathway, through the power source or load.) If a short-circuit is present during cell operation, all useful work would be converted to waste heat and the cell would be damaged. Hydrogen was always introduced to the cell before the HBr/Br_2 solution to prevent crossover, and to check for leaks by closing the connection to the tank and making sure there is no or very low pressure loss over a period of about 5 minutes.

The current-voltage plots were obtained in the following way : 25 mV increment voltage drops from open circuit (close to 1 V) down to 0.6 V, 50 mV increments up to open circuit, 25 mV increments from open circuit to 1.2 V, and 50 mV increments back down to open circuit. Some experiments had larger voltage changes to avoid running out of solution and having to recharge to the initial concentration before the end of the experiment or set of experiments. Making two scans for both charge and discharge checked for reversibility and whether steady state had truly been achieved. At each voltage, a steady state current had been obtained for 2-3 minutes, and the data reported is averaged over this time period.

Charge was limited to 1.2 V to avoid water electrolysis. Discharge was limited to 0.6 V because this was past the voltage where peak power occurred, and it is usually not recommended to operate past this voltage because the efficiency will be less for smaller power densities. Since the total voltage change during discharge (1.0 V to 0.6 V) was larger than for charge (1.0 V to 1.2 V), at the end of each cycle, the solution had been discharged more than charged. Thus, the hydrobromic acid concentration would be slightly larger and the bromine concentration would be slightly smaller than the initial concentrations at the end of each cycle. The discharge and charge

capacities were recorded by Arbin in terms of Ahr, which can be converted to moles reacted. After each cycle or before the feed solution ran out, the battery was recharged until the capacities were equal to keep the concentration of the feed constant.

The data for the case studies will be presented graphically in sections 3.3.2-8, but tables are provided in Appendix C.

3.3.2: Effect of Bromine Concentration

In Figure 3.9 on the next page, the only difference in the operating variables between the three curves was the bromine concentration. The three bromine concentrations are 2 M Br_2, 1 M Br_2 and 0.7 M Br_2. Since the hydrobromic acid concentration is kept constant, as the bromine concentration is increased, the ratio of Br_2 to HBr increases. This would be expected to enhance discharge (for which Br_2 is a reactant) and hinder charge (for which HBr is a reactant), and this was verified experimentally.

There is very little difference between 1 M Br_2 and 0.7 M Br_2 because the concentrations are so similar, with slightly lesser performance during charge for the 1 M Br_2 at the higher current densities. The 2M Br_2/2M HBr solution has enhanced discharge performance and hindered charge performance compared to the 1M Br_2/2M HBr solution. Increased concentration of the reactants will increase the kinetics (if the concentration at the surface of the electrode is increased). Thus, an increase in bromine concentration will increase the reaction rate for discharge, and a decrease in hydrobromic acid concentration will decrease the reaction rate for charge. However, there does not seem to be a change in the kinetic regions of the current-voltage curves (near 0 A/cm^2). Le Chatelier's principle could be playing a role, in which having more of the product hinders its formation, and having more of the reactant drives the reaction in

the forward direction. Increasing the Br_2 concentration will increase the mass transport to the electrode surface, as evidenced by the 2M Br_2 curve reaching mass transport limitations at a lower voltage than the 1 M Br_2 curve. Increasing the bromine concentration also increases the open circuit potential, which was expected by the Nernst equation and from previous studies discussed in section 2.3.2.

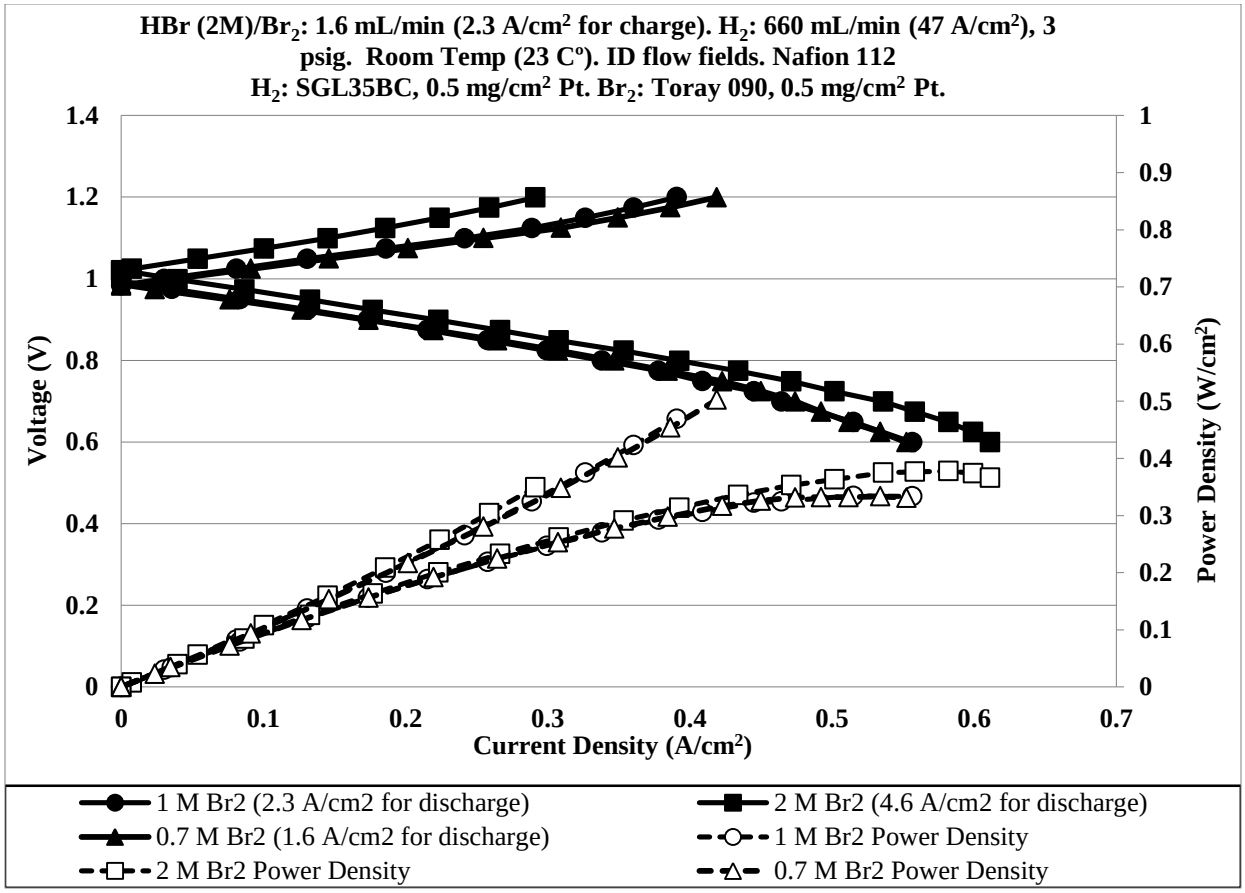

Figure 3.9: Effect of bromine concentration on H_2-Br_2 flow battery performance

Figure 3.10 verifies that the difference in performance is attributable to more than just the shift in open circuit potential. The 1 M Br_2 and 0.7 M Br_2 data is graphed on the left vertical axis, and the 2 M Br_2 voltage is graphed on the right vertical axis, which is shifted so that the open circuit potentials are at the same vertical level. Even accounting for the difference in open

circuit, increasing bromine concentration enhances discharge and hinders charge, although the effect is not substantial.

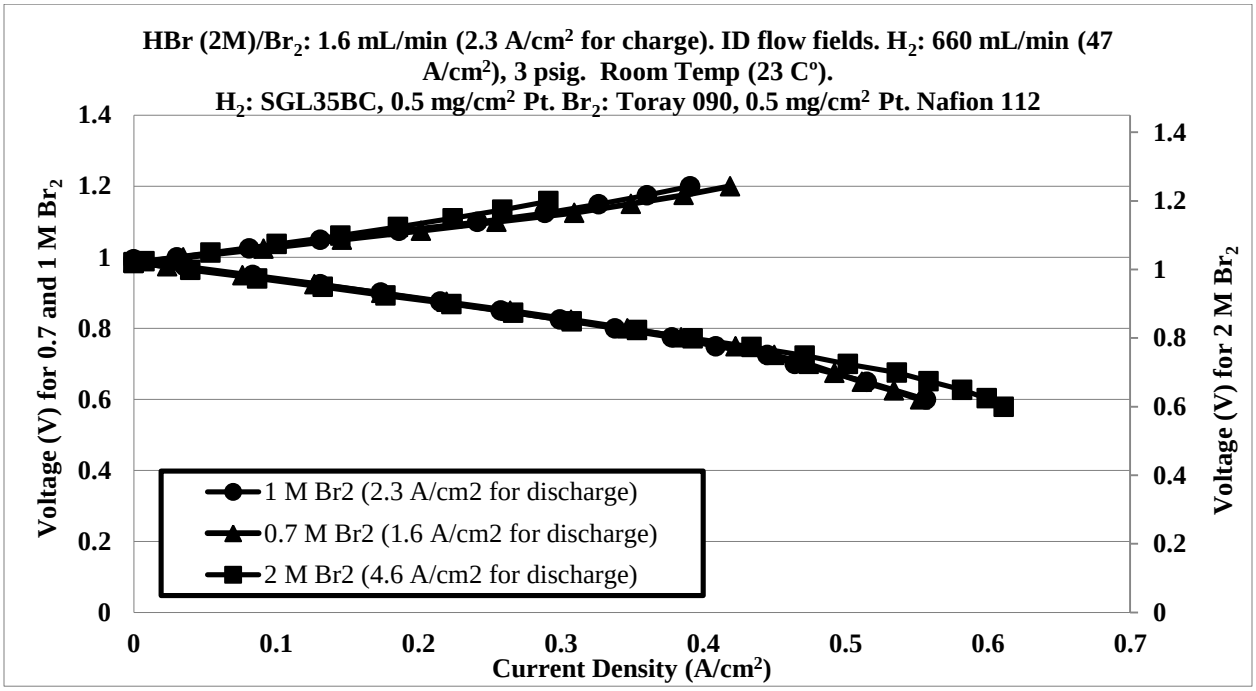

Figure 3.10: Effect of bromine concentration on H_2-Br_2 flow battery performance, adjusted for open circuit potential

Also, it seems that for a voltage change above open circuit potential, there is a higher current than that produced for an equal voltage change below open circuit potential. For example using the 1M Br_2 performance data, at 1.2 V (about 0.2 V above open circuit potential), the current density is about 0.4 A/cm^2 while at 0.8 V (about 0.2 V below open circuit potential), the current density is about 0.35 A/cm^2. Similar behavior is also observed in Figure 3.4 (the comparison to the H_2-O_2 system). The reactions in this system are highly reversible, and so it would be expected based on kinetics that the curves should be very similar, but mirrored over the x-axis. One possible explanation is that the diffusivity of bromine (the reactant for discharge) is lower than the diffusivity of a bromide ion (the reactant for charge) because it is a larger

molecule. Another possibility is that dehydration of the hydrogen electrode – membrane interface is more likely to occur during discharge as the hydronium ion, carrying water, is transported from the hydrogen electrode to the bromine electrode during discharge. The bromine electrode will always be hydrated (unless the HBr concentration is very high) due to the flowing aqueous electrolyte.

3.3.3: Effect of Flow Field Design

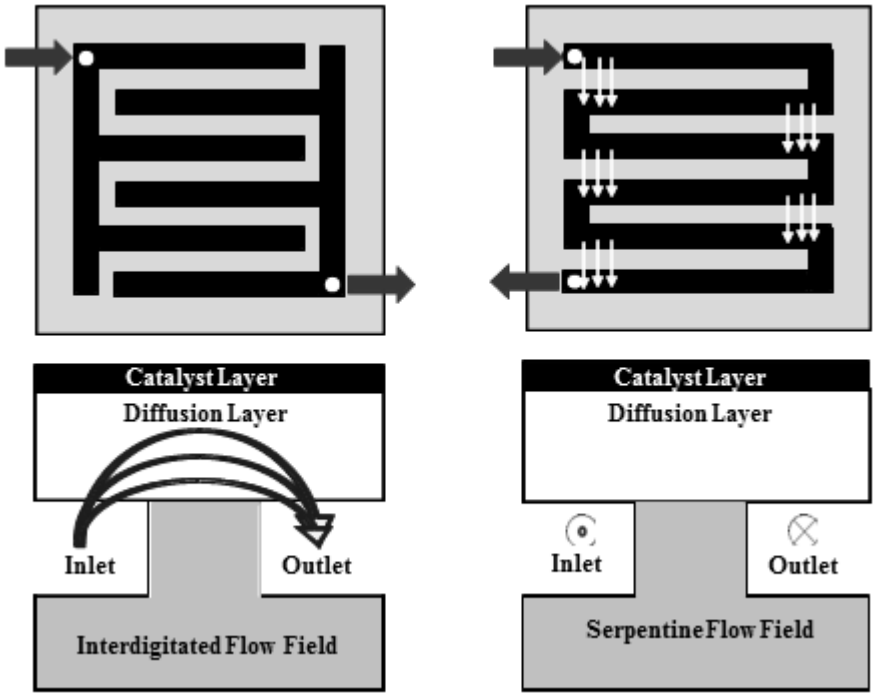

Figure 3.11: Interdigitated and serpentine flow field designs

Since the transport of reactants in the HBr/Br_2 aqueous solution is much slower than the transport of hydrogen in the gas phase (the diffusivity of gas is four orders of magnitude faster than liquid), only the flow field design on the bromine electrode was changed. Interdigitated flow fields were always used for the hydrogen electrode. Changing only the flow field for the HBr/Br_2 solution also ensured that only HBr or Br_2 transport was a factor between the studies.

The flow field channel designs used for the bromine electrode were serpentine and interdigitated, shown in Figure 3.11 on the previous page.

The top blocks in the figure are the flow field designs as seen by the face of the MEA. The bottom parts of the figure are side views illustrating the interface between the electrodes (containing the diffusion and catalyst layers) and the flow channels. In the serpentine flow field on the right, the transport of the reactants is mostly by diffusion. This is because the flow is directed along the electrode, but is not forced up through the porous electrode, except for a small amount of convection due to a pressure difference, as illustrated by the white arrows. The interdigitated flow field, on the left, has dead-ended channels. This design forces the gas or liquid to flow up through the porous electrode, shortening the diffusion distance to the catalyst layer. Thus, transport is enhanced using the interdigitated flow field.[48] This was observed experimentally for the H_2-Br_2 system, as exemplified in Figure 3.12.

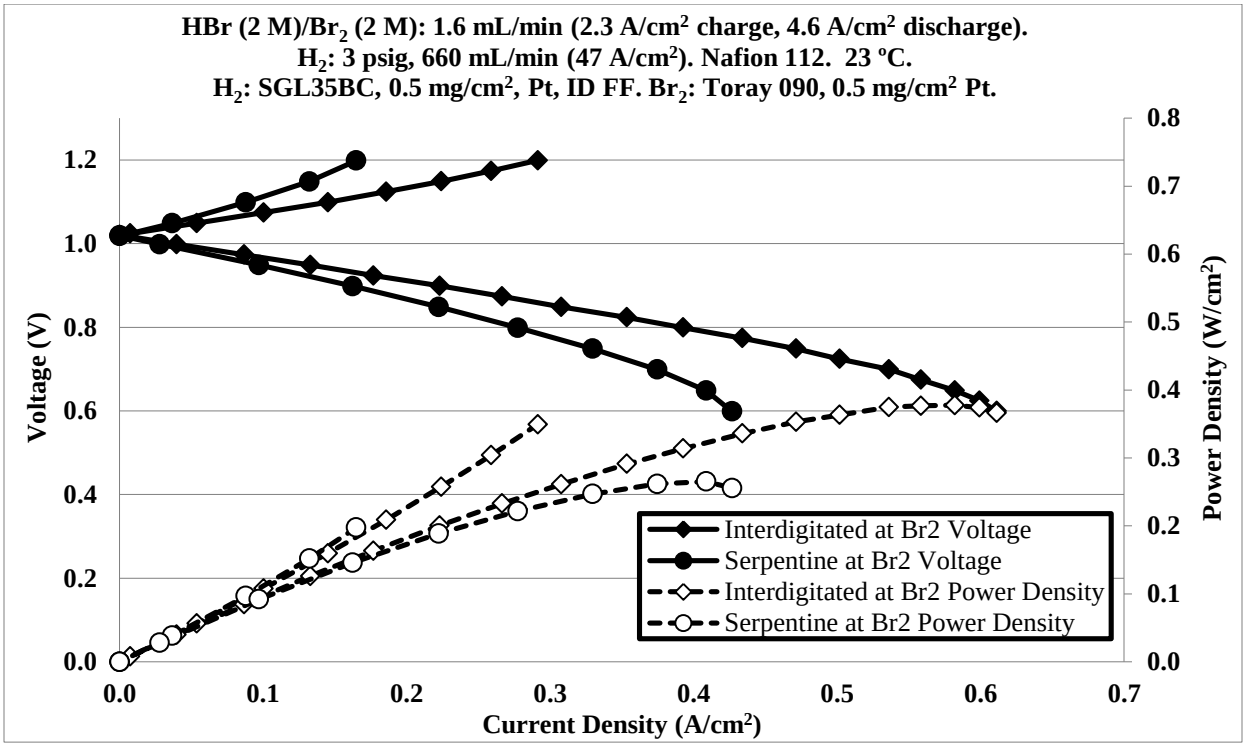

Figure 3.12: Interdigitated and serpentine flow field performance in the H_2-Br_2 flow battery

Using the interdigitated flow field on the bromine side enhanced performance for both discharge and charge. Obtaining higher currents at a specific voltage (for example at 0.6 V, the interdigitated flow field obtained 0.6 A/cm^2 compared to a little over 0.4 A/cm^2 using serpentine) increased the maximum power density 42%. Although the pressure drop will increase using an interdigitated flow field, the pumping costs are likely small compared to the cost of the battery components.

3.3.4: Effect of Br_2/HBr Flow Rate

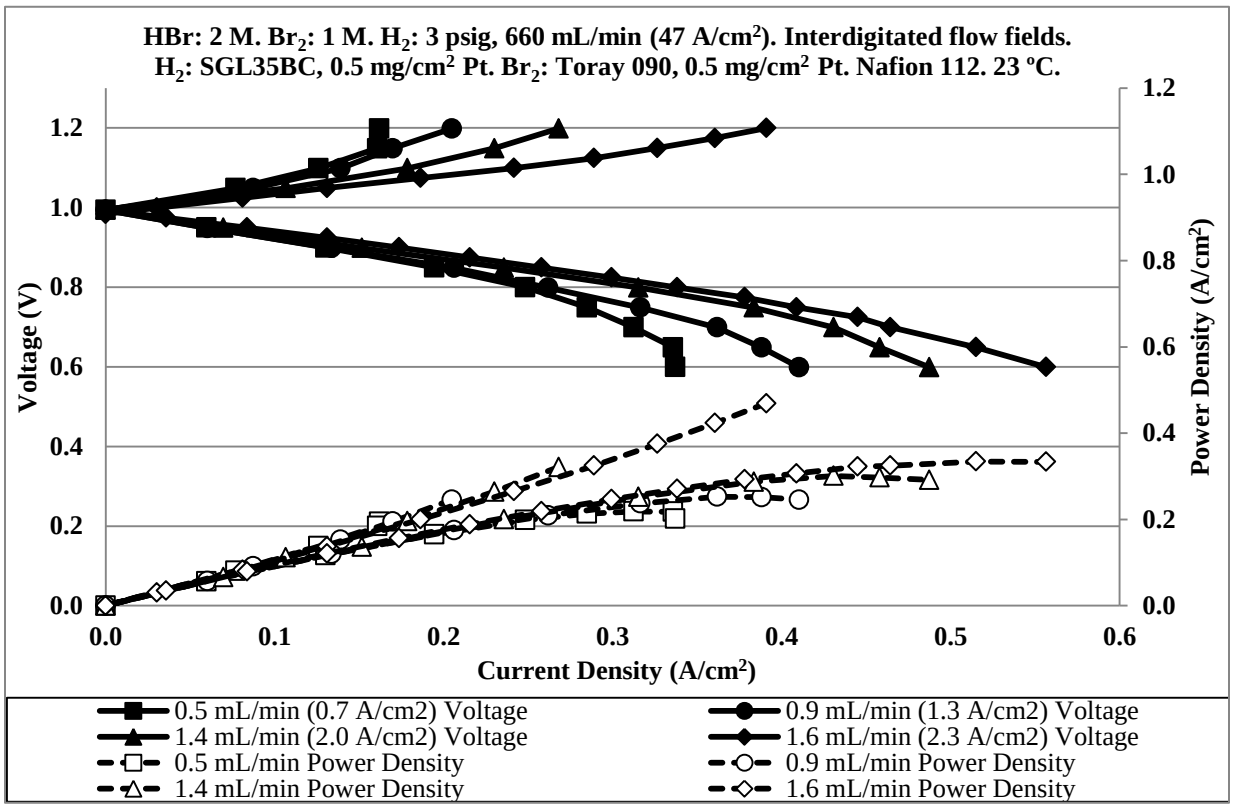

Figure 3.13: Effect of Br_2/HBr flow rate on H_2-Br_2 flow battery performance, interdigitated flow fields

The flow rate of the Br_2/HBr aqueous solution was varied to also look at mass transport effects. If the system was kinetically limited instead of mass transport limited, an increase in

flow rate would not increase the performance of the H_2-Br_2 flow battery. The flow rates were varied using both serpentine and interdigitated flow fields on the bromine electrode. Figures 3.13 and 3.14 demonstrate how increasing the flow rate of the solution to the bromine electrode does indeed increase performance for both charge and discharge for both the serpentine and interdigitated flow fields.

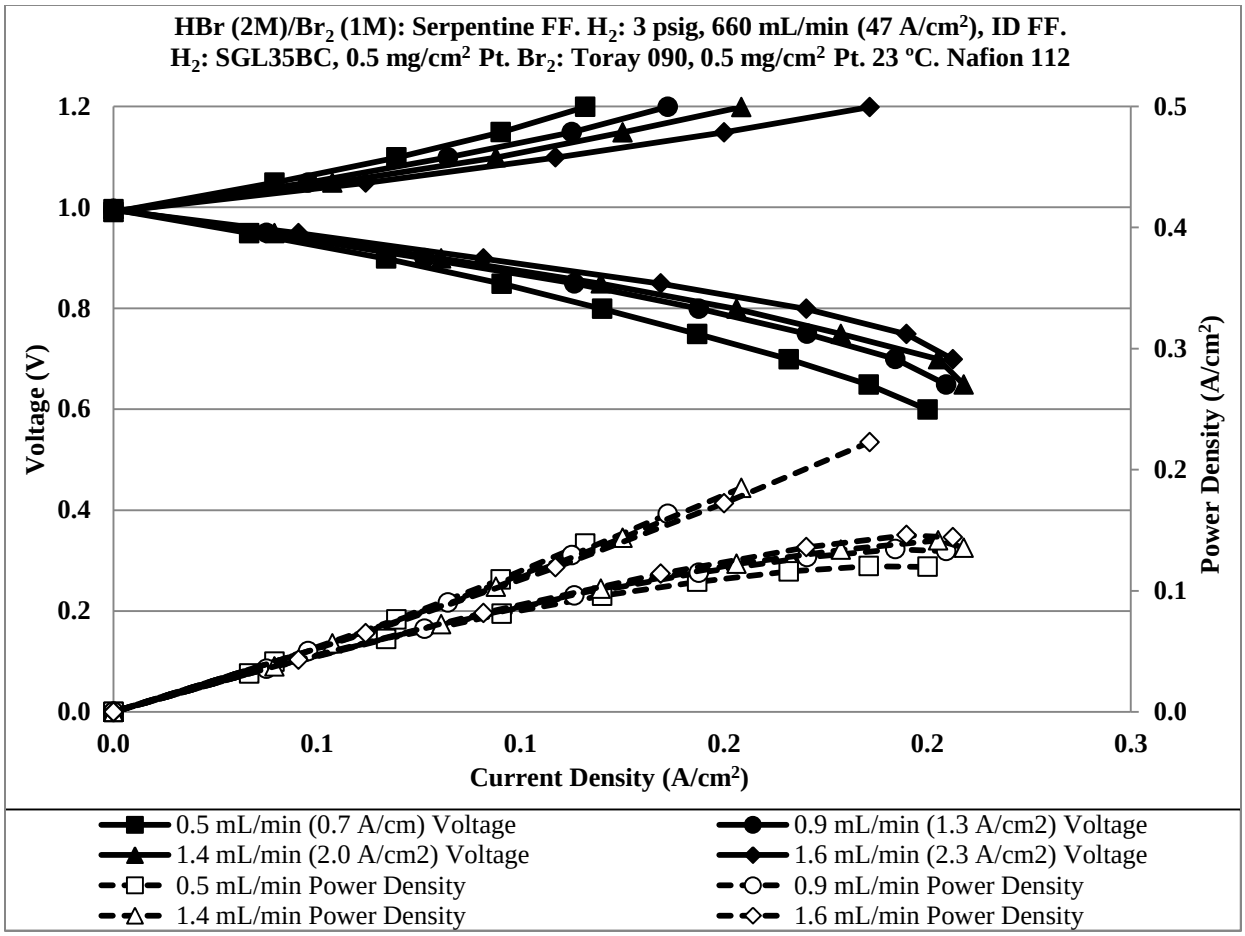

Figure 3.14: Effect of Br_2/HBr flow rate on H_2-Br_2 flow battery performance, serpentine flow field for Br_2/HBr solution, interdigitated flow field for H_2

As the volumetric flow rate is increased and the size of the flow field channels remains the same, the linear velocity is increased, enhancing convective transport. (The term for convective transport is the concentration times the velocity.) For both flow fields, this enhances

mass transport by forcing more of the reactants through the diffusion layer up to the catalyst layer. It appears that this effect is enhanced more so using the interdigitated flow field, probably because convection plays a bigger role in transport in an interdigitated flow field than a serpentine flow field.

3.3.5: Effect of Temperature

Increasing the temperature affects the flow battery performance in several ways. Higher operating temperature increases both the diffusivity of the gaseous and liquid species (molecular transport) and the conductivity of the membrane (ionic transport).[27] Although it also helps to hydrate the hydrogen stream, as increasing the temperature increases the vapor pressure of water, the water traps were not heated. Increasing temperature also increases the vapor pressure of bromine, releasing more of it to the gas phase. Bromine becomes a vapor at 59 ˚C, so temperatures were limited to below this (35 ˚C and 45 ˚C) to keep the reactants in the liquid phase. Previous groups have reported both liquid and gas phase results as high as 80 ˚C. It is not clear why this was so, although there are probably two phases at this temperature due to complexation of bromine by hydrobromic acid, as discussed in section 2.3.6.2.3.[38-39]

For these studies, an aluminum block was assembled within the cell, in between the current collector and end block (to not interfere with the electronic pathway). A PID controller with a thermocouple and a cylindrical heating element was used to control the temperature of the cell. The aluminum block had one large hole to insert the heating element of the PID controller, and two small holes for two thermocouples. One thermocouple was connected to the PID controller, and the other was connected to the Arbin data acquisition system to monitor the temperature of the flow battery. The HBr/Br_2 solution was preheated to around 5 ˚C higher than

the cell temperature, since the solution will likely lose heat travelling through the tubes from storage to cell. A thermocouple connected to the Arbin data acquisition system was inserted into a block underneath the solution. The data is presented in Figure 3.15 below. The increase in temperature slightly decreases the hydrogen flow rate in current equivalence because of the decrease in molar density, but the effect is small (47 A/cm^2 to 44 A/cm^2 from 23 ˚C to 45 ˚C, respectively).

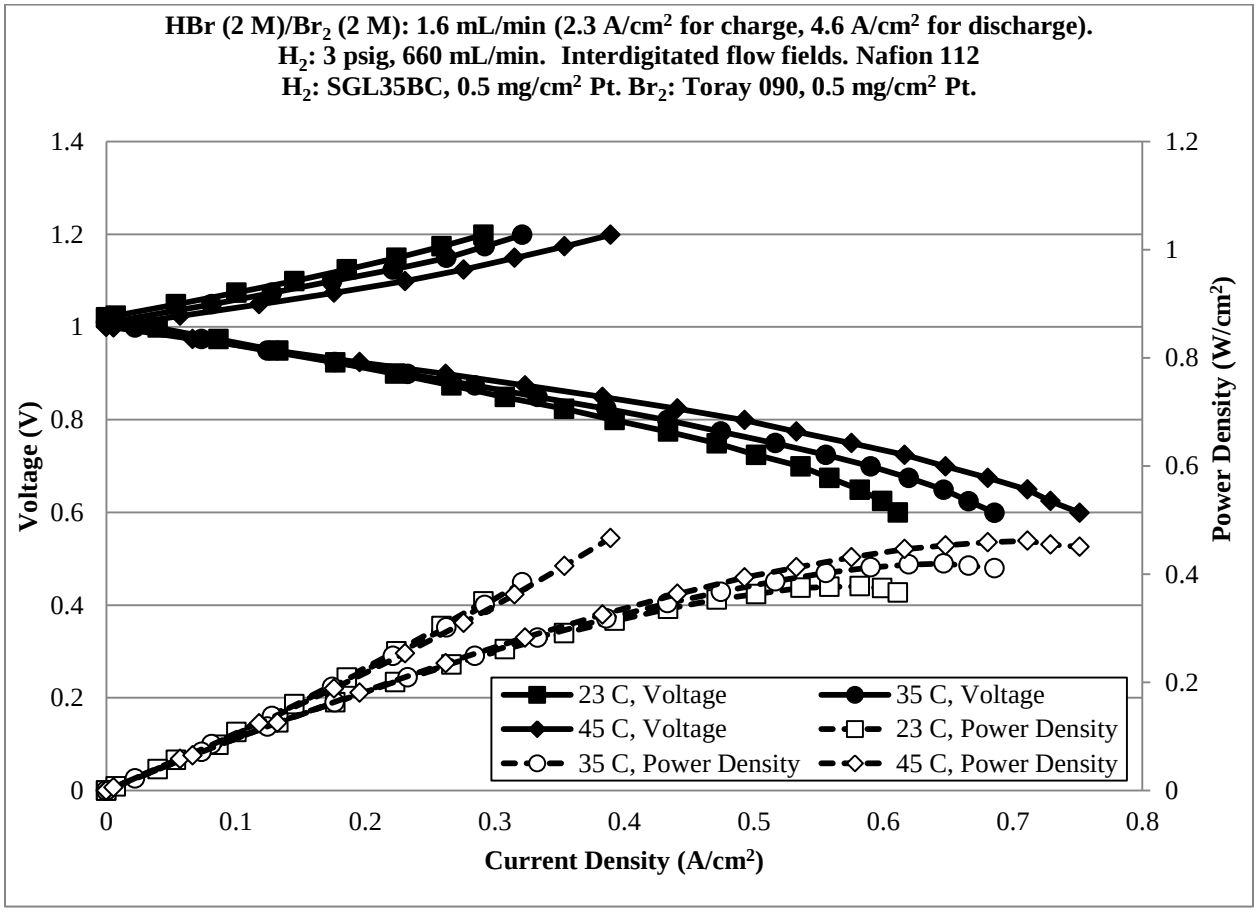

Figure 3.15: Effect of temperature on H_2-Br_2 flow battery performance

Higher temperatures increase both charge and discharge performance because of the higher diffusivity of the species. It is expected that performance would continue to increase if the hydrogen electrode was also heated (the aluminum heating block was on the bromine side).

There does not seem to be a detrimental effect by the possible loss of bromine to the vapor phase, probably because of its complexation with HBr. There is a slight decrease in open circuit potential with increasing temperature, which matches with other studies.[30,32]

The higher operating temperatures could have a negative impact on lifespan, both due to the increasing diffusivity of bromine which would enhance crossover and due to higher corrosion rates and material degradation. The flow field blocks should have a high lifetime in the cell environment, but it was noticed bromine had permeated them, reaching the current collectors and causing corrosion. The flow field blocks are much less prone to corrosion than the stainless steel current collectors. However, increased roughness was observed on the part of the flow field block in contact with the HBr/Br_2 electrode surface that was not observed on the flow field block used for the hydrogen side, indicating a slow corrosion and resulting increase in electrical resistance.

3.3.6: Effect of H_2 Pressure and Flow Rate

The studies in sections 3.3.2-4 looked at liquid-phase transport by changing Br_2 concentration, flow rate of the HBr/Br_2 solution, and flow field design on the bromine side. It was assumed that hydrogen transport would have little effect on performance since the diffusivity of a gas is four orders of magnitude larger than a liquid. This has been confirmed experimentally, as presented in Figure 3.16 on the next page.

It should be noted that the hydrogen flow rate is also a lot higher than the HBr/Br_2 solution flow rate if it is converted to stoichiometric equivalent. There is no difference in performance during discharge. The performance is also similar during charge, although there is a slight discrepancy between 1.175 and 1.2 V. Charge was limited to 1.2 V to avoid electrolysis

of water, so there may be a slight difference in performance at voltages above 1.2 V, but it is unclear from this experiment.

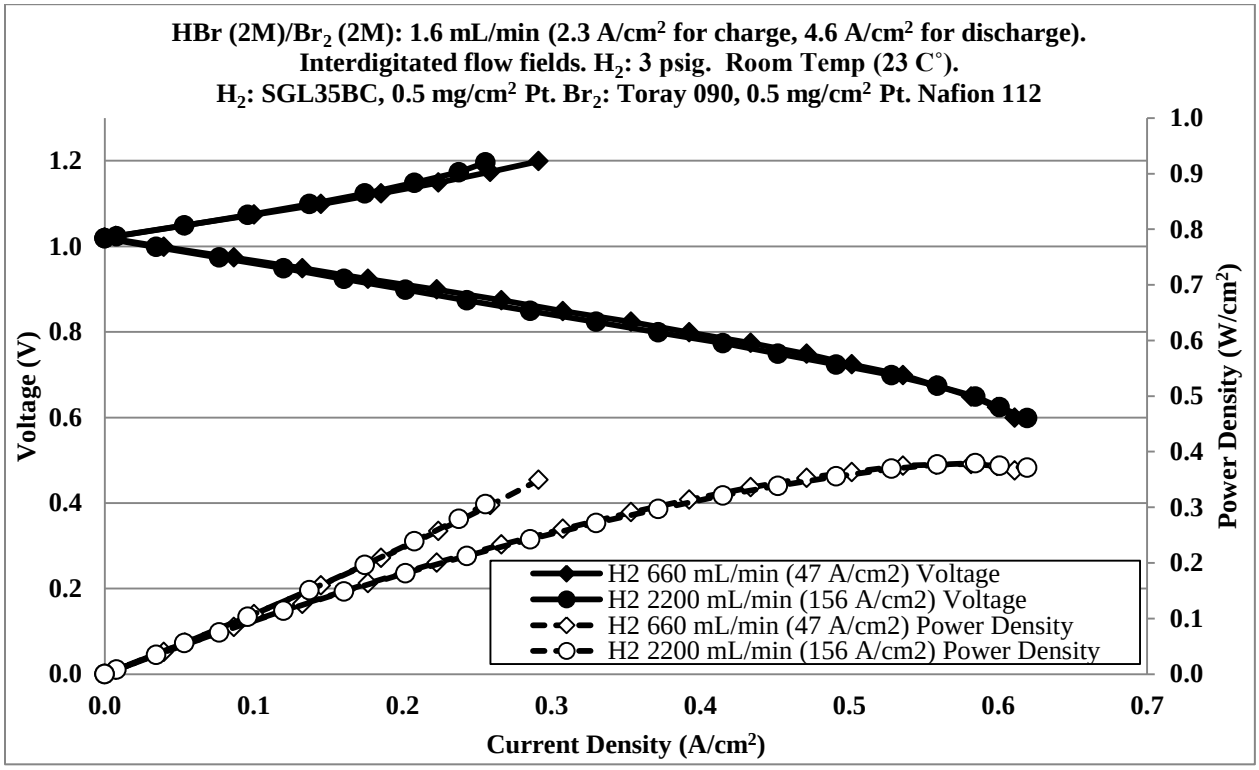

Figure 3.16: Effect of H_2 flow rate on H_2-Br_2 flow battery performance

Another way of looking at hydrogen transport would be to change the pressure. Figure 3.17 on the next page compares the pressure used in the rest of the studies (3 psig) to higher and lower pressures, 6 psig and 1 psig respectively.

Increasing the hydrogen pressure from 3 psig to 6 psig improves the performance for discharge, which might have indicated improved transport and kinetics due to the increased concentration. However, decreasing the pressure from 3 psig to 1 psig also improves the discharge performance. This may be due to a competing effect of increasing the hydrogen pressure. At a constant temperature, when the pressure is increased, the mole fraction of water (given by the ratio of the vapor pressure to the total pressure) in the gas phase is decreased.

Thus, the membrane becomes more dehydrated, increasing the ohmic resistance. This effect matches the trend given at 1.2 V (increasing pressure decreases performance), although this is inconclusive since the performances between the pressures during charge is mostly similar and the voltage is limited to 1.2 V. Also, this is not the trend observed during discharge.

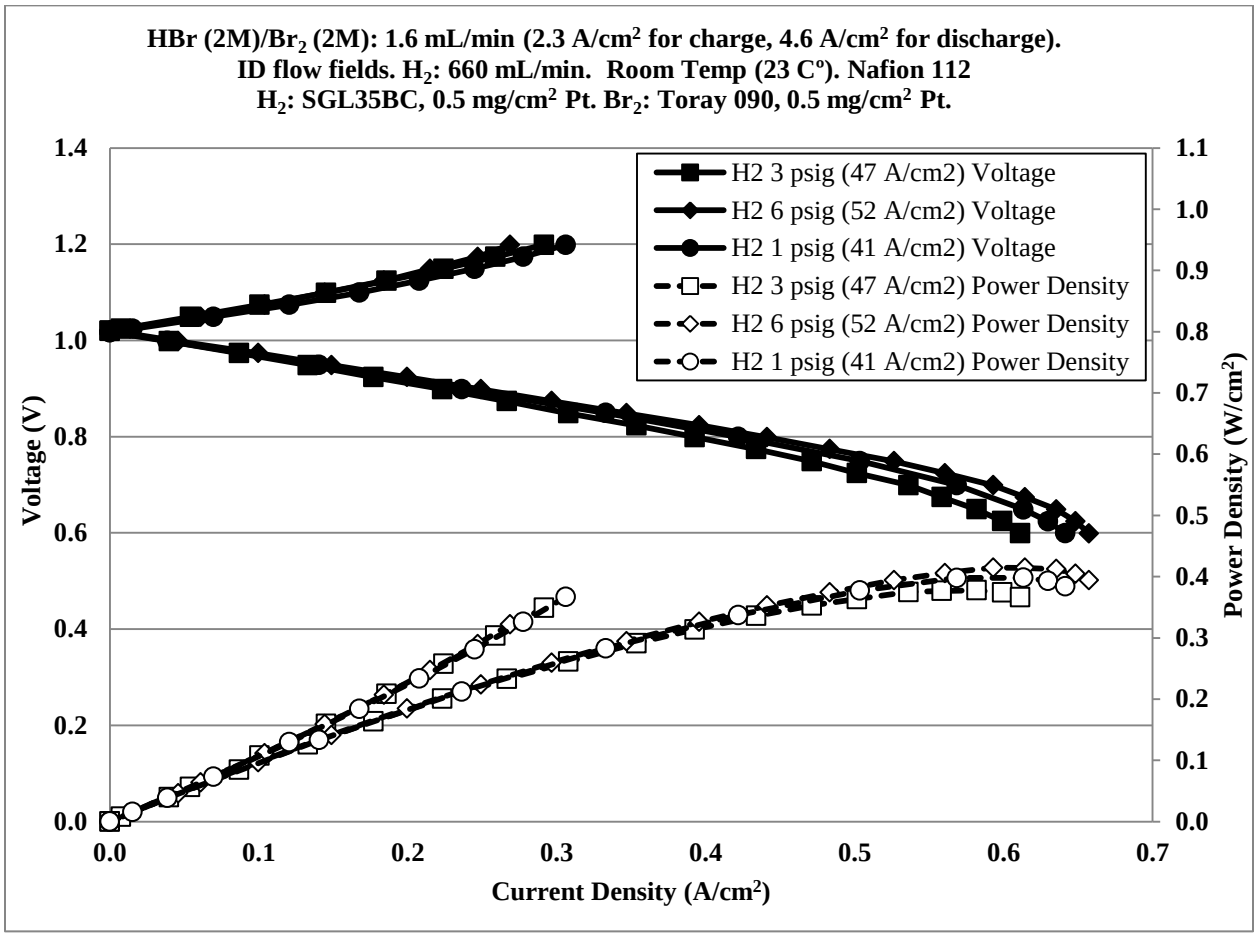

Figure 3.17: Effect of H_2 pressure on H_2-Br_2 flow battery performance

3.3.7: Effect of Membrane Thickness

The previous experiments looked at mostly molecular transport, which is the transport of the reactants in the gas or liquid phase. Another component is the transport of the proton within the cation exchange membrane, ionic transport. The speed of ionic transport is determined by

the conductivity within the membrane and the distance the proton has to travel. Hydration enhances a Nafion membrane's conductivity. As discussed in section 2.3.4.2, the conductivity reaches a maximum near 3 M HBr because of competing effects of increasing proton concentration and decreasing water amount with increasing acid concentration.[27]

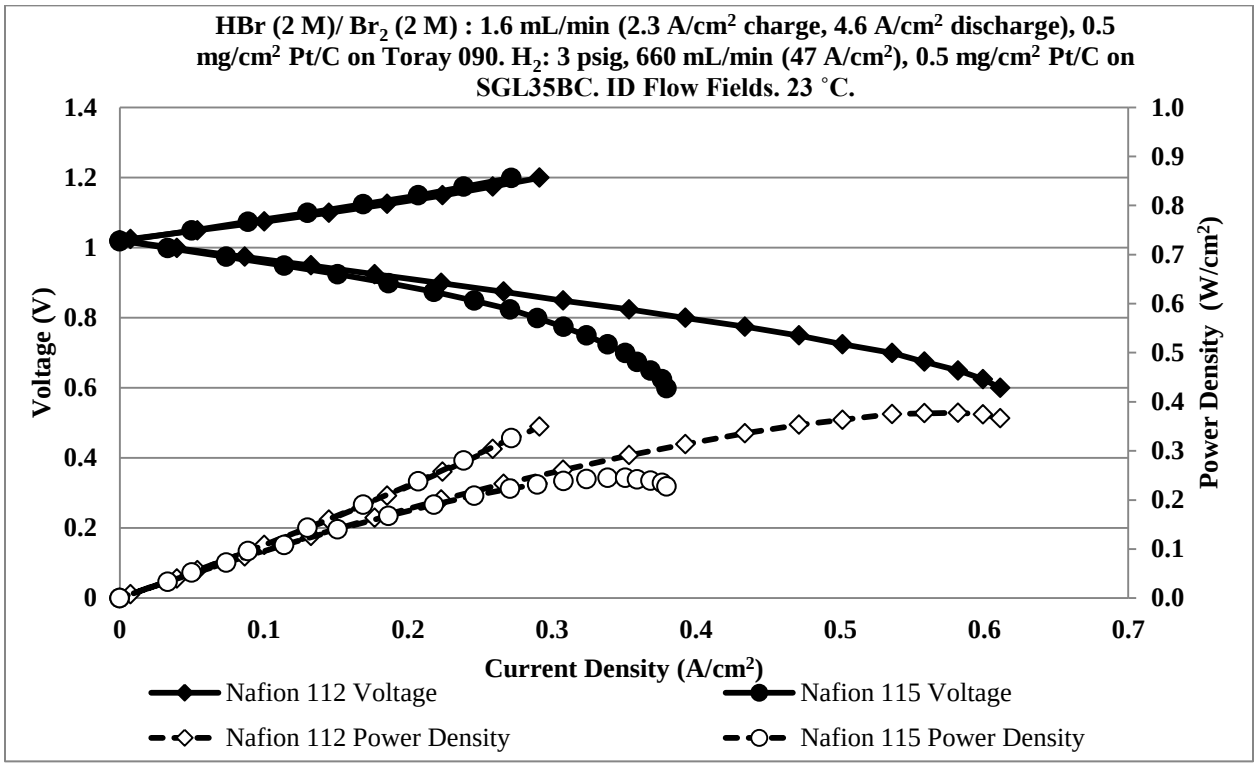

Figure 3.18: Effect of membrane thickness on H_2-Br_2 flow battery performance

The two experiments in Figure 3.18 above have identical operating conditions, with the exception of the membrane thickness. Nafion 112 and Nafion 115 have the same conductivity (EW = 1100), but Nafion 112 is 0.002 inches thick and Nafion 115 is 0.005 inches thick. Mass transport limitations are reached at a much lower current density with the thicker membrane, and maximum power during discharge is decreased. Although the charge data is limited to 1.2 V, it seems that the performance is enhanced more for discharge than charge by the thinner membrane. The current density for the Nafion 115 membrane is much closer to that for the

Nafion 112 membrane at 0.2 V above open circuit (at 1.2 V) than at 0.2 V below open circuit (at 0.8 V).

This can be explained by dehydration effects being more likely to occur during discharge because the hydronium ion transports water from the hydrogen electrode to the bromine electrode after being dissociated from hydrogen gas and before being combined with the bromide ions at the cathode. The bromine electrode is wetted by the electrolyte, and therefore is not going to be dehydrated. While the hydrogen electrode is fed with hydrogen that has been through a water trap, the trap is at room temperature, and thus the hydrogen is not likely to be well-hydrated. Although increasing the membrane thickness decreases performance, there may be a benefit for long-term use due to decreased bromine permeation.

3.3.8: Effect of Br_2/HBr Electrode

While platinum is needed as a catalyst on the hydrogen electrode, the reactions occurring at the bromine electrode are active on a much cheaper material, graphite.[22,32,34] Platinum is a much more expensive material due to it being a rare metal, so using graphite as a catalyst will greatly reduce the cost of the cell. To explore the performance of different catalyst types, several electrodes were made. The electrodes were made in the lab by painting on a solution of either XC-72 carbon or graphene on Toray 090 plain substrate, so the catalyst loading may not be as evenly distributed as for the Pt/C electrodes provided for the experiments in sections 3.3.2-7. Graphene and XC-72 carbon do not necessarily need to be added to the substrate, as the graphite support itself is active for both bromine reduction and evolution. One MEA had no added catalyst to test this, with just SGL 10AA as the bromine electrode. Since both hydrogen

oxidation and evolution reactions are not active on graphite material, the same platinum electrodes were used for the hydrogen electrode as the other case study experiments.

Figure 3.19 compares the performance of a bromine electrode of Toray 090 with platinum catalyst (the same type and loading used in sections 3.3.2-7) to Toray 090 with 2.1 mg/cm^2 XC-72 carbon and to an electrode of SGL 10AA with no added catalyst.

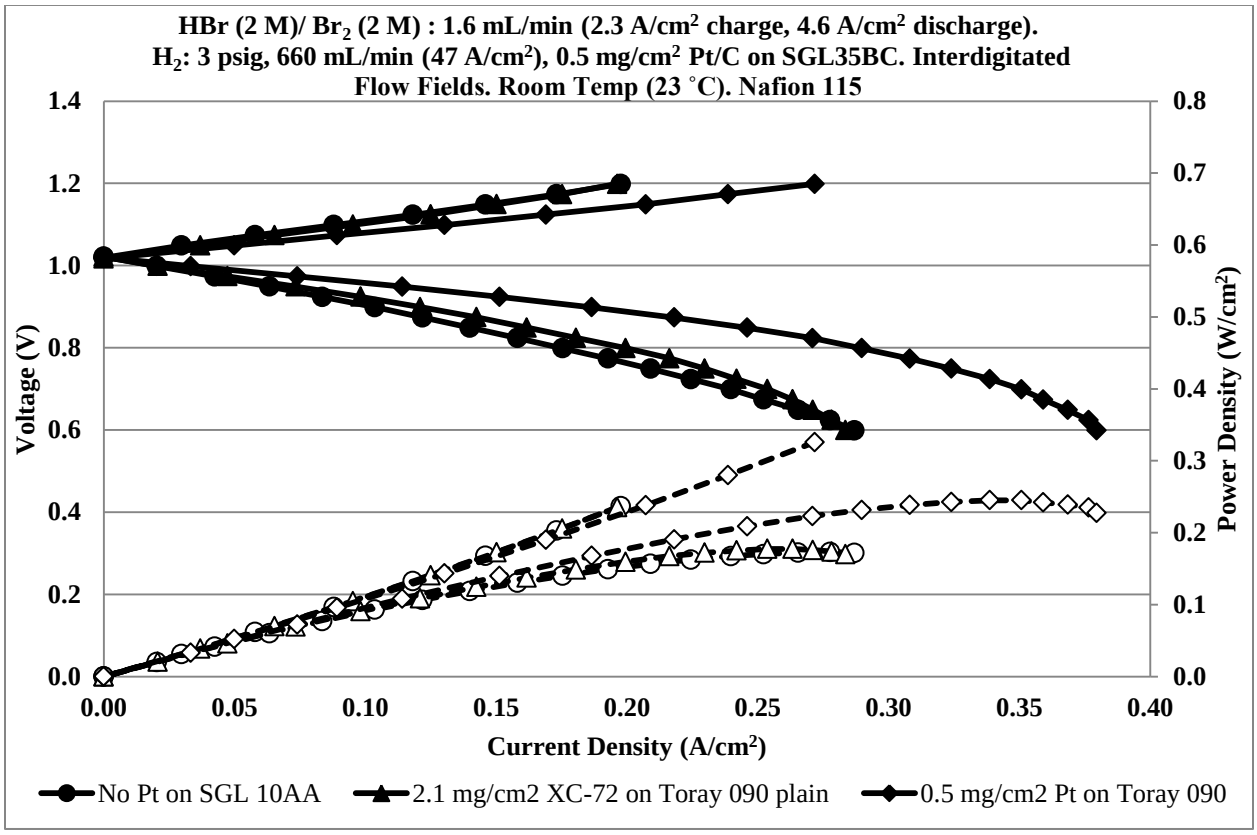

Figure 3.19: Effect of bromine electrode catalyst on H_2-Br_2 flow battery performance, platinum or XC-72 on Toray 090 and plain SGL 10AA

The performance of 2.1 mg/cm^2 XC-72 carbon was similar using SGL 10AA with no added catalyst for the bromine electrode, demonstrating that adding catalyst is not necessary when using a carbon-based substrate. The XC-72 carbon was added in an attempt to increase the surface area of the electrode. The maximum power density is reduced when platinum catalyst is

not used from 0.25 W/cm^2 to about 0.18 W/cm^2. This reflects the higher exchange current density of a platinum electrode for the bromine reactions.[22] It is not clear what power density would be a good target for an energy storage application, because most targets are given in terms of power output per cost. However, the current densities and power densities achieved using a graphite-based electrode on the bromine side are similar to that of vanadium redox batteries, which have been tested at the utility scale.[17,19]

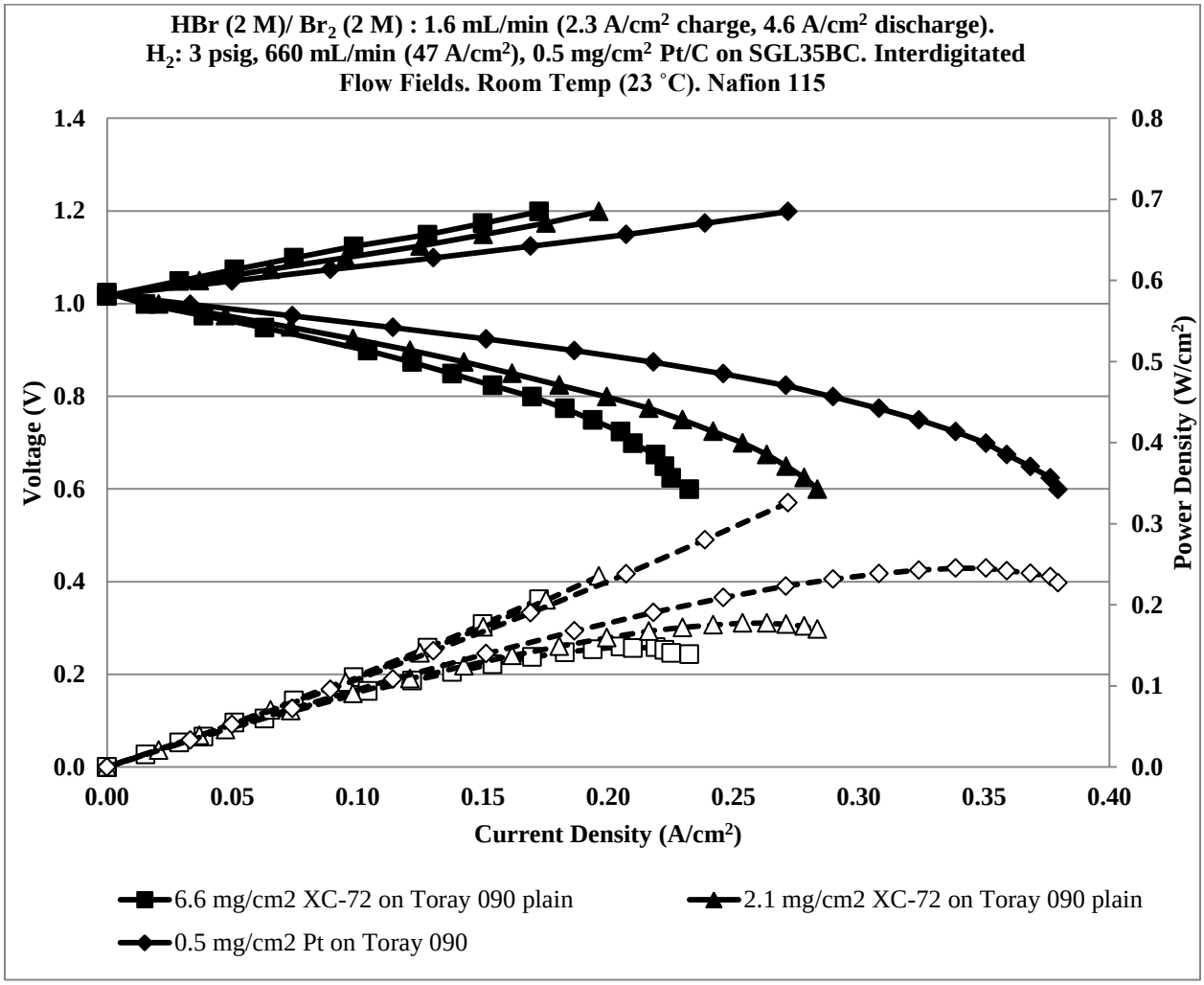

Figure 3.20: Effect of bromine electrode catalyst on H_2-Br_2 flow battery performance, platinum or XC-72 on Toray 090

Figure 3.20 compares the performance data of two different loadings of XC-72 to platinum, all on Toray 090. The performance for both charge and discharge is better for the 2.1 mg/cm^2 XC-72 loading than for the 6.6 mg/cm^2 XC-72 loading. This is probably because of increased mass transport resistance. Although the XC-72 carbon should act to increase the surface area of the electrode, the added material also increases the catalyst layer thickness. This hinders reactants from reaching inner surface areas and increases the ohmic resistance of the cell.

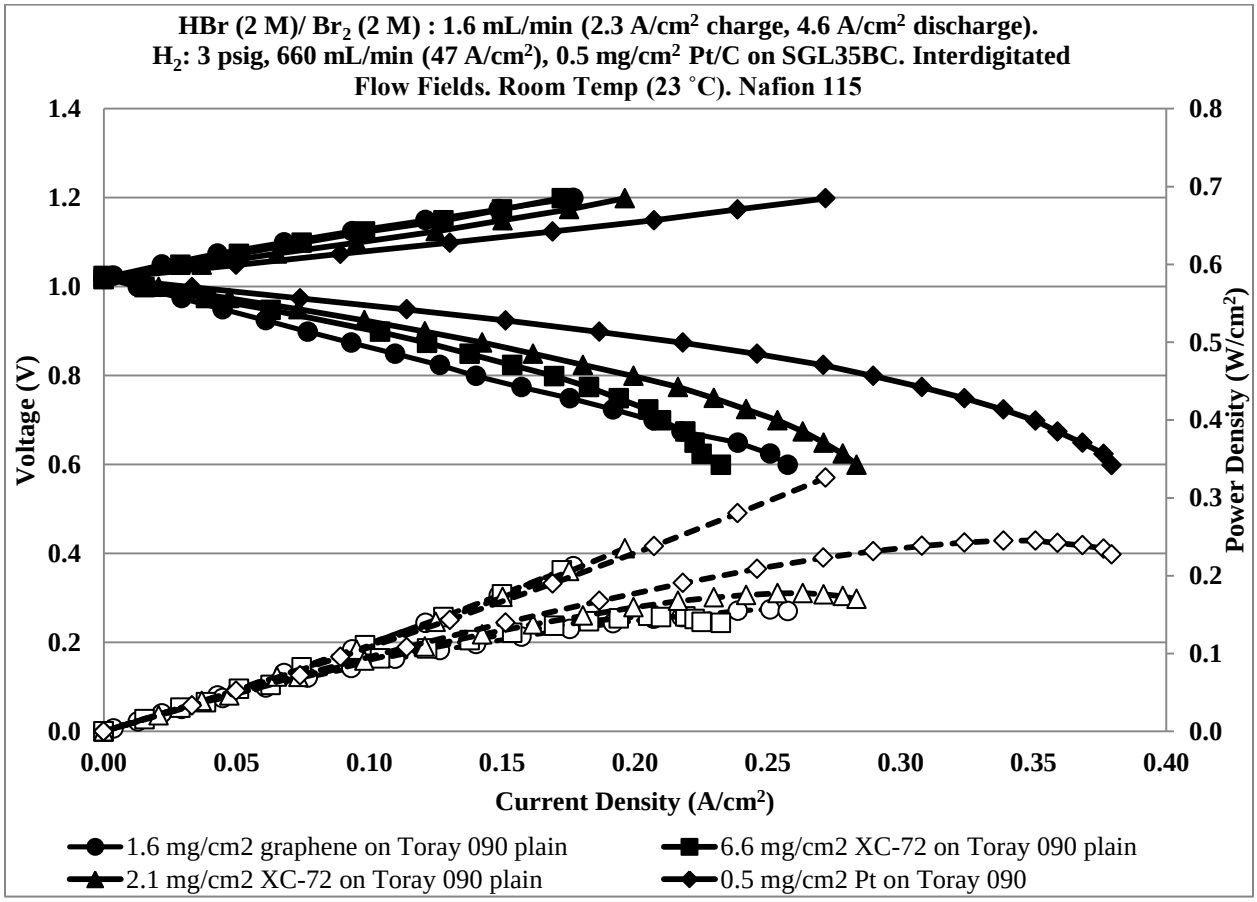

Figure 3.21: Effect of bromine electrode catalyst on H_2-Br_2 flow battery performance, XC-72 or graphene on Toray 090 plain

Figure 3.21 includes performance data for 1.6 mg/cm^2 graphene on Toray to the two XC-72 carbon loadings and to platinum. Graphene was tested because it is supposed to be more

electronically conductive than XC-72 carbon. Another clue the loss in performance at the higher XC-72 loadings is due to transport effects is that the 6.6 mg/cm^2 XC-72 loading performs better than graphene with lower loading of 1.6 mg/cm^2 until 0.3 V below open circuit, when the XC-72 curve becomes nonlinear (reaching mass transport limitations) and the graphene curve remains linear (mass transport limitations have not yet been reached). Not using platinum does decrease the performance for both charge and discharge, but losses will decrease if the graphite catalyst is dispersed in a way that minimizes interference with mass transport.

The performance for both discharge and charge is better using the 2.1 mg/cm^2 XC-72 carbon than the 1.6 mg/cm^2 graphene, with a larger difference in performance at 0.2 V below open circuit (discharge) than 0.2 V above open circuit (charge). It is difficult to make a conclusion on the activity of graphene to XC-72 carbon because the catalyst loading is also lower. Graphene and XC-72 catalysts as well as the plain SGL 10AA electrode do seem to achieve closer results to platinum during charge than discharge.

3.4: Summary of Experimental Findings

The performance of the hydrogen-bromine flow battery is predominantly affected by transport as demonstrated by showing the effects of HBr/Br_2 flow rate, flow field design, membrane thickness and temperature. The flow rate of hydrogen had no effect on performance, as expected since its reactants are in the gas phase while the reactants at the bromine electrode (HBr, Br_2) are in the liquid phase. Although lower overvoltages and higher maximum power densities are achieved when platinum catalyst is used on both sides, the flow battery is still mass transport limited when platinum catalyst is not used, as demonstrated by lower carbon-based catalyst loadings achieving higher performance.

Chapter 4: Recommendations for Further Studies

4.1: Catalyst Design

Platinum achieves the highest performance for both electrodes.[22,32,34] While using only graphite materials for the bromine electrode lowered the flow battery performance, it is recommended to use this type of electrode due to its much lower cost and suitable performance. The exchange current density when carbon is used at the bromine electrode is still four orders of magnitude higher than the electrodes used in the all vanadium redox battery, which is commercially developed.[22]

Unfortunately, a low-cost catalyst with high activity for both reactions occurring at the hydrogen electrode is not available. Active materials for hydrogen oxidation and evolution are expensive metals, such as platinum, tantalum and iridium.[32] Another downside of platinum is poisoning by bromide.[28-29,37] If the membrane is not completely impermeable to bromine and bromide crossover, bromide will reach the hydrogen electrode or bromine will reach the electrode and be reduced to bromide, which adsorbs onto the reactant surface, inhibiting the reactions at the hydrogen electrode. It is not likely that bromine will corrode the platinum, since this occurs very slowly, and any bromine that crosses over will be reduced to bromide as soon as it reaches the hydrogen electrode due to the voltage being lower than the open circuit potential for the reduction of bromine.[32] This poisoning of the hydrogen electrode is reversible, but it would be impractical for a commercial flow battery to have to stop operations to clear the platinum on the hydrogen electrode by oxidizing the bromide and flushing out the bromine.

Although platinum is the most active for hydrogen materials, rhodium is active and is resistant to bromide poisoning, but is similarly high cost. To make the hydrogen-bromine flow

battery a viable commercial option, a catalyst needs to be developed which is inexpensive, active for the reactions at the hydrogen electrode, and resistant to bromide poisoning. This is the objective of The University of California-Santa Barbara team within the collaborative effort of developing the hydrogen-bromine flow battery.

Until a resistant catalyst can be found, design can minimize the likelihood of bromine contamination on the hydrogen side. The carbon paper on which the platinum catalyst is dispersed, SGL 35BC, is a very hydrophobic material. This allows any water (which may contain bromide or bromine) to more easily be flushed from the cell. The catalyst solution also contains Teflon to increase the hydrophobicity of the catalyst and enhance liquid flushing from the reactive surface. Increasing the amount of Teflon in the catalyst will increase the hydrophobicity of the electrode, but will also increase electrical resistance.[37]

4.2: Membrane Design

If the membrane could eliminate bromine and bromide crossover, there would be no need to find a hydrogen electrode catalyst that was resistant to halide poisoning. For Nafion, bromine permeability increases with increasing bromine concentration and decreasing hydrobromic acid concentration. Increasing acid concentration dehydrates the membrane, hindering bromine transport. Unfortunately, dehydration also reduces conductivity within the Nafion membrane.[27] Conductivity and permeability to bromine and bromide are often competing properties within membranes other than and including Nafion. Membranes with lower water content, such as a sulfonated polystyrene membrane, are more resistant to bromine crossover, but also have higher ohmic resistance.[30]

The team at Vanderbilt University is working on developing a membrane that is low-cost and highly conductive to protons while being resistant to crossover of hydrogen, bromine or bromide. The membrane must also be resistant to chemical attack by bromine or hydrobromic acid and durable to changes in hydration. As discussed, the membrane needs competing properties of conductivity and resistance to crossover, so the team uses electrospinning to combine different membrane materials and achieve an optimum structure.

To minimize contamination at the hydrogen electrode while a cell is operated with a membrane permeable to bromine or bromide, the hydrogen should be introduced to the cell before the HBr/Br_2 solution, and the pressure at the hydrogen electrode should always be higher than the pressure at the bromine electrode. Any liquid that may reach the hydrogen electrode is more likely to be flushed from the system if the hydrogen electrode contains hydrophobic materials, and a water trap after the cell is necessary to prevent flushed acid or bromine from reaching the gas pump. High charge rates and prolonged charge should be avoided as water is transported to the hydrogen electrode during charge, increasing the likelihood of bromine and bromide crossover. A thick Nafion membrane will reduce crossover, but will also increase electrical resistance, as seen in Figure 3.19.

4.3: Cell Design

Since the hydrogen-bromine flow battery is transport limited, interdigitated flow field design should be used to maximize transport through the diffusion layer to the catalyst surface. This may increase pressure drop, but pumping costs are likely to be small compared to the cost of the cell materials. Although the blocks made of compressed graphite powder are more electronically resistive than the blocks made of layers of graphite, they are recommended

because of their higher durability in the HBr/Br_2 environment. A thin flow field would reduce the electrical resistance, but the thicker blocks allow the connections from the reactant storage to the power conversion unit to be connected through the side. This simplifies the design, eliminating the need of gaskets and reducing the chance of leaking in between the flow field block and the current collector, which would also increase electrical resistance.

The current collectors in these studies are made of stainless steel, which is prone to corrosion by the hydrobromic acid and bromine. This corrosion increases the electrical resistance by roughening the contact surface between the back of the flow field blocks and the current collectors. The graphite-based flow field blocks are not completely impermeable to the aqueous HBr/Br_2 solution, although polymer sealant can help reduce this at the expense of increasing electrical resistance. Although tantalum is not corroded by bromine or hydrobromic acid, its use as a current collector or as a film over the flow field block would be impractical due to its high cost.[30,32]

4.4: Development of Model

Development of a model is crucial for optimizing design variables such as flow field block length that would be costly and time-consuming to test in the lab. The experimental work in this thesis can serve as a large data bank for model verification. Besides as an optimization tool, the model can be used to explore scale-out effects and to calculate parasitic losses from pumping or other auxiliary components. The hydrogen-bromine flow battery model is essential for the team at The University of Texas-Arlington to simulate its connection to the electrical grid, and identify any obstacles or other components needed to successfully implement the battery.

References

1. Septimus van der Linden, "Bulk energy storage potential in the USA, current developments and future prospects," *Energy*, Vol. 31, 3446-3457 (2006).
2. Haisheng Chen, Thang Ngoc Cong, Wei Yang, Chunqing Tan, Yongliang Li, Yulong Ding, "Progress in electrical energy storage system: A critical review," *Progress in Natural Science*, Vol. 19, 291-312 (2009).
3. IUPAP Working Group on Energy, "Report on Research and Development of Energy Technologies," *International Union of Pure and Applied Physics* (2004). <http://www.iupap.org/wg/energy/report-a.pdf>
4. United States. Dept. of Energy/Energy Information Agency. *International Energy Outlook 2011*. U.S. Energy Information Agency, Office of Communications (2011). <http://205.254.135.7/forecasts/ieo/pdf/0484(2011).pdf>
5. Alfred Cavallo, "Energy Storage Technologies for Utility Scale Intermittent Renewable Energy Systems," *Journal of Solar Energy Engineering*, Vol. 123, 387-389 (2001).
6. Herbert Inhaber, "Why wind power does not deliver the expected emissions reductions," *Renewable and Sustainable Energy Reviews*, Vol. 15, 2557-2562 (2011).
7. Martin Winter and Ralph Brodd, "What are Batteries, Fuel Cells, and Supercapacitors?," *Chem. Rev.*, Vol. 104, 4245-4269 (2004).
8. X.D. Xue, K.W.E. Cheng and D. Sutanto, "A study of the status and future of superconducting magnetic energy storage in power systems," *Supercond. Sci. Techol.*, Vol. 19, R31-R39 (2006).

9. Paul Denholm and Gerald L. Kulcinski, "Life cycle energy requirements and greenhouse gas emissions from large scale energy storage system," *Energy Conversion and Management*, Vol. 45, 2153-2172 (2004).
10. *Pumped Storage diagram at TVA's Racoon Mountain*. Digital image. *Wikipedia*. Web. 12 Dec. 2011 <http://en.wikipedia.org/wiki/File:Pumpstor_racoon_mtn.jpg>
11. Trung Nguyen and Robert F. Savinell, "Flow Batteries," *The Electrochemical Society Interface*, Fall 2010, 52-54 (2010).
12. Grigorii L. Soloveichik, "Battery Technologies for Large-Scale Stationary Energy Storage," *Annu. Rev. Chem. Biomol. Eng.*, Vol. 2, 503-527 (2011).
13. L.H. Thaller, "Electrically Rechargeable Redox Flow Cell." US Patent 3996064. 7 Dec. 1976.
14. L.H. Thaller, "Redox Flow Cell Energy Storage Systems," *NASA Technical Memorandum 79143*. National Aeronautics and Space Administration, Lewis Research Center (1979).
15. Adam Z. Weber, Matthew M. Mench, Jeremy P. Meyers, Philip N. Ross, Jeffrey T. Gostick and Qinghua Liu, "Redox flow batteries: a review," *Journal of Applied Electrochemistry*, Vol. 41, 1137-1164 (2011).
16. Maria Skyllas-Kazacos, Miron Rychick, and Robert Robins, "All-Vanadium Redox Battery." US Patent 4786567. 22 Nov. 1988.
17. M. Skyllas-Kazacos, M.H. Chakrabarti, S.A. Hajimolana, F.S. Mjalli, and M. Saleem, "Progress in Flow Battery Research – a Review," *Journal of the Electrochemical Society*, Vol. 158, R55-R79 (2011).
18. M. Skyllas-Kazacos, "Novel vanadium chloride/polyhalide redox flow battery," *Journal of Power Sources*, Vol. 124, 299-302 (2003).

19. M. Skyllas-Kazacos, G. Kazacos, G. Poon, and H. Verseema, "Recent advances with UNSW vanadium-based redox flow batteries," *International Journal of Energy Research*, Vol. 34, 182-189 (2010).
20. Robert P. Remick and Peter G.P. Ang, "Electrically Rechargeable Anionically Active Reduction-Oxidation Electrical Storage-Supply System." US Patent 4485154. 27 Nov. 1984.
21. DTI, "Regenesys Utility Scale Energy Storage: Project Summary," *Contract number K/EL/00246/00/00 URN Number 04/1049* (2004). http://webarchive.nationalarchives.gov.uk/+/http://www.berr.gov.uk/files/file16056.pdf
22. Paul Ridgway, Kyu Taek Cho, Vincent Battaglia, Adam Z. Weber, and Venkat Srinivasan, "Redox Kinetics of the Bromine-Bromide Reaction for Flow Batteries," *The Electrochemical Society 220th Meeting*, Abstract #695 (2011).
23. E.N. Balko, "Heat rejection and thermal efficiency in model hydrogen-halogen fuel cell systems," *Journal of Applied Electrochemistry*, Vol. 11, 91-102 (1981).
24. *Technology Comparison*. Digital image. *Electricity Storage Association.* Web. 8 Jan. 2012. <http://www.electricitystorage.org/images/uploads/static_content/technology/technology_resources/comparison_large.gif>
25. *Capital Cost*. Digital image. *Electricity Storage Association.* Web. 8 Jan. 2012. < http://www.electricitystorage.org/images/uploads/static_content/technology/technology_resources/capital-cost_large.gif>
26. R.S. Yeo and D-T. Chin, "A Hydrogen-Bromine Cell for Energy Storage Applications," *Journal of the Electrochemical Society*, Vol. 127, 549-555 (1980).

27. Richard S. Baldwin, "Electrochemical Performance and Transport Properties of a Nafion Membrane in a Hydrogen-Bromine Cell Environment," *NASA Technical Memorandum 89862*. National Aeronautics and Space Administration, Lewis Research Center (1987).
28. M.W. Breiter, "Voltammetric Study of Halide Ion Adsorption on Platinum in Perchloric Acid Solution," *Electrochimica Acta*, Vol. 8, 925-935 (1963).
29. V.S. Bagotzky, Yu B. Vassilyev, J. Weber, and J.N. Pirtskhalava, "Adsorption of Anions on Smooth Platinum Electrodes," *Electroanalytical Chemistry and Interfacial Electrochemistry*, Vol. 27, 31-46 (1970).
30. Werner Glass and G.H. Boyle, "Performance of Hydrogen-Bromine Fuel Cells." Fuel Cell Systems. Ed. George J. Young and Henry R. Linden. Washington, D.C.: American Chemical Society, 203-222 (1969).
31. G.H. Schuetz, "Hydrogen Producing Cycles Using Electricity and Heat – Hydrogen Halide Cycles: Electrolysis of HBr," *International Journal of Hydrogen Energy*, Vol. 1, 379-388 (1977).
32. G.H. Schuetz and P.J. Fiebelmann, "Electrolysis of Hydrobromic Acid," *International Journal of Hydrogen Energy*, Vol. 5, 305-316 (1980).
33. G.H. Schuetz, "Recent Advances and Possible Improvements in the Electrolysis of HBr," *Hydrogen Energy Progress*, Vol. 4, 493-504 (1982).
34. J.A. Kosek and A.B. LaConti, "Investigation of Bromine Complexed Hydrogen/Bromine Regenerative Fuel Cells for Portable Electric Power," *Final Report for U.S. Army Mobility Equipment Research and Development Command*. General Electric, Electrochemical Energy Conversion Programs (1984).

35. E.L. Johnson, “The Texas Instruments Solar Energy System Development,” *Proceedings of the Intersociety Energy Conversion Engineering Conference*, Vol. 16, 798-804 (2001).

36. William R. McKee, Kent R. Carson, and Jules D. Levine, “Development and Evaluation of the Texas Instruments Solar Energy Systems,” *Conference record of the IEEE Photovoltaic Specialists Conference*. Vol. 16, 257-262 (1982).

37. G.G. Barna, S.N. Frank, T.H. Teherani, and L.D. Weedon, “Lifetime Studies in H_2/Br_2 Fuel Cells,” *Journal of the Electrochemical Society*, Vol. 131, 1973-1980 (1984).

38. V. Livshits, A. Ulus, and E. Peled, “High-power H_2/Br_2 fuel cell,” *Electrochemistry Communications*, Vol. 8, 1358-1362 (2006).

39. Rui Zhang and John W. Weidner, “Analysis of a gas-phase Br2-H2 redox flow battery,” *J. Applied Electrochem.*, Vol. 41, 1245-1252 (2011).

40. J.A. Kosek and A.B. LaConti, “Advanced Hydrogen Electrode for a Hydrogen-Bromine Battery,” *Journal of Power Sources*, Vol. 22, 293-300 (1988).

41. *Nafion-Polymer*. Digital image. *Wikipedia.* Web. 11 Dec. 2011. <http://en.wikipedia.org/wiki/File:Nafion2.svg>

42. T.D. Gierke and W.Y. Hsu, “The Cluster-Network Model of Ion Cluster in Perfluorosulfonated Membranes,” Perfluorinated Ionomer Membranes. Ed. Adi Eisenberg and Howard L. Yeager. Lake Buena Vista, FL: ACS Symposium Series, 283-310 (1982).

43. *Cluster Network Model*. Digital image. *Wikipedia*. Web. 11 Dec. 2011. <http://en.wikipedia.org/wiki/File:Cluster_network_model.png>

44. R.S. Yeo and J. McBreen, “Transport Properties of Nafion Membranes in Electrochemically Regenerative Hydrogen/Halogen Cells,” *Journal of the Electrochemical Society*, Vol. 126, 1682-1687 (1979).

45. F.G. Will, “Bromine Diffusion Through Nafion Perfluorinated Ion Exchange Membranes,” *Journal of the Electrochemical Society*, Vol. 126, 36-43 (1979).

46. S.D. Fritts and R.F. Savinell, “Simulation Studies on the Performance of the Hydrogen Electrode Bonded to Proton Exchange Membranes in the Hydrogen-Bromine Fuel Cell,” *Journal of Power Sources*, Vol. 28, 301-315 (1989).

47. R.F. Savinell and S.D. Fritts, “Theoretical Performance of a Hydrogen-Bromine Rechargeable SPE Fuel Cell,” *Journal of Power Sources*, Vol. 22, 423-440 (1988).

48. T.V. Nguyen, “A Gas Distributor Design for Proton-Exchange-Membrane Fuel Cells,” *Journal of the Electrochemical Society*, Vol. 143, L103-L105 (1996).

Appendix A: Calibration Data

This appendix includes the HBr/Br_2 peristaltic pump calibration data and H_2 rotameter calibration data. Table A.1 includes the pump calibration data used for the preliminary studies (the data presented in section 3.2.4-5). This data is plotted in Figure A.1. The pump was re-calibrated for the case studies (the data presented in sections 3.3.2-8) to obtain more accurate data at the lower pump settings by using more trials and smaller increments between the data points. Table A.2 includes the raw data for the three HBr/Br_2 pump calibration trials. The averages of these three trials are presented in Table A.3 and Figure A.2. The HBr/Br_2 pump calibration data for the preliminary and case studies was obtained by weighing the water added to a flask by the pump over a recorded period of time for each pump setting. M_1 is the mass of the flask and water before the run and M_2 is the mass of the flask and water after the end of the time period for each pump setting.

The soap bubble method was used to obtain the H_2 flow rate indicated by the rotameter. The data presented in Table A.4 includes the level the bubble reached when the stopwatch was started and stopped (reading began and reading end columns, respectively), the volume the bubble travelled, and the time it took to travel this volume. This was used to calculate the flow rate. The averages of three trials are presented in Figure A.3.

Table A.1: HBr/Br_2 calibration data for the preliminary studies (sections 3.2.4-5).

M_1 (g)	M_2 (g)	(M_2 - M_1) (g)	Time (min)	Setting	Flow Rate (ml/min)
109.2704	107.3676	1.9028	4	0.5	0.5
107.3554	104.2438	3.1116	4	1	0.8
99.3246	91.5616	7.763	4	1.5	1.9
112.7338	102.5862	10.1476	4	2	2.5
112.4833	99.327	13.1563	4	2.5	3.3
117.728	102.2311	15.4969	4	3	3.9
116.8375	97.3915	19.446	4	3.5	4.9
101.7762	80.5651	21.2111	4	4	5.3
118.3748	92.9893	25.3855	4	4.5	6.3
114.5817	87.6068	26.9749	4	5	6.7
118.3745	87.9469	30.4276	4	5.5	7.6
119.4922	78.3872	41.105	5	6	8.2
117.3622	80.4156	36.9466	4	6.5	9.2
119.0603	80.5684	38.4919	4	7	9.6

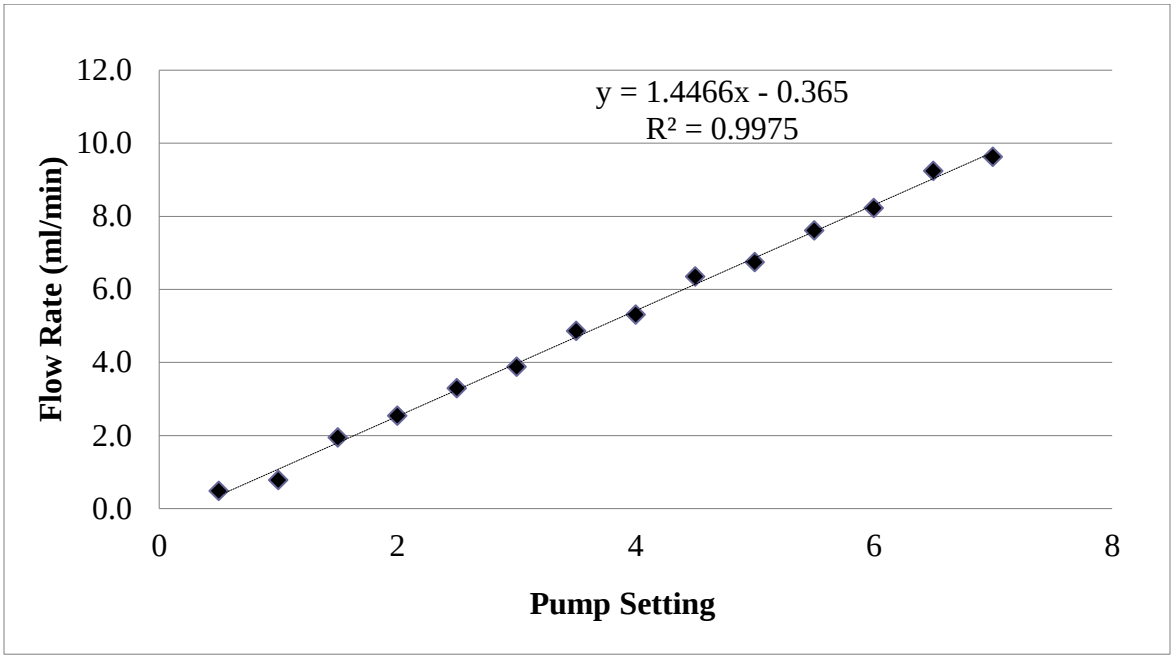

Figure A.1: HBr/Br_2 pump calibration chart for the preliminary studies (sections 3.2.4-5)

Table A.2: HBr/Br_2 pump calibration data for the case studies (sections 3.3.2-8), all three trials

	M_1 (g)	M_2 (g)	(M_2 - M_1) (g)	Time (min)	Setting	Flow Rate (ml/min)
Trial 1	85.3952	82.4278	2.9674	5	0.5	0.6
	82.4278	78.6193	3.8085	5	0.75	0.8
	78.6139	72.3844	6.2295	5	1	1.2
	72.3844	62.5828	9.8016	5	1.25	2.0
	82.9874	69.8012	13.1862	5	1.5	2.6
	69.8012	56.8124	12.9888	5	1.75	2.6
	92.4428	77.1023	15.3405	5	2	3.1
Trial 2	74.5894	71.4915	3.0979	5	0.5	0.6
	77.9341	74.5894	3.3447	5	0.75	0.7
	69.7842	63.6692	6.115	5	1	1.2
	79.044	69.7842	9.2598	5	1.25	1.9
	91.4101	79.044	12.3661	5	1.5	2.5
	92.6669	77.4219	15.245	5	1.75	3.0
	93.3748	78.1474	15.2274	5	2	3.0
Trial 3	91.7894	88.6974	3.092	5	0.5	0.6
	88.6974	84.2565	4.4409	5	0.75	0.9
	84.2565	77.9663	6.2902	5	1	1.3
	90.1596	80.5446	9.615	5	1.25	1.9
	80.5446	68.1663	12.3783	5	1.5	2.5
	92.3029	79.807	12.4959	5	1.75	2.5
	91.7109	76.4329	15.278	5	2	3.1

Table A.3: HBr/Br_2 pump calibration data for the case studies (sections 3.3.2-8), average of three trials

Setting	Flow Rate (ml/min)
0.5	0.6
0.75	0.8
1	1.2
1.25	1.9
1.5	2.5
1.75	2.7
2	3.1

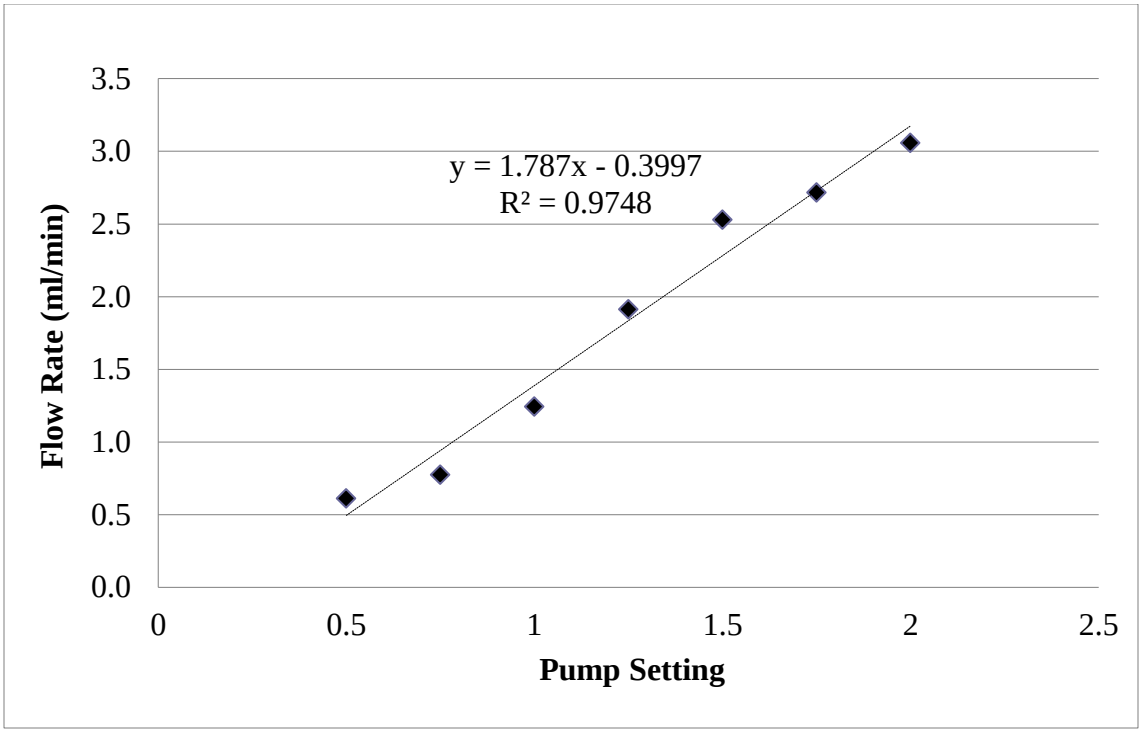

Figure A.2: HBr/Br_2 pump calibration chart for the case studies (sections 3.3.2-8)

Table A.4: H_2 rotameter calibration data

	Time (s)											
Rota-meter Reading	**Trial 1**	**Trial 2**	**Trial 3**	**Avg.**	**Reading Began (mL)**	**Reading End (mL)**	**Amount (mL)**	**Flow Rate 1 (ml/s)**	**Flow Rate 2 (ml/s)**	**Flow Rate 3 (ml/s)**	**Average Flow Rate (mL/min)**	**Std. Deviation (mL/min)**
0								0.00	0.00	0.00	0	0
20	9.91	9.44	9.90	9.75	70	40	30	3.03	3.18	3.03	185	5
40	4.35	4.40	4.57	4.44	70	40	30	6.90	6.82	6.56	406	10
60	4.34	4.37	4.43	4.38	80	30	50	11.52	11.44	11.29	685	7
80	3.00	3.00	2.94	2.98	80	30	50	16.67	16.67	17.01	1007	12
100	2.13	2.09	2.04	2.09	80	30	50	23.47	23.92	24.51	1438	31
120	2.28	2.25	2.28	2.27	90	20	70	30.70	31.11	30.70	1850	14
140	1.72	1.69	1.79	1.73	90	30	60	34.88	35.50	33.52	2078	61

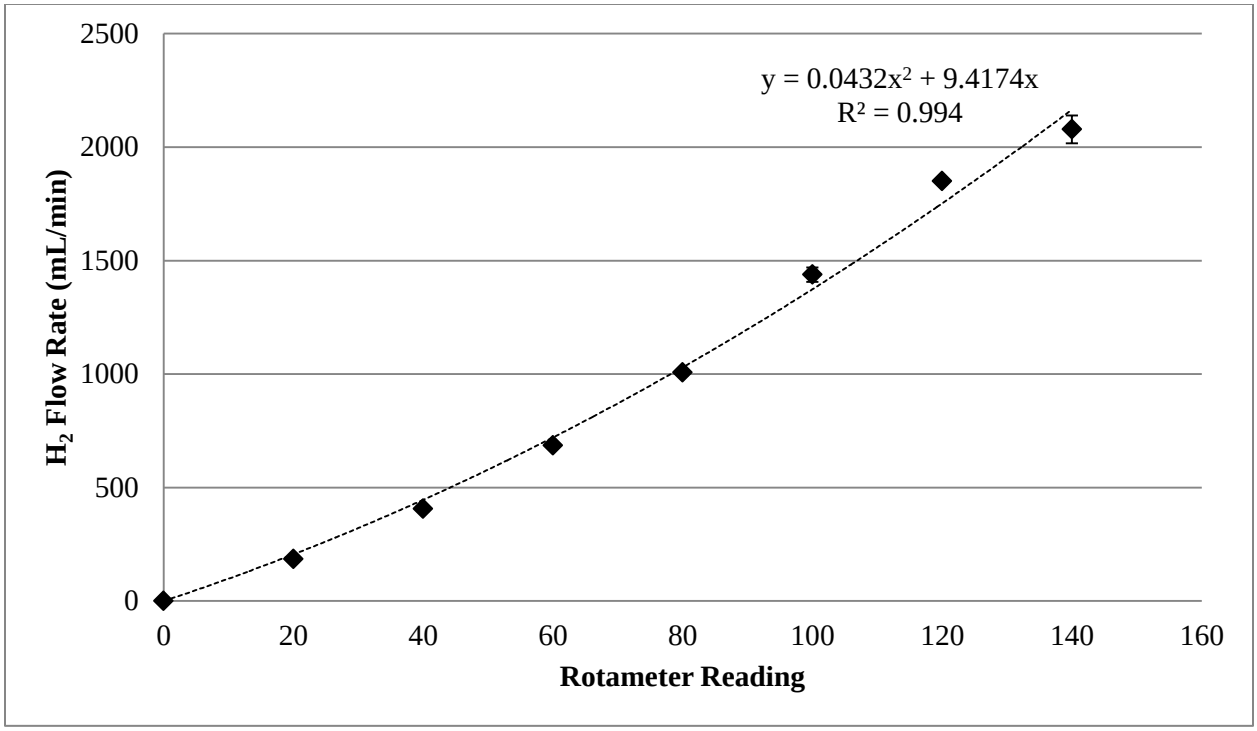

Figure A.3: H_2 rotameter calibration chart

Appendix B: Experimental Data from Preliminary Studies (Sections 3.2.4-5)

This appendix includes the numerical data that is presented in the figures for the preliminary studies. Tables B.1 and B.2 include the H_2-Br_2 and H_2-Air data, respectively, compared in Figure 3.4. Table B.3 contains the H_2-Br_2 data in the looping example, Figure 3.5.

Table B.1: H_2-Br_2 experimental data presented in Figure 3.4

Voltage (V)	Current Density (A/cm^2)	Power Density (W/cm^2)
1.2497	0.6916	
1.2261	0.6086	
1.1998	0.5550	
1.1747	0.5039	
1.1498	0.4467	
1.1249	0.3904	
1.0997	0.3411	
1.1994	0.5489	
1.0744	0.2821	
1.0498	0.2278	
1.0249	0.1647	
0.9997	0.1055	
0.9751	0.0477	
0.9551	0.0000	
0.9600	0.0000	0.0000
0.9548	0.0000	0.0000
0.8991	0.1110	0.0998
0.8491	0.2167	0.1840
0.7993	0.3074	0.2457
0.7490	0.3747	0.2806
0.6993	0.4343	0.3037
0.6495	0.4805	0.3121
0.5995	0.5118	0.3068
0.5497	0.5302	0.2914

Table B.2: H_2-Air experimental data presented in Figure 3.4

Voltage(V)	**Current Density (A/cm^2)**	**Power Density (W/cm^2)**
1.0200	0.0000	0.0000
0.9299	0.0000	0.0000
0.8992	0.0009	0.0008
0.8745	0.0033	0.0029
0.8491	0.0087	0.0074
0.8243	0.0179	0.0148
0.7993	0.0312	0.0250
0.7742	0.0473	0.0366
0.7493	0.0655	0.0491
0.7242	0.0837	0.0606
0.6995	0.1006	0.0704
0.6744	0.1080	0.0728
0.6496	0.1385	0.0900
0.6245	0.1647	0.1029
0.5993	0.1780	0.1067
0.5745	0.1945	0.1118
0.5494	0.2113	0.1161
0.5243	0.2278	0.1194
0.4992	0.2453	0.1224
0.4746	0.2626	0.1246
0.4496	0.2773	0.1246
0.4248	0.2931	0.1245

Table B.3: H_2-Br_2 experimental data presented in Figure 3.5

Current (A)	**Voltage (V)**	**Current Density (-A/cm^2)**	**Power Density (W/cm^2)**
-1.5236	0.4000	0.2645	0.1058
-1.8784	0.4504	0.3261	0.1469
-2.1653	0.5005	0.3759	0.1881
-2.3657	0.5503	0.4107	0.2260
-2.4877	0.6004	0.4319	0.2593
-2.4092	0.6503	0.4183	0.2720
-2.2039	0.7000	0.3826	0.2678
-1.8899	0.7498	0.3281	0.2460
-1.4727	0.8000	0.2557	0.2045
-0.9541	0.8499	0.1656	0.1408
-0.4037	0.8999	0.0701	0.0631
	0.9444	0.0000	0.0000

Appendix C: Experimental Data from Case Studies (Sections 3.3.2-8)

This appendix includes the current, voltage, and calculated current and power densities from the case studies. Each table includes the data from one discharge-charge experiment. Table C.1 is considered the base case, and is used in several of the figures. The operating conditions were as follows: 2M HBr, 2M Br_2, HBr/Br_2 flow rate of 1.6 mL/min (2.3 A/cm^2 for charge and 4.6 A/cm^2 for discharge), H_2 at 3 psig, 660 mL/min (47 A/cm^2 for discharge), and interdigitated flow fields. The MEAs were as described in section 3.3.1.2. All other experiments changed only one of these operating conditions to look at their effects.

Tables C.1 through C.3 contain each of the curves from the Br_2 concentration studies (Figures 3.9 and 3.10). The data in Table C.1 is also included in the flow field comparison, Figure 3.12, along with the data in Table C.4 (serpentine flow field for the HBr/Br_2 solution). Tables C.5 through C.8 contain the data used to look at the effects of HBr/Br_2 flow rate using interdigitated flow fields, compared in Figure 3.13. Tables C.9 through C.12 contain the data in Figure 3.14, which compares different flow rates when serpentine is used for the HBr/Br_2 flow field, and interdigitated flow field is used for H_2. The data in Table C.1 is also used as the base for the studies looking at the effects of higher temperatures, contained in Tables C.13 and C.14 and displayed in Figure 3.15. Table C.15 contains the higher hydrogen flow rate data that was compared to Table C.1 data in Figure 3.16. Tables C.16 and C.17 contain the higher and lower pressures that were compared to the base case (Table C.1) in Figure 3.17. The data used to compare the performance of cells with different membrane thickness in Figure 3.18 is contained in Table C.18. Since the thicker Nafion 115 was used in the membrane electrode assemblies containing the graphite-based bromine electrodes, the data in Table C.18 is used for the platinum

electrode curve compared to the performance data for the graphite-based bromine electrodes in Figures 3.19 through 3.21.

The graphite-based electrode data displayed in Figures 3.19 through 3.21 are contained in Tables C.19 through C.22. Table C.19 contains the performance data using SGL 10AA with no added catalyst as the bromine electrode. Tables C.20 and C.21 contain the performance data for the Toray 090 electrodes with 2.1 mg/cm^2 and 6.6 mg/cm^2 XC-72 carbon, respectively. The performance data using a bromine electrode of 1.6 mg/cm^2 graphene on Toray 090 is enclosed in Table C.22.

Table C.1: H_2-Br_2 flow battery data, base case conditions (Figures 3.9, 3.10, 3.12, 3.15, 3.16, 3.17, 3.18)

Current (A)	**Voltage (V)**	**Current Density (A/cm^2)**	**Power Density (W/cm^2)**
0.6556	1.1989	0.2914	0.3494
0.5824	1.1739	0.2588	0.3039
0.5041	1.1490	0.2241	0.2574
0.4178	1.1240	0.1857	0.2087
0.3266	1.0989	0.1451	0.1595
0.2259	1.0741	0.1004	0.1078
0.1211	1.0489	0.0538	0.0565
0.0168	1.0241	0.0075	0.0076
0.0000	1.0196	0.0000	0.0000
0.0000	1.0206	0.0000	0.0000
-0.0893	0.9984	0.0397	0.0396
-0.1952	0.9737	0.0868	0.0845
-0.2989	0.9487	0.1328	0.1260
-0.3980	0.9236	0.1769	0.1634
-0.5020	0.8989	0.2231	0.2006
-0.5996	0.8739	0.2665	0.2329
-0.6926	0.8487	0.3078	0.2613
-0.7956	0.8235	0.3536	0.2912
-0.8836	0.7990	0.3927	0.3138
-0.9765	0.7741	0.4340	0.3359
-1.0608	0.7488	0.4715	0.3530
-1.1289	0.7241	0.5017	0.3633
-1.2063	0.6991	0.5361	0.3748
-1.2566	0.6743	0.5585	0.3766
-1.3095	0.6489	0.5820	0.3777
-1.3484	0.6243	0.5993	0.3741
-1.3753	0.5993	0.6112	0.3663

Table C.2: H_2-Br_2 flow battery data from Figures 3.9 and 3.10, 1 M Br_2

Current (A)	**Voltage (V)**	**Current Density (A/cm^2)**	**Power Density (W/cm^2)**
0.8796	1.1996	0.3909	0.4690
0.8111	1.1742	0.3605	0.4233
0.7347	1.1492	0.3265	0.3752
0.6501	1.1242	0.2889	0.3248
0.5434	1.0990	0.2415	0.2654
0.4191	1.0742	0.1862	0.2001
0.2945	1.0491	0.1309	0.1373
0.1823	1.0243	0.0810	0.0830
0.0678	0.9995	0.0302	0.0301
0.0000	0.9838	0.0000	0.0000
0.0000	0.9941	0.0000	0.0000
-0.0802	0.9747	0.0357	0.0348
-0.1880	0.9497	0.0836	0.0794
-0.2948	0.9241	0.1310	0.1211
-0.3904	0.8998	0.1735	0.1561
-0.4847	0.8747	0.2154	0.1884
-0.5803	0.8494	0.2579	0.2191
-0.6737	0.8243	0.2994	0.2468
-0.7609	0.7996	0.3382	0.2704
-0.8506	0.7745	0.3781	0.2928
-0.9199	0.7492	0.4088	0.3063
-1.0013	0.7245	0.4450	0.3224
-1.0449	0.6995	0.4644	0.3248
-1.1590	0.6493	0.5151	0.3345
-1.2522	0.5994	0.5565	0.3336

Table C.3: H_2-Br_2 flow battery data from Figures 3.9 and 3.10, 0.7 M Br_2

Current (A)	**Voltage (V)**	**Current Density (A/cm^2)**	**Power Density (W/cm^2)**
0.9427	1.1996	0.4190	0.5026
0.8694	1.1746	0.3864	0.4539
0.7860	1.1498	0.3493	0.4017
0.6962	1.1246	0.3094	0.3480
0.5735	1.0995	0.2549	0.2802
0.4539	1.0745	0.2017	0.2167
0.3290	1.0492	0.1462	0.1534
0.2054	1.0241	0.0913	0.0935
0.0783	0.9989	0.0348	0.0348
0.0000	0.9827	0.0000	0.0000
0.0000	0.9861	0.0000	0.0000
-0.0530	0.9740	0.0236	0.0229
-0.1719	0.9490	0.0764	0.0725
-0.2856	0.9237	0.1269	0.1172
-0.3914	0.8990	0.1740	0.1564
-0.4944	0.8739	0.2197	0.1920
-0.5950	0.8491	0.2645	0.2245
-0.6914	0.8240	0.3073	0.2532
-0.7805	0.7993	0.3469	0.2773
-0.8652	0.7742	0.3845	0.2977
-0.9515	0.7489	0.4229	0.3167
-1.0128	0.7242	0.4501	0.3260
-1.0670	0.6992	0.4742	0.3316
-1.1078	0.6744	0.4924	0.3321
-1.1514	0.6493	0.5117	0.3322
-1.2017	0.6245	0.5341	0.3335
-1.2431	0.5993	0.5525	0.3311

Table C.4: H_2-Br_2 flow battery data from Figure 3.12, serpentine flow field

Current (A)	Voltage (V)	Current Density (A/cm^2)	Power Density (W/cm^2)
0.3709	1.1985	0.1648	0.1976
0.2976	1.1485	0.1323	0.1519
0.1979	1.0987	0.0880	0.0967
0.0822	1.0487	0.0365	0.0383
0.0000	1.0179	0.0000	0.0000
0.0000	1.0195	0.0000	0.0000
-0.0631	0.9986	0.0280	0.0280
-0.2184	0.9486	0.0971	0.0921
-0.3656	0.8984	0.1625	0.1460
-0.5006	0.8486	0.2225	0.1888
-0.6244	0.7987	0.2775	0.2216
-0.7418	0.7488	0.3297	0.2469
-0.8429	0.6989	0.3746	0.2618
-0.9200	0.6485	0.4089	0.2652
-0.9602	0.5988	0.4267	0.2555

Table C.5: H_2-Br_2 flow battery data from Figure 3.13, 0.5 mL/min

Current (A)	Voltage (V)	Current Density (A/cm^2)	Power Density (W/cm^2)
0.3642	1.1984	0.1619	0.1940
0.3615	1.1486	0.1606	0.1845
0.2830	1.0985	0.1258	0.1382
0.1728	1.0485	0.0768	0.0805
0.0000	0.9938	0.0000	0.0000
-0.1339	0.9495	0.0595	0.0565
-0.2927	0.8995	0.1301	0.1170
-0.4374	0.8498	0.1944	0.1652
-0.5585	0.7998	0.2482	0.1985
-0.6407	0.7493	0.2848	0.2134
-0.7030	0.6990	0.3124	0.2184
-0.7554	0.6486	0.3357	0.2178
-0.7582	0.5991	0.3370	0.2019

Table C.6: H_2-Br_2 flow battery data from Figure 3.13, 0.9 mL/min

Current (A)	Voltage (V)	Current Density (A/cm^2)	Power Density (W/cm^2)
0.4610	1.1984	0.2049	0.2455
0.3820	1.1485	0.1698	0.1950
0.3126	1.0985	0.1389	0.1526
0.1960	1.0485	0.0871	0.0914
0.0000	0.9937	0.0000	0.0000
-0.1353	0.9485	0.0601	0.0570
-0.3007	0.8984	0.1337	0.1201
-0.4638	0.8486	0.2061	0.1749
-0.5892	0.7986	0.2619	0.2091
-0.7121	0.7488	0.3165	0.2370
-0.8140	0.6988	0.3618	0.2528
-0.8736	0.6485	0.3882	0.2518
-0.9232	0.5989	0.4103	0.2457

Table C.7: H_2-Br_2 flow battery data from Figure 3.13, 1.4 mL/min

Current (A)	Voltage (V)	Current Density (A/cm^2)	Power Density (W/cm^2)
0.6031	1.1984	0.2681	0.3213
0.5176	1.1484	0.2300	0.2642
0.4016	1.0985	0.1785	0.1961
0.2399	1.0485	0.1066	0.1118
0.0000	0.9953	0.0000	0.0000
-0.1567	0.9488	0.0696	0.0661
-0.3413	0.8984	0.1517	0.1363
-0.5305	0.8487	0.2358	0.2001
-0.7093	0.7990	0.3152	0.2519
-0.8630	0.7489	0.3836	0.2873
-0.9693	0.6988	0.4308	0.3011
-1.0306	0.6489	0.4580	0.2972
-1.0965	0.5988	0.4873	0.2918

Table C.8: H_2-Br_2 flow battery data from Figure 3.13, 1.6 mL/min

Current (A)	**Voltage (V)**	**Current Density (A/cm^2)**	**Power Density (W/cm^2)**
0.8796	1.1996	0.3909	0.4690
0.8111	1.1742	0.3605	0.4233
0.7347	1.1492	0.3265	0.3752
0.6501	1.1242	0.2889	0.3248
0.5434	1.0990	0.2415	0.2654
0.4191	1.0742	0.1862	0.2001
0.2945	1.0491	0.1309	0.1373
0.1823	1.0243	0.0810	0.0830
0.0678	0.9995	0.0302	0.0301
0.0000	0.9838	0.0000	0.0000
0.0000	0.9941	0.0000	0.0000
-0.0802	0.9747	0.0357	0.0348
-0.1880	0.9497	0.0836	0.0794
-0.2948	0.9241	0.1310	0.1211
-0.3904	0.8998	0.1735	0.1561
-0.4847	0.8747	0.2154	0.1884
-0.5803	0.8494	0.2579	0.2191
-0.6737	0.8243	0.2994	0.2468
-0.7609	0.7996	0.3382	0.2704
-0.8506	0.7745	0.3781	0.2928
-0.9199	0.7492	0.4088	0.3063
-1.0013	0.7245	0.4450	0.3224
-1.0449	0.6995	0.4644	0.3248
-1.1590	0.6493	0.5151	0.3345
-1.2522	0.5994	0.5565	0.3336

Table C.9: H_2-Br_2 flow battery data from Figure 3.14, 0.5 mL/min

Current (A)	Voltage (V)	Current Density (A/cm^2)	Power Density (W/cm^2)
0.2608	1.1989	0.1159	0.1390
0.2142	1.1488	0.0952	0.1094
0.1565	1.0985	0.0696	0.0764
0.0891	1.0487	0.0396	0.0415
0.0000	0.9906	0.0000	0.0000
0.0000	0.9958	0.0000	0.0000
-0.0752	0.9485	0.0334	0.0317
-0.1508	0.8984	0.0670	0.0602
-0.2148	0.8486	0.0955	0.0810
-0.2703	0.7985	0.1201	0.0959
-0.3227	0.7488	0.1434	0.1074
-0.3735	0.6987	0.1660	0.1160
-0.4177	0.6485	0.1856	0.1204
-0.4502	0.5988	0.2001	0.1198

Table C.10: H_2-Br_2 flow battery data from Figure 3.14, 0.9 mL/min

Current (A)	Voltage (V)	Current Density (A/cm^2)	Power Density (W/cm^2)
0.3066	1.1990	0.1363	0.1634
0.2534	1.1488	0.1126	0.1294
0.1850	1.0991	0.0822	0.0904
0.1077	1.0489	0.0479	0.0502
0.0000	0.9916	0.0000	0.0000
0.0000	0.9967	0.0000	0.0000
-0.0847	0.9489	0.0376	0.0357
-0.1720	0.8989	0.0765	0.0687
-0.2548	0.8490	0.1133	0.0961
-0.3237	0.7990	0.1439	0.1150
-0.3835	0.7493	0.1705	0.1277
-0.4323	0.6994	0.1921	0.1344
-0.4605	0.6489	0.2047	0.1328
-0.4491	0.5992	0.1996	0.1196

Table C.11: H_2-Br_2 flow battery data from Figure 3.14, 1.4 mL/min

Current (A)	Voltage (V)	Current Density (A/cm^2)	Power Density (W/cm^2)
0.3472	1.1984	0.1543	0.1849
0.2816	1.1485	0.1252	0.1438
0.2115	1.0985	0.0940	0.1033
0.1210	1.0485	0.0538	0.0564
0.0000	0.9909	0.0000	0.0000
0.0000	0.9964	0.0000	0.0000
-0.0891	0.9488	0.0396	0.0376
-0.1812	0.8985	0.0806	0.0724
-0.2696	0.8487	0.1198	0.1017
-0.3445	0.7986	0.1531	0.1223
-0.4022	0.7488	0.1788	0.1338
-0.4561	0.6988	0.2027	0.1417
-0.4703	0.6485	0.2090	0.1356
-0.4020	0.5988	0.1787	0.1070

Table C.12: H_2-Br_2 flow battery data from Figure 3.14, 1.6 mL/min

Current (A)	Voltage (V)	Current Density (A/cm^2)	Power Density (W/cm^2)
0.4182	1.1984	0.1859	0.2227
0.3377	1.1484	0.1501	0.1724
0.2445	1.0985	0.1087	0.1194
0.1396	1.0485	0.0620	0.0650
0.0000	0.9914	0.0000	0.0000
0.0000	0.9944	0.0000	0.0000
-0.1023	0.9485	0.0455	0.0431
-0.2047	0.8984	0.0910	0.0817
-0.3027	0.8488	0.1345	0.1142
-0.3831	0.7986	0.1703	0.1360
-0.4386	0.7488	0.1949	0.1460
-0.4642	0.6989	0.2063	0.1442
-0.4506	0.6486	0.2003	0.1299
-0.3418	0.5988	0.1519	0.0910

Table C.13: H_2-Br_2 flow battery data from Figure 3.15, 35 ˚C

Current (A)	**Voltage (V)**	**Current Density (A/cm_2)**	**Power Density (W/cm_2)**
0.7225	1.1988	0.3211	0.3849
0.6576	1.1736	0.2923	0.3430
0.5909	1.1489	0.2626	0.3017
0.4979	1.1239	0.2213	0.2487
0.3923	1.0990	0.1744	0.1916
0.2880	1.0738	0.1280	0.1375
0.1830	1.0489	0.0814	0.0853
0.0000	1.0095	0.0000	0.0000
0.0000	1.0105	0.0000	0.0000
-0.0501	0.9985	0.0223	0.0222
-0.1656	0.9738	0.0736	0.0717
-0.2802	0.9489	0.1245	0.1182
-0.3969	0.9238	0.1764	0.1630
-0.5235	0.8987	0.2327	0.2091
-0.6406	0.8739	0.2847	0.2488
-0.7491	0.8490	0.3330	0.2827
-0.8687	0.8237	0.3861	0.3180
-0.9752	0.7989	0.4334	0.3463
-1.0681	0.7740	0.4747	0.3674
-1.1623	0.7491	0.5166	0.3870
-1.2502	0.7239	0.5556	0.4022
-1.3284	0.6991	0.5904	0.4127
-1.3945	0.6742	0.6198	0.4179
-1.4552	0.6489	0.6467	0.4197
-1.4984	0.6241	0.6660	0.4156
-1.5436	0.5992	0.6860	0.4111

Table C.14: H_2-Br_2 flow battery data from Figure 3.15, 45 ˚C

Current (A)	Voltage (V)	Current Density (A/cm^2)	Power Density (W/cm^2)
0.8760	1.1985	0.3893	0.4666
0.7960	1.1736	0.3538	0.4152
0.7095	1.1489	0.3153	0.3623
0.6208	1.1238	0.2759	0.3101
0.5194	1.0990	0.2309	0.2537
0.3956	1.0737	0.1758	0.1888
0.2656	1.0489	0.1181	0.1238
0.1283	1.0241	0.0570	0.0584
0.0000	0.9999	0.0000	0.0000
0.0000	1.0012	0.0000	0.0000
-0.0125	0.9986	0.0056	0.0055
-0.1500	0.9738	0.0667	0.0649
-0.2972	0.9489	0.1321	0.1253
-0.4402	0.9239	0.1956	0.1808
-0.5896	0.8988	0.2620	0.2355
-0.7276	0.8740	0.3234	0.2826
-0.8621	0.8490	0.3831	0.3253
-0.9925	0.8238	0.4411	0.3634
-1.1093	0.7990	0.4930	0.3939
-1.1993	0.7741	0.5330	0.4126
-1.2951	0.7491	0.5756	0.4312
-1.3869	0.7239	0.6164	0.4462
-1.4582	0.6992	0.6481	0.4532
-1.5319	0.6742	0.6808	0.4590
-1.6005	0.6490	0.7113	0.4616
-1.6405	0.6241	0.7291	0.4550
-1.6913	0.59921	0.75167	0.45041

Table C.15: H_2-Br_2 flow battery data from Figure 3.16, 2200 mL/min

Current (A)	Voltage (V)	Current Density (A/cm^2)	Power Density (W/cm^2)
0.5752	1.1961	0.2556	0.3058
0.5351	1.1732	0.2378	0.2790
0.4679	1.1485	0.2080	0.2388
0.3932	1.1235	0.1747	0.1963
0.3094	1.0986	0.1375	0.1511
0.2162	1.0734	0.0961	0.1031
0.1202	1.0486	0.0534	0.0560
0.0178	1.0237	0.0079	0.0081
0.0000	1.0191	0.0000	0.0000
0.0000	1.0186	0.0000	0.0000
-0.0777	0.9986	0.0345	0.0345
-0.1729	0.9738	0.0768	0.0748
-0.2703	0.9490	0.1201	0.1140
-0.3617	0.9239	0.1607	0.1485
-0.4543	0.8986	0.2019	0.1815
-0.5474	0.8737	0.2433	0.2126
-0.6430	0.8488	0.2858	0.2426
-0.7426	0.8236	0.3300	0.2718
-0.8365	0.7987	0.3718	0.2969
-0.9340	0.7738	0.4151	0.3212
-1.0172	0.7490	0.4521	0.3386
-1.1055	0.7235	0.4913	0.3555
-1.1891	0.6990	0.5285	0.3694
-1.2584	0.6739	0.5593	0.3769
-1.3157	0.6487	0.5848	0.3793
-1.3523	0.6238	0.6010	0.3749
-1.3942	0.5988	0.6197	0.3711

Table C.16: H_2-Br_2 flow battery data from Figure 3.17, 1 psig

Current (A)	Voltage (V)	Current Density (A/cm^2)	Power Density (W/cm^2)
0.8003	1.2489	0.3557	0.4442
0.7489	1.2225	0.3328	0.4069
0.6890	1.1989	0.3062	0.3671
0.6246	1.1740	0.2776	0.3259
0.5507	1.1489	0.2448	0.2812
0.4673	1.1242	0.2077	0.2335
0.3768	1.0993	0.1675	0.1841
0.2712	1.0741	0.1205	0.1295
0.1566	1.0492	0.0696	0.0730
0.0341	1.0242	0.0152	0.0155
0.0000	1.0172	0.0000	0.0000
0.0000	1.0172	0.0000	0.0000
-0.0868	0.9990	0.0386	0.0385
-0.3158	0.9491	0.1404	0.1332
-0.5315	0.8988	0.2362	0.2123
-0.7493	0.8493	0.3330	0.2828
-0.9495	0.7993	0.4220	0.3373
-1.1331	0.7493	0.5036	0.3773
-1.2796	0.6994	0.5687	0.3977
-1.3803	0.6488	0.6135	0.3980
-1.4173	0.6241	0.6299	0.3931
-1.4436	0.5991	0.6416	0.3844

Table C.17: H_2-Br_2 flow battery data from Figure 3.17, 5 psig

Current (A)	Voltage (V)	Current Density (A/cm^2)	Power Density (W/cm^2)
0.6048	1.1987	0.2688	0.3222
0.5556	1.1736	0.2469	0.2898
0.4839	1.1487	0.2151	0.2471
0.4140	1.1239	0.1840	0.2068
0.3248	1.0991	0.1443	0.1586
0.2338	1.0740	0.1039	0.1116
0.1373	1.0490	0.0610	0.0640
0.0000	1.0202	0.0000	0.0000
0.0000	1.0207	0.0000	0.0000
-0.1035	0.9983	0.0460	0.0459
-0.2241	0.9736	0.0996	0.0970
-0.3348	0.9487	0.1488	0.1412
-0.4491	0.9238	0.1996	0.1844
-0.5608	0.8986	0.2492	0.2240
-0.6676	0.8738	0.2967	0.2593
-0.7805	0.8487	0.3469	0.2944
-0.8905	0.8236	0.3958	0.3259
-0.9930	0.7988	0.4413	0.3525
-1.0876	0.7739	0.4834	0.3741
-1.1846	0.7489	0.5265	0.3943
-1.2615	0.7237	0.5606	0.4058
-1.3345	0.6991	0.5931	0.4146
-1.3825	0.6741	0.6145	0.4142
-1.4298	0.6486	0.6355	0.4122
-1.4588	0.6239	0.6484	0.4045
-1.4794	0.5990	0.6575	0.3938

Table C.18: H_2-Br_2 flow battery data from Figures 3.18 through 3.21, Nafion 115 and 0.5 mg/cm^2 Pt/C

Current (A)	Voltage (V)	Current Density (A/cm^2)	Power Density (W/cm^2)
0.6116	1.1985	0.2718	0.3258
0.5370	1.1736	0.2387	0.2801
0.4661	1.1489	0.2072	0.2380
0.3803	1.1237	0.1690	0.1899
0.2931	1.0986	0.1303	0.1431
0.2005	1.0735	0.0891	0.0956
0.1122	1.0486	0.0499	0.0523
0.0000	1.0176	0.0000	0.0000
0.0000	1.0197	0.0000	0.0000
-0.0746	0.9985	0.0332	0.0331
-0.1663	0.9736	0.0739	0.0720
-0.2567	0.9486	0.1141	0.1082
-0.3403	0.9237	0.1513	0.1397
-0.4197	0.8985	0.1866	0.1676
-0.4907	0.8737	0.2181	0.1905
-0.5535	0.8487	0.2460	0.2088
-0.6097	0.8234	0.2710	0.2231
-0.6519	0.7988	0.2897	0.2315
-0.6932	0.7737	0.3081	0.2383
-0.7291	0.7488	0.3240	0.2427
-0.7621	0.7236	0.3387	0.2451
-0.7893	0.6988	0.3508	0.2451
-0.8081	0.6739	0.3592	0.2420
-0.8292	0.6485	0.3685	0.2390
-0.8472	0.6238	0.3765	0.2349
-0.8540	0.5988	0.3796	0.2273

Table C.19: H_2-Br_2 flow battery data from Figure 3.19, SGL 10 AA without catalyst

Current (A)	**Voltage (V)**	**Current Density (A/cm^2)**	**Power Density (W/cm^2)**
0.4447	1.1986	0.1977	0.2369
0.3894	1.1733	0.1731	0.2031
0.3283	1.1485	0.1459	0.1676
0.2659	1.1236	0.1182	0.1328
0.1977	1.0986	0.0879	0.0966
0.1300	1.0735	0.0578	0.0620
0.0667	1.0485	0.0296	0.0311
0.0000	1.0191	0.0000	0.0000
0.0000	1.0216	0.0000	0.0000
-0.0455	0.9987	0.0202	0.0202
-0.0954	0.9738	0.0424	0.0413
-0.1426	0.9489	0.0634	0.0601
-0.1879	0.9239	0.0835	0.0771
-0.2332	0.8987	0.1036	0.0931
-0.2740	0.8739	0.1218	0.1064
-0.3147	0.8490	0.1399	0.1187
-0.3559	0.8237	0.1582	0.1303
-0.3945	0.7990	0.1754	0.1401
-0.4336	0.7740	0.1927	0.1492
-0.4703	0.7490	0.2090	0.1566
-0.5051	0.7237	0.2245	0.1625
-0.5393	0.6991	0.2397	0.1676
-0.5676	0.6742	0.2523	0.1701
-0.5972	0.6489	0.2654	0.1723
-0.6247	0.6240	0.2777	0.1733
-0.6456	0.5991	0.2870	0.1719

Table C.20: H_2-Br_2 flow battery data from Figures 3.19 through 3.21, 2.1 mg/cm^2 XC-72 carbon on Toray 090 plain

Current (A)	Voltage (V)	Current Density (A/cm^2)	Power Density (W/cm^2)
0.4416	1.1987	0.1962	0.2352
0.3944	1.1739	0.1753	0.2058
0.3379	1.1491	0.1502	0.1725
0.2812	1.1241	0.1250	0.1405
0.2143	1.0992	0.0952	0.1047
0.1469	1.0740	0.0653	0.0701
0.0831	1.0492	0.0369	0.0388
0.0000	1.0168	0.0000	0.0000
0.0000	1.0215	0.0000	0.0000
-0.0465	0.9989	0.0207	0.0206
-0.1064	0.9739	0.0473	0.0460
-0.1650	0.9491	0.0733	0.0696
-0.2208	0.9241	0.0982	0.0907
-0.2722	0.8990	0.1210	0.1088
-0.3207	0.8742	0.1425	0.1246
-0.3638	0.8491	0.1617	0.1373
-0.4061	0.8240	0.1805	0.1487
-0.4488	0.7991	0.1995	0.1594
-0.4866	0.7742	0.2163	0.1675
-0.5168	0.7492	0.2297	0.1721
-0.5443	0.7240	0.2419	0.1751
-0.5707	0.6993	0.2537	0.1774
-0.5924	0.6742	0.2633	0.1775
-0.6099	0.6490	0.2711	0.1759
-0.6262	0.6242	0.2783	0.1737
-0.6379	0.5993	0.2835	0.1699

Table C.21: H_2-Br_2 flow battery data from Figures 3.20 and 3.21, 6.6 mg/cm^2 XC-72 carbon on Toray 090 plain

Current (A)	Voltage (V)	Current Density (A/cm^2)	Power Density (W/cm^2)
0.3880	1.1986	0.1725	0.2067
0.3374	1.1734	0.1499	0.1760
0.2877	1.1486	0.1279	0.1469
0.2215	1.1236	0.0984	0.1106
0.1678	1.0987	0.0746	0.0820
0.1145	1.0736	0.0509	0.0546
0.0649	1.0487	0.0288	0.0303
0.0000	1.0164	0.0000	0.0000
0.0000	1.0235	0.0000	0.0000
-0.0346	0.9988	0.0154	0.0154
-0.0865	0.9740	0.0385	0.0375
-0.1414	0.9477	0.0628	0.0596
-0.2340	0.8984	0.1040	0.0934
-0.2740	0.8736	0.1218	0.1064
-0.3100	0.8487	0.1378	0.1169
-0.3460	0.8234	0.1538	0.1266
-0.3817	0.7988	0.1696	0.1355
-0.4112	0.7738	0.1828	0.1414
-0.4363	0.7488	0.1939	0.1452
-0.4613	0.7236	0.2050	0.1484
-0.4721	0.6988	0.2098	0.1466
-0.4927	0.6740	0.2190	0.1476
-0.5005	0.6487	0.2225	0.1443
-0.5067	0.6240	0.2252	0.1405
-0.5228	0.5990	0.2323	0.1392

Table C.22: H_2-Br_2 flow battery data from Figure 3.21, 1.6 mg/cm^2 graphene on Toray 090 plain

Current (A)	Voltage (V)	Current Density (A/cm^2)	Power Density (W/cm^2)
0.3978	1.1992	0.1768	0.2120
0.3346	1.1740	0.1487	0.1746
0.2726	1.1493	0.1212	0.1392
0.2105	1.1244	0.0936	0.1052
0.1528	1.0995	0.0679	0.0747
0.0965	1.0743	0.0429	0.0461
0.0493	1.0494	0.0219	0.0230
0.0082	1.0246	0.0037	0.0038
0.0000	1.0170	0.0000	0.0000
0.0000	1.0195	0.0000	0.0000
-0.0289	0.9993	0.0128	0.0128
-0.0659	0.9738	0.0293	0.0285
-0.1008	0.9489	0.0448	0.0425
-0.1372	0.9244	0.0610	0.0564
-0.1728	0.8986	0.0768	0.0690
-0.2097	0.8738	0.0932	0.0814
-0.2469	0.8489	0.1097	0.0931
-0.2848	0.8236	0.1266	0.1043
-0.3154	0.7990	0.1402	0.1120
-0.3539	0.7740	0.1573	0.1217
-0.3948	0.7490	0.1755	0.1314
-0.4316	0.7238	0.1918	0.1388
-0.4659	0.6991	0.2071	0.1448
-0.4896	0.6742	0.2176	0.1467
-0.5373	0.6488	0.2388	0.1549
-0.5646	0.6241	0.2509	0.1566
-0.5796	0.5991	0.2576	0.1543